2011

Experimental and numerical investigation of effect of stick-slip friction transition on lateral vibration of magnetic tapes

Sameer Jape
Iowa State University

Experimental and numerical investigation of effect of stick-slip friction transition on lateral vibration of magnetic tapes

by

Sameer Sanjay Jape

A thesis submitted to the graduate faculty

in partial fulfillment of the requirements for the degree of

MASTER OF SCIENCE

Major: Mechanical Engineering

Program of Study Committee:
Jonathan Wickert
Baskar Ganapathysubramanian
Umesh Vaidya

Iowa State University

Ames, Iowa

2011

Table of Contents

List of Figures

List of Tables

Acknowledgements

I would like to express my heartfelt gratitude to my advisors, Dr. Jonathan Wickert and Dr. Baskar Ganapathysubramanian for their encouragement and support throughout my stay at Iowa State University. Their guidance and suggestions greatly helped me focus on this research work. I would also like to thank Dr. Umesh Vaidya for his time and support throughout by graduate studies.

I would also like to thank INSIC for their technical and financial support to this research. I express my gratitude towards Douglas Johnson and Mark Weber from Imation Inc. and Daniel Underkofler and Peter Coburn from Sun Microsystems for providing the experimental setup and their expert guidance from time to time. Lastly, I would like to thank my family, friends and colleagues for their support during my stay at Iowa State University.

Abstract

Magnetic tape storage which is primarily used for long-term archival and backup of digital data, has historically been the most efficient, high-capacity and least expensive storage technology for huge quantities of data. Tape storage applications are in diverse fields such as corporate and government financial records, satellite imagery, credit card databases and patient medical records. Recently, the Linear Tape-Open (LTO) Ultrium format has emerged as the most dominant tape technology option in the mid-range tape drive market, with the LTO generation 5 (LTO-5) being capable of holding as much as 1.5 TB of uncompressed data on a single cartridge. Tape storage however has been traditionally challenged by competing technologies like hard disk drives (HDD), consumer optical storage devices which include CDs, DVDs and Blu-ray disk technologies, optical library systems and holographic storage systems. Thus, one of main goals of the tape industry is to design and manufacture advanced tape storage technologies that aim at reducing the price per unit data storage ($/GB).

In commercial tape drives, a flexible magnetic tape is transported between the supply and take-up packs at a fixed axial tension and transport speed and over edge and surface guides and read/write heads. The tape decks must assure accurate guiding and transport of the tape while it accelerates and decelerates by holding the axial tension constant. During transport, lateral in-plane vibration of tape's narrow edge causes misalignment between data tracks on the tape and position of read/write head and leads to reduced storage capacity. Lateral vibration (low and high frequency) is caused by excitation sources viz. pack run-out, flange impacts, pack tilts and tape edge weave. High frequency lateral vibration is more detrimental

as it is difficult to move the read/write head to follow the tape's high frequency motion. To attenuate this vibration, surface guides (rollers or stationary guides) which control the lateral displacement of tape by applying friction on its wider surface, are used. Choice of an appropriate surface guide (or roller) is possible with an understanding of the physics involved in the surface friction between magnetic tape's wide surface and the roller.

This thesis is motivated by the need to conduct a detailed investigation into the frictional interaction between roller surface and magnetic tape and contribute towards the advancement of tape technology to meet the growing market needs. A parametric study is carried out with respect to the tape's axial tension and axial velocity in the following two aspects:

- An experimental setup is used to control these tape parameters and obtain lateral vibration measurements at two points equidistant from the tape-roller interface to understand the effect of stick-slip friction at the interface on tape's lateral vibration
- A numerical model is developed to study stick-slip friction between the roller surface and the tape that travels over it. The tape is modeled as an axially moving, tensioned, viscoelastic Euler-Bernoulli beam subjected to boundary disturbances arising from supply and take-up pack run-out and stick-slip friction between tape and roller surface.

These analyses are used to predict the possibility of sticking or slipping between the surfaces in contact, as a function of parameters viz. axial tension, axial velocity, surface roughness of roller and span length. A 'dynamic phase diagram' is constructed to determine the regions in

the stiffness-velocity phase-space where steady stick-slip motion occurs and its effects on lateral vibration of the magnetic tape.

Chapter 1

Introduction

1.1 Digital data storage

With the rapidly growing influence of information technology in virtually all walks of life, viz. entertainment, business, politics, military etc., the quantities of digital information generated and stored on a daily basis is staggering. In an estimate in 2008, roughly 3.6 Zettabytes (1 Zettabyte = 10^{21} bytes) of information totaling 10,845 trillion words was consumed by Americans, corresponding to 34 Gigabytes and 100,500 words for an average person per day [1]. There is thus, a huge market demand for low cost per unit storage capacity ($/GB) of digital data. Some of the major storage technologies are magnetic storage media such as audio and video tapes, hard disk drives (HDD), consumer optical storage devices which include CDs, DVDs and Blu-ray disk technologies, optical library systems and holographic storage systems.

Magnetic tape storage technology consists of tape libraries (Fig. 1.1) which are used for long-term data retention, archive, and backup of digital data and commercial tape drives (Fig. 1.2) which are used primarily for backup and recovery of smaller magnitudes of digital data. Advances in computational power, electronics, material science and mechanics have revolutionized the areas of hard disk drives, dramatically dropping their price. Facing this competition, tape media prices and storage capacities have also seen tremendous growth over the past few decades. Recent advancements in technologies like Linear Tape-Open (LTO)

drives of Ultrium format viz. LTO-4 with a capacity of 800 GB and LTO-5 with a capacity 1.5 TB have boosted the sales of magnetic tape based storage in the mid-range market.

1.2 Issues in cost per unit storage capacity

INSIC (Information Storage Industry Consortium) in 2008 provided a roadmap projecting the price of magnetic tape storage for the next 10 years and identified issues that need to be resolved to reach the projected capacity [3]. In the mechanical transport area, which encompasses technology associated with tensioning and transporting the flexible magnetic tape in a linear tape drive and keeping the read/write head in contact with the data tracks on the tape, tape's lateral motion has been identified as a key issue leading to low storage capacity. Lateral Tape Motion (LTM) is caused by excitation sources viz. pack run-out, flange impacts, pack tilts and tape edge weave and leads to misalignment between data tracks on the tape and position of the read/write head ultimately leading to reduced storage capacity, as shown in Fig. 1.3.

LTM issues fall into four broad areas:

- Minimizing LTM introduced in the system
- Mechanically attenuating LTM
- Servo compensation
- Controlling relative slope between head and tape

Careful design and manufacture of tape drive components can ensure minimizing the effects of excitation sources and avoid the introduction of LTM. The read/write head can be mounted on a servo-tracking mechanism so it follows the high-amplitude and low-frequency

vibration of the tape, significantly removing the low-frequency component of the LTM. However, as tape velocity increases, high frequency disturbances are introduced in the system and the LTM can't be tracked by the servo system [3].

1.3 Mechanical Isolation of LTM

Mechanical isolation of LTM includes edge and surface friction guiding to limit the high frequency lateral vibration. Fig. 1.4 depicts the area of mechanical isolation of LTM divided into edge guiding and surface guiding. Conventional edge guides use rigid or compliant flanges that apply lateral force on the narrow edge of the tape to constrain the lateral motion. However, edge guiding can lead to excessive damage and wear of the fragile edge and can introduce LTM via flange-edge contacts. Surface friction guides, such as grooved, porous or roughened rollers and non-rotating cylindrical posts, apply distributed lateral forces on the wider tape surface. Surface friction eliminates the possibility of edge wear and can be used to mitigate high-frequency LTM. However, surface friction guiding also suffers from limitations such as insufficient contact pressure and poor tape slope control [3]. An investigation in the stick-slip frictional interaction between magnetic tape and surface friction guide is thus necessary for tackling these issues and to suggest appropriate roller characteristics.

1.4 Thesis organization

This thesis qualitatively investigates the nature of stick-slip friction between the tape and surface friction guide with regards to tape parameters such as axial tension and axial velocity on the. To get an insight into the complex interplay between surface friction and tape's lateral

motion (LTM) near the tape-roller interface, lateral vibration of tape is observed through experiments and is modeled through numerical analysis.

Chapter 2 analyzes the experimental lateral vibration measurements of tape which is transported between supply and take-up packs, two stationary guides and a rotating roller. LTM is observed at distance 1 cm on the upstream and downstream side of the tape roller interface for five values of tape's axial tension (0.5 N, 0.55 N, 0.6 N, 0.65 N & 0.7 N) and axial velocity (2 m/s, 2.5 m/s, 3 m/s, 3.5 m/s & 4 m/s). The effect of stick-slip surface friction at the interface on LTM is analyzed over this experimental stiffness-velocity phase-space.

Chapter 3 consists of the construction of a finite element model of magnetic tape as an axially moving tensioned Euler-Bernoulli beam supported between a stationary guide and a roller. Stick-slip friction is applied at one end of the beam and numerical lateral displacement is calculated for different values of axial tension and axial velocity of beam and transition frequency of stick-slip friction. Results from the experimental analysis in chapter 1 are used to validate the numerical model.

Chapter 4 deals with applying similar vibration analysis techniques as in chapter 1, to the flanged grooved roller and flangeless smooth roller. Stick-slip friction between roller surface and tape is then investigated over the experimental stiffness-velocity place for these two rollers.

Finally, chapter 5 summarizes the thesis and lists conclusions based on the experimental and numerical results in the thesis and identifies future work. A summary of literature is provided at the end of the thesis.

References

[1] Roger E. Bohn, James E. Short, How Much Information? - Report on American Consumers, (2009)

[2] Sun Microsystems, http://www.oracle.com/us/sun

[3] International magnetic storage roadmap, Information Storage Industry Consortium, September (2008) 117-120

[4] http://hmi.ucsd.edu/howmuchinfo_research.php

[5] http://lto.org/technology/generations.html

Figure 1.1: StorageTek SL3000 modular library system

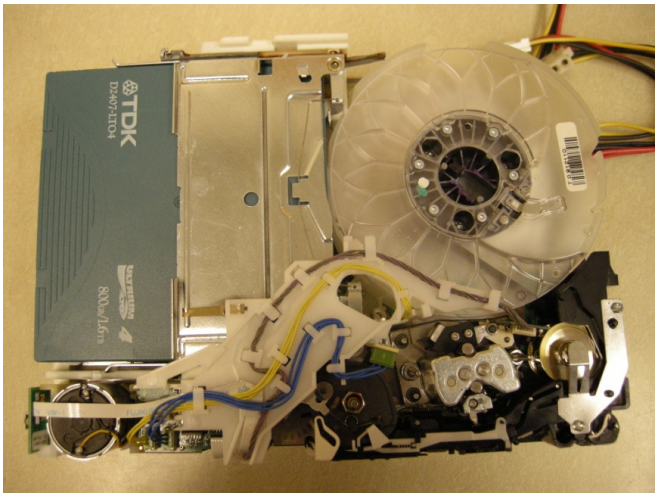

Figure 1.2: HP commercial magnetic tape drive with TDK LTO-4 Ultrium cartridge

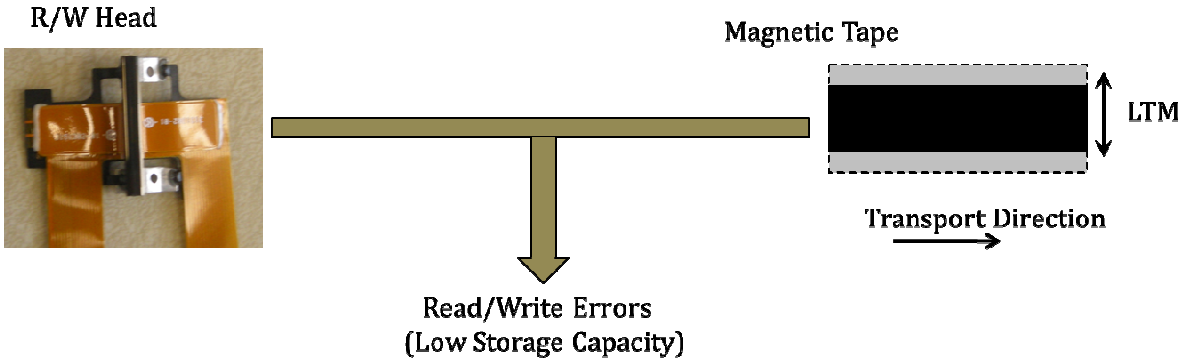

Figure 1.3: Lateral tape motion causing misalignment between R/W head and data tracks on tape and leading to reduced storage capacity

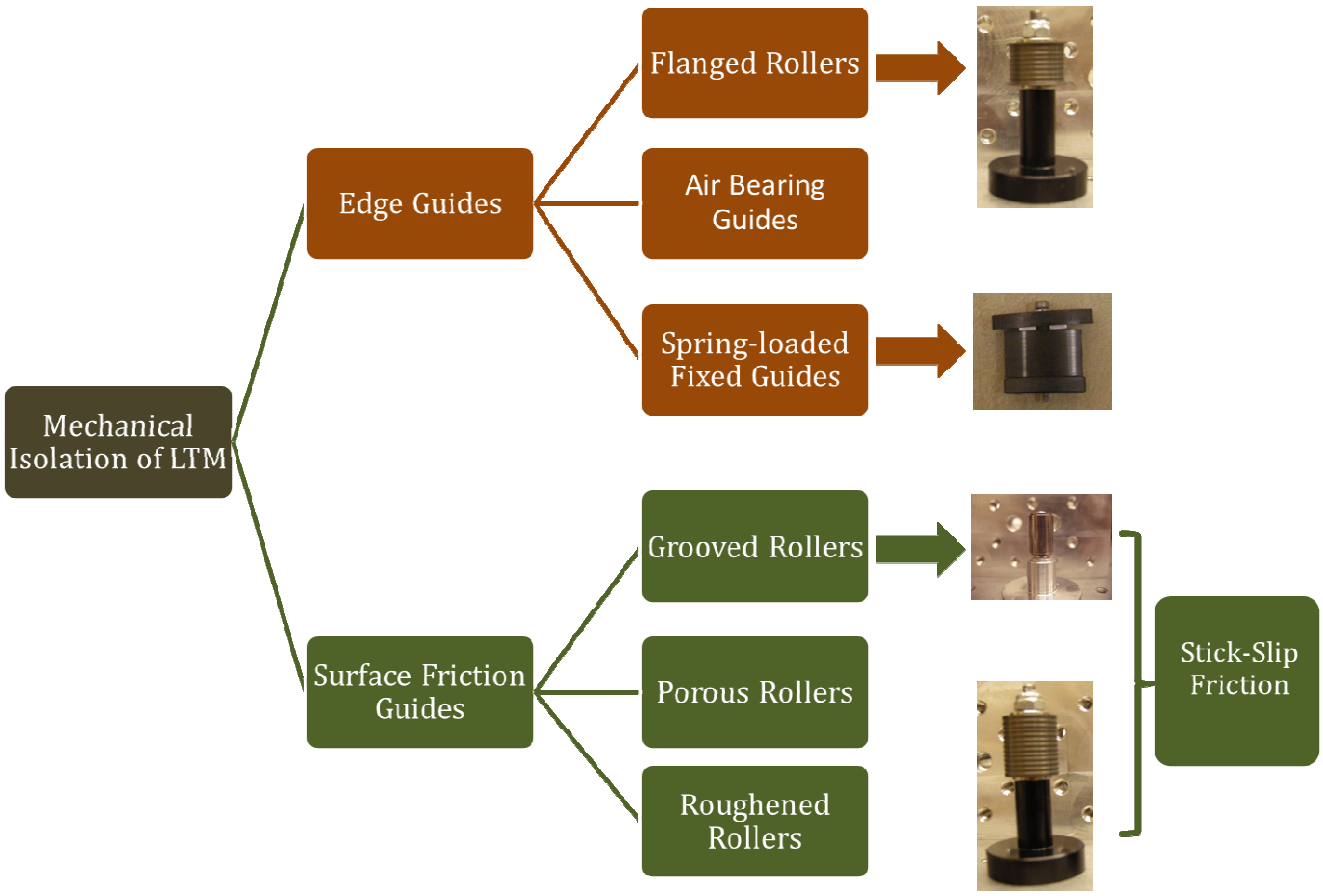

Figure 1.4: Hierarchical chart depicting mechanical isolation of LTM with edge guides and surface friction guides

Chapter 2

Exploring effect of stick-slip friction transition on the lateral vibration of magnetic tapes

S. S. Jape, J.A. Wickert and B. Ganapathysubramanian

Department of Mechanical Engineering, Iowa State University, Ames, IA-50011, U.S.A.

Abstract

Magnetic tape libraries are used for long-term archival and backup of digital data since they offer the least expensive storage for huge quantities of data. The magnetic tape's lateral in-plane vibration leads to misalignment between data tracks on the tape and position of the read/write head and can cause reduced storage capacity in tape drives. Lateral vibration of tape, also known as lateral tape motion (LTM) can be caused by excitation sources viz. pack run-out, flange impacts, pack tilts and tape edge weave. To attenuate this vibration, surface guides, which include grooved rollers, porous rollers, or roughened rollers, are used. A good understanding of the physical phenomena involved in the frictional interaction between magnetic tape and surface friction guides will allow the appropriate and optimal choice of roller characteristics.

In this article, we have conducted a parametric study of the frictional interaction between the roller surface and magnetic tape traveling over it, with respect to two parameters viz. axial tension and axial transport velocity of the tape. An experimental setup is used to control these

tape parameters and obtain lateral vibration measurements at two points equidistant from the tape-roller interface - one on upstream and other on downstream side. Because of friction constraints at roller surface, the tape will have two states in axial motion: if axial force is smaller than frictional force, the end sticks; if axial force increases above frictional force, the end starts slipping. We apply correlation techniques from spectral analysis to upstream and downstream signals to investigate the effect of stick-slip frictional behavior on LTM. The coherence estimate between upstream and downstream LTM signals provides a valuable insight into the nature of stick-slip friction at the interface. It is used as a metric to construct and understand the 'dynamic phase diagram', i.e. to demarcate regions in the stiffness-velocity phase-space where predominance of stick or slip occurs. This phase diagram can then be used as a look-up table to choose roller characteristics.

Keywords: lateral vibration, stick-slip friction, magnetic tape drives

2.1 Introduction

Lateral tape motion (LTM) is one of the chief factors contributing to reduced digital storage capacity in magnetic tape libraries and commercial magnetic tape drives to be investigated, understood and minimized. LTM arises from excitation sources such as supply and take-up pack run-out, guide run-out and tilt, tape and guide flange impacts and imperfections or weave in the tape edge. Various ways of addressing current LTM issues are: (1) minimizing LTM introduced in the system, (2) mechanical isolation of LTM, (3) compensation using a servo system and (4) controlling the head/tape slope [1].

Mechanical isolation of LTM includes edge and surface friction guiding to limit high frequency lateral vibration. Conventional edge guides use rigid or compliant flanges that

apply lateral force on the narrow edge of the tape to constrain the lateral motion. However, edge guiding can lead to excessive damage and wear of the fragile edge and can introduce LTM via flange-edge contacts. Surface friction guides, such as grooved, porous or roughened rollers and non-rotating cylindrical posts, apply distributed lateral forces on the wider tape surface. Surface friction eliminates the possibility of edge wear and can be used to mitigate high-frequency LTM. Surface friction guiding, however, suffers from limitations such as insufficient contact pressure and poor tape slope control. An investigation in the frictional coupling between axially moving medium and a surface friction guide is thus necessary for tackling these issues [1].

Previous work in this area has addressed the frictional interaction between a moving media modeled as either a string or a beam and a surface of a rotating roller. Ono [2] addressed the problem of transfer of lateral vibration of an axially moving string from one side of a cylindrical guide surface to the other side, where Coulomb friction between the string and guide surface was approximated by viscous damping for lateral velocities much smaller than the transport velocity. The amplitude ratio and phase delay of the lateral vibration depends on coefficient of dry friction between string and guide in the axial direction, cylinder contact length and radius and axial speed of the string. Yang [3] studied the dynamics of a string over rotating arbitrary axisymmetric rollers and compared solutions for the case of a cylindrical roller to that of tapered and parabolic rollers. Rhodes [4] investigated the parametric self-excitation of a belt into transverse vibration caused by the recording and playing back of varying tension from one span to another, leading to a similar tension variation into the second span.

Shelton and Reid [5] [6] analyzed the dynamic behavior of idealized and real web over a roller for a single web span and derived the transfer functions for various elements found in practical web guide control systems. Young, Shelton and Fang [7] investigated the statics and dynamics of interactive web systems. Three modes of interaction viz. interaction free for small steering angles (Shelton and Reid, 1971 a & b), circumferential slippage for greater steering and lateral slippage for still greater steering were studied along with the negative steering effect invoked by the circumferential slippage mode. These papers provide boundary conditions that clearly established occurrence of the modes and serve as a guideline for choosing system parameters to avoid undesirable regions, for example, the negative steering effect.

Kartik and Wickert [10] studied the free and forced lateral vibration of axially moving media in the presence of distributed friction guiding with sub-ambient pressure features. The authors performed parameter studies with respect to the pressure coefficient, transport speed, and guide placement and established their effects on the dissipation of the lateral vibration amplitude. Brake and Wickert [11] developed a model for the frictional vibration transmission from a laterally moving surface to a traveling beam, investigating the design parameters that affect the extent of vibration transmission. The authors discovered that by choosing an engagement length between the surface and the beam that is approximately an integral multiple of a vibration mode, vibration transmission from the surface to the beam can be minimized. They also concluded that vibration transmission over a range of frequencies and a particular set of modes could be reduced by choosing a surface having multiple contact regions.

In an experimental analysis involving the frictional interaction between tape and roller, Taylor and Talke [12] investigated the effect of roller axial runout on lateral displacement of tape close to the roller-tape interface. Comparing smooth and grooved roller, the authors found out that axial runout of an unlubricated grooved roller had higher correlation with tape's lateral displacement than the same roller with lubrication or a smooth roller. Raeymakers and Talke [13] investigated the lateral displacement of tape on a cylindrical guide surface and concluded that the amplitude ratio of input and output lateral displacements depends on the bending stiffness of the tape, guide radius and wrap angle.

Previous analytical and experimental work in the area of coupling between an axially moving tensioned media and a frictional surface has thus focused on incorporating friction as a static phenomenon. Stick-slip friction between axially moving tensioned tape and roller surface is another important factor that determines their frictional coupling and needs to be analyzed to control LTM near the tape-roller interface. In the present study, we investigate the frictional coupling between tape and roller surface by experimentally studying lateral vibration of tape at upstream and downstream of the tape-roller interface. Relationship between upstream and downstream lateral vibration signals is used to establish the nature of stick-slip at tape-roller interface. The contributions of this work are: (1) Outlining effects of changing axial tension and axial velocity on magnitude and frequency content of lateral vibration, lateral velocity and lateral acceleration signals at both upstream and downstream (2) Using coherence analysis between upstream and downstream signals to study the frictional nature of tape-roller interface and identify it as predominantly stick or slip and, (3) Demarcation of areas on

the experimental stiffness-velocity phase-space where the frictional coupling shows predominantly stick or predominantly slip behavior.

2.2 Stick-Slip in tape-roller interface

Stick-slip motion arises in sliding friction systems because of the difference between static and kinetic friction coefficients. A single degree-of-freedom spring-block system can be used to illustrate stick-slip friction [14-17]. The system shown in Fig. 2.1(a) consists of a block of mass M with elastic properties represented by spring constant k, sliding on a rough surface with velocity v and tension T. Assuming an initial state where the block sticks to the rough surface, the system will start steady sliding if tensile spring force overcomes static friction. However, for a kinetic frictional force that is lower than static friction and tensile spring force, the block moves at a velocity greater than that of the spring, restoring the spring towards its original length. This reduces the spring force below static friction and causes the block to stick again, thus resulting in a series of stick/slip phases. If motion of the block alternates between periodic stick and slip, spring force F has the profile of a saw-tooth waveform in time with respect to the kinetic friction force F_b (Fig. 2.1(b)).

In the tape-roller frictional interface, an axially tensioned magnetic tape travels over the roller surface with a constant velocity v and axial tension T. The tape is modeled according to the Kelvin-Voigt model for viscoelastic materials, with a purely elastic spring and a purely viscous damper in parallel as shown in Fig. 2.2. Fig. 2.2 depicts an arbitrarily small mass (dM) of tape in contact with the roller surface acted upon by viscoelastic restoring forces given by $\mathrm{F} = -\mathrm{kx} - \mathrm{cv},$ where parameters k and c represent the spring constant and damper constant respectively.

The axially moving tape when pulled in axial direction undergoes a small local elongation resulting in a change in restoring force of the system. When viscoelastic restoring force in the tape increases beyond static friction in tape-roller interface, the tape slips on roller surface. In this slipping phase, frictional force between the tape and roller surface drops to its lower value of kinetic friction (assuming Stribeck friction [18]) and causes the mass (dM) to slide at higher speed than rest of the tape material. Increased local velocity will rapidly reduce the local elongation in tape material, subsequently reducing the viscoelastic force, causing the mass to stick. The tape-roller interface thus undergoes steady stick-slip oscillations, wherein the tape periodically sticks and slips on the roller surface.

Axial tension and axial velocity are two important parameters that determine the occurrence of stick or slip friction between the magnetic tape and roller surface. Stick or slip friction and the transition between stick and slip at tape-roller interface directly influence the tape's lateral vibration near the interface. In this experimentally driven analysis, tape's lateral vibration near the interface is measured using an experimental test-stand JAWS and the predominance of stick or slip friction or both and its effect on the lateral vibration is studied for a range of tape parameters viz. axial tension and axial transport velocity. Stick-slip behavior is analyzed over the experimental domain of axial tension and axial velocity using spectral analysis tools and conclusions are derived to suggest optimum tape and roller parameters.

2.3 Experimental setup

The test-stand "JAWS" (Fig. 2.3) provided by Imation Inc. mimics an industrial magnetic tape drive and consists of a deck, a motion control system, supply and take-up packs, LTO-4

generation tape cartridge, R/W heads and an assortment of tape-path elements viz. two stationary guides, smooth rollers and grooved rollers as shown in Fig. 2.4. The test-stand is connected to a computer via a serial port and the winding/unwinding of tape from the supply and take-up packs can be controlled using a Matlab program [19].

Throughout each experiment, the tape is maintained at a constant nominal tension and transported with constant axial velocity through the tape-path. The aim of this experiment was to analyze the effect of frictional force at tape-roller interface on the lateral vibration of tape on either side of the interface. The typical setup in Fig. 2.3 shows a simple tape-path with supply and take-up packs, two stationary flanged guides and a flangeless grooved roller placed between the guides. The length of tape's span between the roller and each flanged guide was fixed at 10 cm and two optical edge sensors were placed at a distance approximately 1 cm to the upstream and downstream side of the interface as shown in Fig. 2.5. These sensors are capable of collecting real time displacement measurements of the tape's narrow edge in the lateral direction.

Lateral vibration measurements are performed for three different test rollers viz. two flangeless grooved rollers with different groove widths, which act primarily as surface friction guides and one flanged grooved roller acting primarily as an edge guide, as shown in Fig. 2.4. In all three sets of measurements, LTO generation-4 magnetic tape with 12.65 mm width and 6.6 μm thickness is transported between the supply and take-up packs, guided by the flanged guides and roller. Measurements are taken for a range of axial tensions from 0.5 N to 0.7 N at 0.05N intervals and velocities from 2 m/s to 4 m/s at 0.5 m/s intervals.

Controlling these two parameters, we analyzed and compared the lateral tape motion at the upstream entry point and downstream exit point of each roller.

2.4 Lateral vibration analysis

We investigate lateral vibration of tape for different values of axial tension and axial velocity at points located 1 cm upstream and 1 cm downstream of the flangeless grooved roller (Fig. 2.5). In order to isolate the effects of both axial tension and axial velocity on stick-slip friction at the tape-roller interface, our preliminary analysis focuses on keeping one parameter constant and varying the other. Two sets of lateral vibration measurements with a sampling frequency of 1 kHz are carried out viz. (a) constant axial tension and varying axial velocity and (b) constant axial velocity and varying axial tension. Applying moving average method [20], the LTM signal is smoothed and lateral velocity and acceleration of the tape are also calculated and are compared for a 1s time-span.

2.4.1 Constant Axial Tension

Fig. 2.6(a) shows LTM in microns at the upstream and downstream sensor points for a time span of 1s for T = 0.5 N and v = 2 m/s. It can be seen that the magnitude of LTM decreases as the tape travels over the roller to the downstream side. This damping of lateral vibration is also observed when tension is kept constant at set points of 0.55 N, 0.6 N, 0.65 N and 0.7 N and axial velocities are varied from 2 m/s to 4 m/s for each of these set points. Magnitude of lateral velocity is in the order of a few mm/s whereas acceleration is around 0.2 m/s². At constant tension, as the tape passes through roller surface, its lateral velocity remains approximately constant while acceleration decreases in magnitude and this effect is observed for all values of axial velocities.

Fig. 2.6(b) shows the frequency spectrum of LTM at both sensor positions for a constant tension of 0.5 N and is used to understand the effect of changing axial velocity on frequency content of lateral vibration at upstream and downstream. Since higher frequency vibration is absent in this case, the frequency domain is shortened to 200 Hz. At both sensor positions for a constant tension and increasing the axial velocity, the spectrum shows a steady shift towards higher frequencies for the first two modes of lateral vibration. *A comparison of magnitudes for every value of v in this case shows that vibration at higher frequencies is damped to a greater extent across the tape-roller interface as compared to the vibration at lower frequency.*

The distribution of frequencies in velocity and acceleration spectrum is similar to that in spectrum of lateral displacement of the tape. Higher harmonics become more prominent in case of lateral velocity and acceleration as compared to that in lateral displacement. *A comparison between the ratios of amplitudes of first two harmonics in the frequency spectrum shows that when tape travels through the roller surface, higher harmonics are damped to a greater degree than the lower ones.* This trend is present at all five values of axial velocity and can be attributed to the role surface friction plays as a dominant vibration damping factor in a flangeless grooved roller.

2.4.2 Constant Axial Velocity

In the second set of analysis, axial velocity was maintained constant and axial tension varied from 0.5 N to 0.7 N at 0.05 N intervals for each constant value of axial velocity. Fig. 2.7(a) shows lateral displacement, velocity and acceleration of the tape for axial velocity v = 4 m/s and axial tension T = 0.5 N. Similar to the previous case, LTM, lateral velocity and

acceleration get damped as tape travels through the roller surface. This damping is observed for multiple sets of experiments when velocity is kept constant at 2 m/s, 2.5 m/s, 3 m/s, 3.5 m/s and 4 m/s and tension is varied between 0.5 N and 0.7 N. Moreover, there is no significant observable change in the magnitudes of LTM, lateral velocity or lateral acceleration when tape's axial velocity is maintained constant and axial tension is varied.

Frequency content of lateral vibration is shown in Fig. 2.7(b). Comparing the upstream and downstream LTM measurements, it can be seen that both the high and low frequency lateral vibration is damped by the roller. Moreover, as we make the tape stiffer by increasing tension in the axial direction, frequency distribution of LTM remains constant across the tape-roller interface, for all values of axial tension. For higher tension values like 0.65 N and 0.7 N, there is an introduction of high frequency LTM at approximately 67.14 Hz and 100.7 Hz.

A comparison between frequency spectrum of tape's lateral velocity and acceleration is seen in Fig. 2.7(b). *Increase in axial tension of the tape has no observable effect on frequency content of lateral velocity or acceleration of tape.* However, it causes a significant reduction in their amplitudes for the first two harmonics. Increasing tension also introduces higher frequencies in velocity and acceleration spectrum typically around 67.14 Hz and 100.7 Hz.

We have investigated the tape's lateral displacement, velocity and acceleration at the upstream and downstream sides of tape-roller interface. Increasing axial velocity from 2 m/s to 4 m/s and keeping tension constant, we see a shift towards higher frequencies in the frequency spectrum of tape's lateral displacement, velocity and acceleration. Keeping velocity constant and varying the axial tension from 0.5 N to 0.7 N, on the other hand, shows no change in frequency content of any of the three signals. Despite these trends, it is difficult

to establish a relationship between the upstream and downstream lateral vibration signals that would give us an insight into the frictional behavior of tape roller interface. For a detailed qualitative analysis of stick-slip friction at tape-roller interface at different combinations of axial tension and velocity, we advocate using powerful techniques in spectral analysis.

2.5 Spectral techniques for lateral vibration analysis

2.5.1 Basic definitions

Spectral analysis consists of a wide range of powerful mathematical tools used to analyze discrete time signals in the frequency domain. In our analysis, we apply concepts from spectral analysis to understand the response of tape-roller frictional interface to an incoming lateral vibration signal. The autocorrelation and cross-correlation between signals $x(t)$ and $y(t)$[1] signals are as follows (E stands for "the statistical expectation of"):

$$R_x(\tau) = E[x(t)x(t+\tau)] \qquad \text{Auto-correlation of } x(t)$$

$$R_{xy}(\tau) = E[x(t)y(t+\tau)] \qquad \text{Cross-correlation between } x(t) \text{ and } y(t)$$

Cross power spectral density of a pair of stationary processes or random signals is the Fourier transform of cross-correlation function between those two signals and represents the distribution of power per unit frequency in the cross-correlation function between them [23]. Considering the tape-roller interface as a system represented by upstream and downstream lateral vibration signals, cross power spectral density can be interpreted as a measure of the mutual power between these two signals and identifies signals that are common at both upstream and downstream [25]. It is given by,

[1] We assume finite time records of the vibration measurements to be stationary

$$S_{xy}(\omega) \;=\; \frac{1}{2\pi} \int_{-\infty}^{\infty} R_{xy}(\tau)\; e^{-i\omega t}\, d\,\tau$$

Fig. 2.8(a) shows the cross power spectral density estimate for tension T = 0.7 N and two velocities 2 m/s and 2.5 m/s. It is observed that the mutual power between the signals in these two cases is distributed mostly in the lower frequency range (0 – 0.3) on the normalized frequency[2] scale [19]. Similar trend is observed in case of T = 0.65 N and velocities 2 m/s and 2.5 m/s, with the cross power spectral density function showing peaks mainly in the region 0 – 0.3 on the normalized frequency scale.

Transfer function or frequency response function of a system is defined as the quotient of cross power spectral density $S_{yx}(\omega)$ of $x(t)$ and $y(t)$ and auto-power spectral density $S_{xx}(\omega)$ of $x(t)$. Relationship between upstream and downstream signals of the tape-roller interface is modeled by a linear, time-invariant transfer function

$$T_{xy}(\omega) \;=\; \frac{S_{yx}(\omega)}{S_{xx}(\omega)}$$

A higher magnitude of transfer function in a particular frequency range suggests that the tape-roller interface is transferring maximum power from upstream to downstream in that range. The transfer function in Fig. 2.8(b) for T = 0.7 N and *v* = 2 m/s and 2.5 m/s has higher magnitudes in lower frequency range (< 0.3). Peaks at 0.2031 and 0.25 on normalized frequency scale in these plots show the system's ability to transfer maximum power from upstream signal to downstream signal.

[2] Frequency domain normalized (0 to 1), where 1 corresponds to the Nyquist frequency (500 Hz)

Calculation of cross power spectral density and transfer function of tape-roller interface thus proves to be an efficient tool in understanding frequency response of the interface to tape's upstream lateral vibration signal. However, it is difficult to compare the interface's response for various values of axial tension and velocity by merely observing cross spectral density and transfer function. We therefore introduce another important concept from frequency domain spectral analysis viz. the coherence function.

2.5.2 System coherence function

Coherence function between *x(t)* and *y(t)* is a real valued quantity defined by,

$$\gamma_{xy}^2(\omega) = \frac{\left|S_{yx}(\omega)\right|^2}{S_{xx}(\omega)S_{yy}(\omega)}$$

where $S_{xx}(\omega)$ and $S_{yy}(\omega)$ are the individual auto-power spectral densities. Here $0 \leq \gamma_{xy}^2 \leq 1$ and it represents the degree of correlation between the two vibration signals in the frequency domain [25]. It is also interpreted as the fraction of the mean square output $y(t)$ which can be attributed to the $x(t)$, for every frequency ω and is a measure of the causality between the excitation and the response [26].

For an ideal linear system where all extraneous noise has been eliminated, $\gamma_{xy}^2 = 1$, suggesting that $y(t)$ is completely correlated to $x(t)$ and transfer function T_{xy} represents response of system to the $x(t)$. Thus, coherence γ_{xy}^2 closer to value 1 in a particular frequency range suggests a good frequency domain correlation between the two signals [27]. Due to nonlinear stick-slip friction at the tape-roller interface, coherence function relating upstream and downstream signals is generally less than 1. In our analysis, we consider values roughly in the range 0.7 to 1.0 to be high and those below 0.1 to be low.

Periodogram or average periodogram is a direct estimate of the power spectrum of a random signal and is obtained by Fourier transformation of samples of the random signal [24]. We used Welch's modified average periodogram method to calculate the estimates of cross power spectral density $S_{xy}(\omega)$, transfer function $T_{xy}(\omega)$ and coherence function $\gamma_{xy}^2(\omega)$ between the discrete-time upstream and downstream signals. To reduce the approximation effects on spectral densities calculated and to minimize spectral leakage, a raised cosine Hamming window which minimizes the nearest side lobe is used. The window has length 200 as shown in Fig. 2.9 and is given in frequency domain by,

$$\omega(n) = 0.54 - 0.46 \cos\left(\frac{2\pi n}{N-1}\right)$$

2.5.3 Classification of axial tension and velocity

To simplify our analysis, we have divided our experimental stiffness-velocity phase-space (0.5 N-0.7 N and 2 m/s-4 m/s) into four distinct sections, viz.

(1) High tension-low velocity (T = 0.65 N, 0.7 N and v = 2 m/s, 2.5 m/s)

(2) Low tension-high velocity (T = 0.5 N, 0.55 N and v = 3.5 m/s, 4 m/s)

(3) Low tension-low velocity (T = 0.5 N and v = 2 m/s, 2.5 m/s)

(4) High tension- high velocity (T = 0.7 N and v = 3.5 m/s, 4 m/s)

Using concepts discussed from spectral and statistical signal analysis, we investigate the tape-roller interface as a linear system. We use coherence function to study frequency domain correlation between upstream and downstream LTM signals across the interface for the above four combinations of axial tension and velocity on the experimental stiffness-velocity phase-space.

(1) High tension – low sliding velocity

Coherence function estimates in Fig. 2.10(a) & (b) show that the coherence γ_{xy}^2 has values ~ 1 around the low frequency range 0.15 – 0.25 for tension T = 0.7 N and in a broader range around 0.15 – 0.35 for T = 0.65 N. In high frequency range the coherence function shows values less than 1 everywhere else; although there is weak coherence near 0.45 – 0.75 and 0.9 – 1.0 on the normalized scale. This suggests a good correlation between the upstream and downstream signal's frequencies in the low frequency range but a relatively worse correlation everywhere else.

(2) Low tension – high sliding velocity

The coherence estimate for 0.5 N tension and 3.5 m/s and 4 m/s velocities in Fig. 2.11(a) shows values of γ_{xy}^2 ranging from 0.6 to 0.8 in the high frequency range (0.5 to 0.75) and around 0.3 - 0.45 range. In the lower frequency range, γ_{xy}^2 is very close to 1 in a narrow band of frequencies around 0.15 on the normalized scale. In the 0.55 N tension case in Fig. 12(b), coherence is similar to that in 0.5 N case in high frequency zone, but is better in the lower and mid-frequency zone. This suggests good coherence on a broader range at high and medium frequencies for the low tension – high sliding velocity case.

(3) Low tension – low sliding velocity

Fig. 2.12 for velocity 2 m/s and tensions 0.5 N and 0.55 N shows bad coherence between the upstream and downstream vibration signals at higher frequencies (0.5 – 0.75). In the low frequency region, the coherence estimate is close to 1 for a narrow band of frequencies in the range 0.1 to 0.35, but has a low value elsewhere. Thus, for low tension and low sliding

velocity, the system exhibits bad coherence for most part of the frequency domain, both near the lower and the higher frequency ranges suggesting a weak frequency domain correlation between the signals in these regions.

(4) High tension – high sliding velocity

For high tension and high velocity as shown in Fig. 2.13, coherence between the upstream and downstream signals has values close to 1 in both high and low frequency regions, suggesting a strong frequency domain correlation between the signals in these regions. The high tension – high sliding velocity case is a combination of high tension – low velocity and low tension – high velocity cases, with good coherence across most of the frequency domain. Good coherence in the low frequency range is a result of the high stiffness (tension) of the system and good coherence in the high frequency range is a result of high sliding velocity in the system. An overall greater power transfer between the signals and a good coherence in the frequency domain suggests that most part of the magnitude and frequency content of the lateral displacement signal is being conserved as the tape passes across the roller surface.

2.6 Discussion

2.6.1 Stick/slip predominance

In case of a flangeless grooved roller, surface friction plays a major role in controlling lateral vibration of tape both on the upstream and downstream side of the tape-roller interface. The roller can be assumed to possess a transfer function at tape-roller interface that acts on the upstream LTM signal and produces a definite downstream LTM signal. The nature of this interface is governed by magnitude of surface friction at the tape-roller interface, which in turn depends on axial tension and transport velocity of the magnetic tape. Assuming a

periodic switch in surface friction from stick to slip and vice versa, we can divide a finite amount of tape-roller interface time into discrete periods of sticking and slippage. An investigation into the frequency of this periodic switch (or transition) also gives us some interesting insights into the effect of stick-slip friction on lateral vibration of the tape.

Considering a predominantly stick case, when an arbitrary point on the tape comes in contact with roller surface, its displacement and slope with respect to the tape's neutral axis are frozen on the roller surface; recorded as the tape sticks on the surface for a finite amount of contact time; and finally played back on the downstream side. Predominantly stick case would thus indicate a tape-roller interface that transfers maximum lateral vibration from upstream to the downstream across most of the frequency range and shows a greater frequency domain correlation between the two signals. *Thus, a cross power spectral density that has higher magnitudes and a coherence function that is close to 1 both in the low and high frequency range indicate a system with predominantly stick characteristics.*

When viscoelastic restoring forces are big enough to overcome static friction, the tape slips perfectly on roller surface for entire time of contact. In this case, the arbitrarily small mass dM of tape material overcomes static friction and loses a part of its kinetic energy. This loss of kinetic energy depends on tape's sliding velocity, axial tension, coefficients of static and kinetic friction between the tape-roller surface and the amount of contact time at the interface. Thus, predominantly slip case would indicate a tape-roller interface that transmit minimum amount of power from its upstream to the downstream. *A low cross power spectral density and lower magnitudes of coherence function would thus point towards a tape-roller interface that undergoes slippage for most of the contact time.*

2.6.2 Stick/slip physics for four stiffness-velocity combinations

We return back to our classification of axial tension and velocity into four distinct sections on the experimental stiffness-velocity phase-space in Section 2.5.3. For different combinations of stiffness (axial tension) and axial sliding velocity, we identify four possible scenarios for stick-slip friction, viz. (recall Fig. 2.2, Section 2.2)

1. *Low tension – high sliding velocity:* During an initial stick phase, sufficiently high sliding velocities will cause rapid changes in local values of tensile spring force, raising it above the static friction value (which is low for a low tension) more frequently, causing the tape-roller frictional interface to change state from stick to slip. In slip phase, high velocity will result in smaller kinetic frictional force, given the negative slope relationship of kinetic friction coefficient and sliding velocity from the Stribeck curve, causing the mass dM in Fig. 2.2 to move faster, switching the system back to stick phase.

2. *High tension – low sliding velocity:* Lower velocities will result in less frequent changes in local tensile spring force, rarely raising it above the static friction (which will be comparatively higher owing to higher value of tension). Once the system switches state to slip, it will result in a higher value of kinetic friction force, owing to the relatively lower velocity of mass dM in this case. This will cause the system to remain in slip for longer time before it switches back to stick phase and for the same amount of sliding time between the tape and roller surface, there will be fewer switches between stick and slip phases of the frictional interface for a high tension – low velocity case as compared to that in the low tension – high velocity case.

3. *Low tension – low sliding velocity:* Owing to low static friction (due to low axial tension), the system will switch from stick to slip in a comparatively shorter time for lower values of velocity. However in steady sliding at lower velocity, behavior of system will depend largely on the negative slope of the Stribeck curve of the sliding surfaces. For a high negative slope, kinetic friction force will drop quickly for a small rise in velocity during the system's switch from stick to slip, bringing the system back to stiction in less time. For a relatively lower negative value of the slope, kinetic friction will increase slowly, taking longer time for slip to stick switch. Thus, stick-slip switching frequency will be higher for a higher negative value of slope of Stribeck curve and will be lower for a lower value of this slope.

4. *High tension – high sliding velocity:* For high tension and high velocity system behavior will be similar as described in the previous case. A high value of slope of the Stribeck curve will cause high frequency stick-slip transitions whereas a lower value will cause relatively less frequent transitions.

It can be argued that sticking and slipping times are unequal in last two cases; sticking period will dominate in case of high tension-high velocity owing to a larger static friction while slipping period will dominate in case of low tension-low velocity because of the lower value of static friction. However, stick-slip transition in these cases is more complex and will depend on sliding friction between the surfaces at microscale and needs an accurate stiffness-velocity phase diagram for prediction. Sticking and slipping time-period in each case will be a function of system parameters such as axial tension (T), axial velocity (v), lubrication and

roughness of roller surface and area of contact between tape and roller surface, and varies with every combination of tape-roller interface.

2.6.3 Coherence as a metric to qualitatively understand stick-slip

Out of the four cases analyzed in Section 2.5.3 and Section 2.6.2, for high tension – low velocity case, coherence function is close to 1 for a small band of frequencies in the lower range. High tension – low velocity leads to a low stick/slip switching frequency between the surfaces in contact, whereby the systems stays in stick and slip phase for longer durations of time. This low switching frequency causes the interface to transmit maximum power from upstream to downstream in the lower frequency range and produce better frequency domain correlation between upstream and downstream signals in this range.

On the other hand, low tension – high velocity case shows a coherence function with values closer to 1 in the high frequency zone. Owing to a relatively higher stick/slip switching frequency, the tape-roller interface performs better in high-frequency zone as compared to high-tension low velocity case, where it performs well in the low-frequency region. Thus, lower rate of switching between stick and slip phases across the tape roller interface enables the interface to transmit high-frequency lateral vibration of the tape with greater efficiency.

In case of low tension – low velocity, it is observed that the coherence estimate shows values close to 1 at distinct frequencies in lower and higher frequency range; it suggests the existence of harmonics at which power transfer takes place across the tape-roller interface. However, the overall frequency range in which the interface operates is narrower as compared to the above two cases. Relatively bad coherence across the frequency domain

suggests that the system undergoes slip for most of the time tape is in contact with the roller surface.

Finally, for high tension – high velocity case, system exhibits good coherence over both lower and higher frequency ranges. In contrast to the previous case, overall good coherence of the system across the frequency domain suggests that the interface stays in stick phase for most of the contact time.

Summarizing the discussion, lateral vibration of tape shows the following definite trends as a result of the combination of different excitation sources in the tape-path and surface friction at the tape-roller interface:

(1) For low tension – high velocity, stick/slip transition frequency increases and leads to better coherence and system response in the high frequency domain

(2) For high tension – low velocity, stick/slip transition frequency decreases and leads to better coherence and system response in the low frequency domain

(3) For low tension – low velocity/high tension – high velocity, above discussion points towards complex stick-slip dynamics in these cases. Depending on the Stribeck curve, the stick-slip switching frequency will be higher for a higher negative slope of the curve and lower for a lower value of slope.

2.6.4 Area under coherence function

To compare the four cases, we calculated area enclosed under the coherence curve and plotted its normalized form on the experimental domain, as shown in Fig. 2.14. The normalized area is used as a measure of total amount of coherence between upstream and

downstream signals across the entire frequency domain. Greater value of the area indicates better coherence which in turn suggests that the system stays in stick phase for a comparatively longer time. Smaller value of the area denotes a comparatively bad coherence which suggests the system's tendency to slip more often.

2.7 Conclusion and future work

The effect of stick/slip friction between tape and roller surface on the lateral vibration of the tape is analyzed experimentally by controlling parameters viz. axial tension and axial transport velocity of the tape. The main conclusions of this work are:

(1) When axial tension is kept constant, high frequency vibration is introduced with increasing axial velocity; and higher harmonics are damped to a greater degree than the lower ones in tape's lateral vibration, velocity and acceleration across the tape-roller interface. On the other hand, at constant axial velocity, increase in axial tension of the tape has no observable effect on frequency content of lateral velocity or acceleration of tape.

(2) Since conventional techniques of comparing time and frequency domain lateral vibration data prove inadequate for a detailed understanding of stick-slip friction at the interface, use of advanced correlation techniques (cross power spectral density, transfer function and coherence function) from spectral analysis are advocated.

(3) Nature of friction between tape and roller surface is qualitatively understood from Fig. 2.15, which shows areas of stick predominance, slip predominance and a combination of both. The coherence function metric in Fig. 2.15 indicates that normalized area under coherence function is highest at approximately T = 0.65-0.7 N and v = 3.5-4 m/s. This is the

stiffness-velocity region where the tape and roller surface stick to a greater degree. The region on the left half in Fig. 2.15, especially at T= 0.5 N and v = 2 m/s shows relatively low value of normalized area under coherence. This region is where the two surfaces in contact slip to a greater extent.

We have implemented the coherence analysis technique to investigate frictional interaction between the tape and a flanged (Fig. 2.5(b)) and a flangeless finely grooved (Fig. 2.5(c)) roller for the experimental axial tension and axial velocity range of 0.5 N - 0.7 N and 2 m/s - 4m/s. We are also developing a finite element framework that models the magnetic tape as an axially moving tensioned Euler-Bernoulli beam with stick-slip boundary condition and predicts its lateral vibration near the interface. Results from experiments are used to validate this numerical model.

Acknowledgements

The authors would like to thank INSIC for their technical and financial support to this research. We would also like to thank Douglas Johnson and Mark Weber from Imation Inc. and Daniel Underkofler and Peter Coburn from Sun Microsystems for providing the experimental setup and their expert guidance from time to time.

References

[1] International magnetic storage roadmap, Information Storage Industry Consortium, September (2008) 117-120

[2] K. Ono, Lateral motion of an axially moving string on a cylindrical guide surface, ASME Journal of Applied Mechanics 46 (1979) 905-912

[3] R.J. Yang, Steady motion of a thread over a rotating roller, ASME Journal of Applied Mechanics 61 (1994) 16-22

[4] J.E. Rhodes, Parametric self-excitation of a belt into transverse vibration, ASME Journal of Applied Mechanics 37 (1970) 1055-1060

[5] J.J. Shelton, K.N. Reid, Lateral dynamics of an idealized moving web, ASME Journal of Dynamic Systems, Measurement, and Control 3 (1971) 187-192

[6] J.J. Shelton, K. N. Reid, Lateral dynamics of a real moving web, ASME Journal of Dynamic Systems, Measurement, and Control 3 (1971) 180-186

[7] G.E. Young, J. J. Shelton, B. Fang, Interaction of web spans: Part II—Dynamics, ASME Journal of Dynamic Systems, Measurement, and Control 111 (1989) 497-504

[8] G.E. Young, K.N. Reid, Lateral and longitudinal dynamic behavior and control of moving webs, ASME Journal of Dynamic Systems, Measurement, and Control 115 (1993) 309-317

[9] V. Kartik, J.A. Wickert, Vibration and guiding of moving media with edge weave imperfections, Journal of Sound and Vibration 291 (2006) 419-436

[10] V. Kartik, J.A. Wickert, Surface friction guiding for reduced high frequency lateral vibration of moving media, ASME Journal of Vibration and Acoustics 129 (2007) 371-379

[11] M.R. Brake, J.A. Wickert, Frictional vibration transmissions from a laterally moving surface to a traveling beam, Journal of Sound and Vibration 310 (2008) 663-675

[12] Ryan J. Taylor, Frank E. Talke, Investigation of roller interactions with flexible tape medium, Tribology International 38 (2005) 599-605

[13] Bart Raeymaekers, Frank E. Talke, Lateral Motion of an axially moving tape on a cylindrical guide surface, Journal of Applied Mechanics 74 (2007) 1053-1056

[14] R.N. Miles, S.P. Bigelow, Random vibration of a beam with a stick-slip end condition, Journal of Sound and Vibration 169 (1994) 445-457

[15] R.A. Ibrahim, Friction-induced vibration, chatter, squeal, and chaos Part II: Dynamics and modeling, Applied Mechanics Review 47 (1994) No. 7

[16] Mark Denny, Stick-slip motion: an important example of self-excited oscillation, European Journal of Physics 25 (2005) 311-322

[17] K. Popp, P. Stelter, Stick-slip vibration and chaos, Philosophical Transactions of the Royal Society London 332 (1990) 89-105

[18] Chun Bo, D. Pavelescu, The friction-speed relation and its influence on the critical velocity of stick-slip motion, Wear 82 (1982) 277-289

[19] www.mathworks.com

[20] http://www.mathworks.com/help/toolbox/curvefit/smooth.html

[21] Dean Karnopp, Computer simulation of stick-slip friction in mechanical dynamic systems, ASME Journal of Dynamic Systems, Measurement, and Control 107 (1985) 100-103

[22] Barney E. Klamecki, A catastrophe theory description of stick-slip motion in sliding, Wear 101 (1985) 325-332

[23] D E Newland, An introduction to random vibrations and spectral analysis, Longman Group Limited, 2nd edition, 21-51

[24] A.V. Oppenheim, R.W. Schafer, Discrete-Time Signal Processing, Upper Saddle River, NJ: Prentice-Hall, (1999) 730-754

[25] Michael Norton, Denis Karczub, Fundamentals of noise and vibration analysis for engineers Second Edition, Cambridge University Press, (2003) 352-380

[26] André Preumont, Random vibration and spectral analysis, Kluwer Academic Publishers, (1994) 135-141

[27] Julius S. Bendat, Allan G. Piersol, Engineering applications of correlation and spectral analysis, John Wiley & Sons, (1980) 78-96

(a)

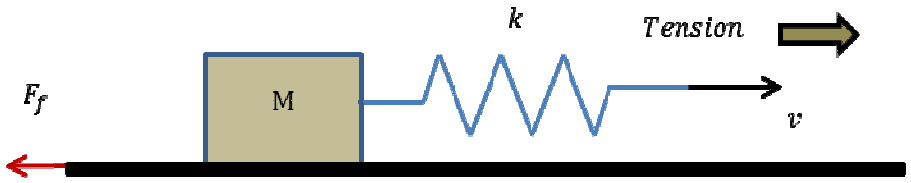

(b)

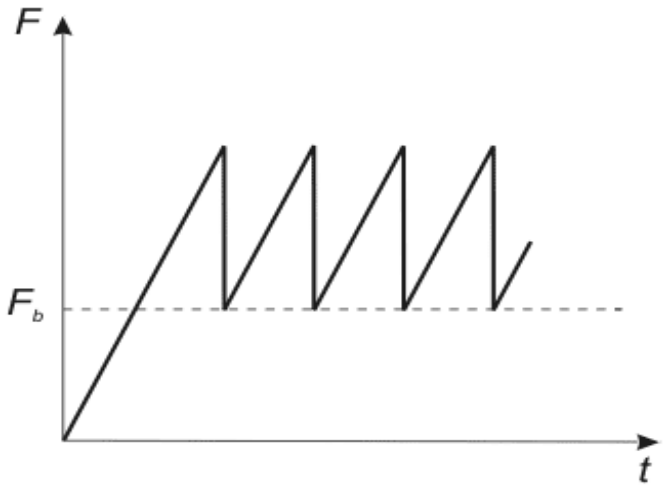

Figure 2.1: (a) Spring-mass system to demonstrate stick-slip (b) Sawtooth profile of spring force

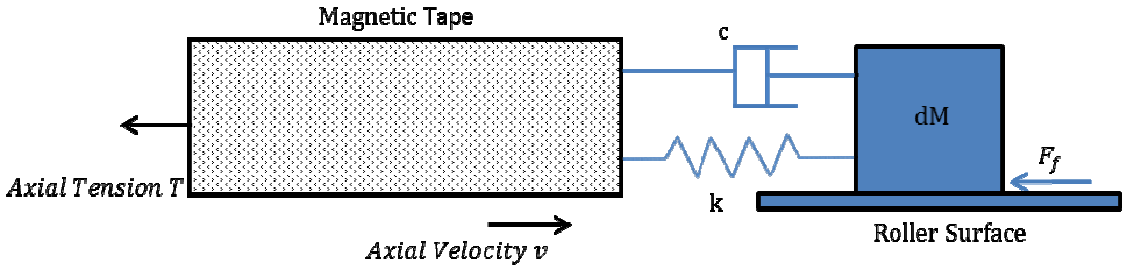

Figure 2.2: Kelvin-Voight viscoelastic model of magnetic tape

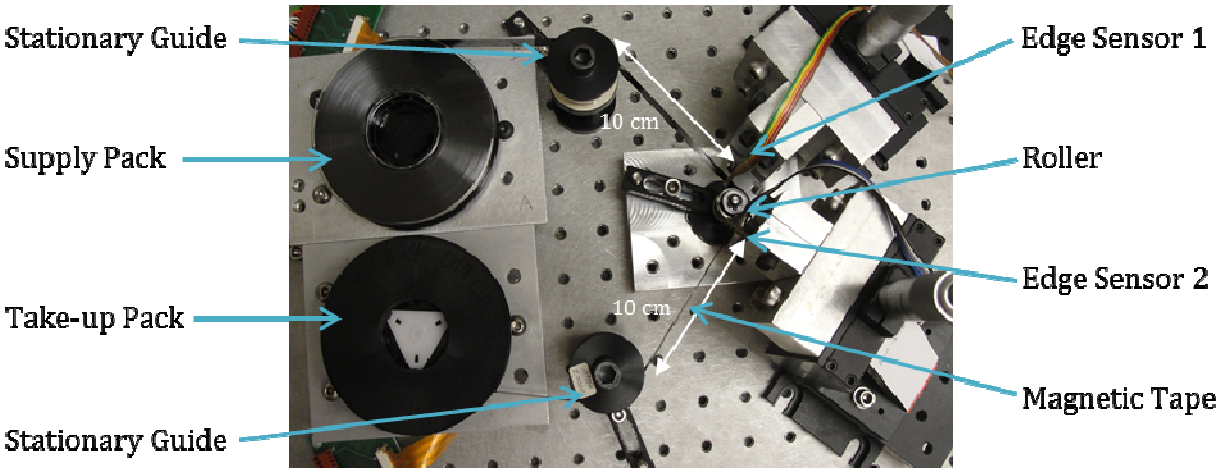

Figure 2.3: Photograph of "JAWS" experimental setup showing tape-path with supply and take-up packs, two stationary flanged guides, flangeless grooved roller and two edge sensors to measure LTM

(a)

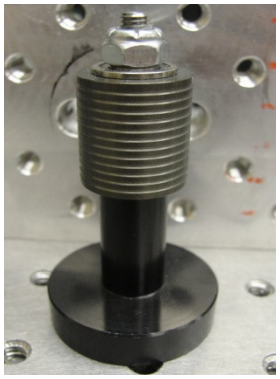

(b)

(c)

Figure 2.4: (a) Flangeless grooved roller (b) Flanged grooved roller (c) Flangeless Grooved Roller

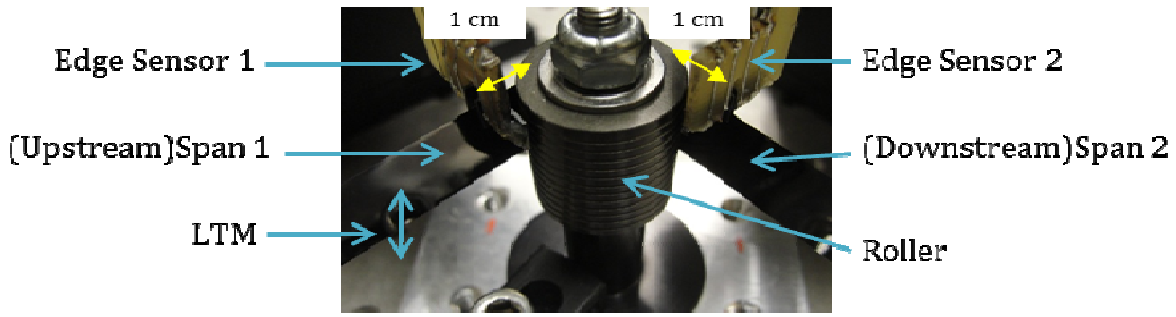

Figure 2.5: Flangeless grooved roller with two edge sensors, depicting LTM direction and upstream and downstream spans

(a)

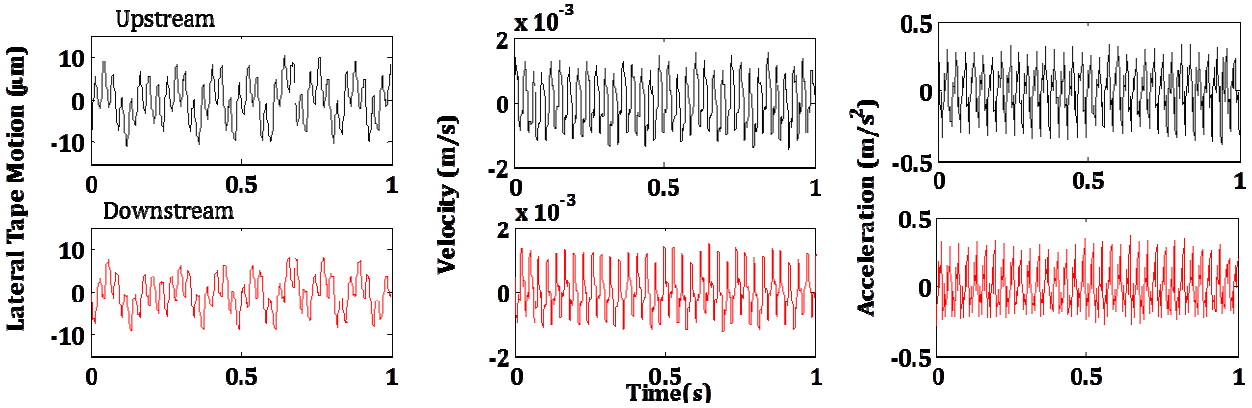

(b)

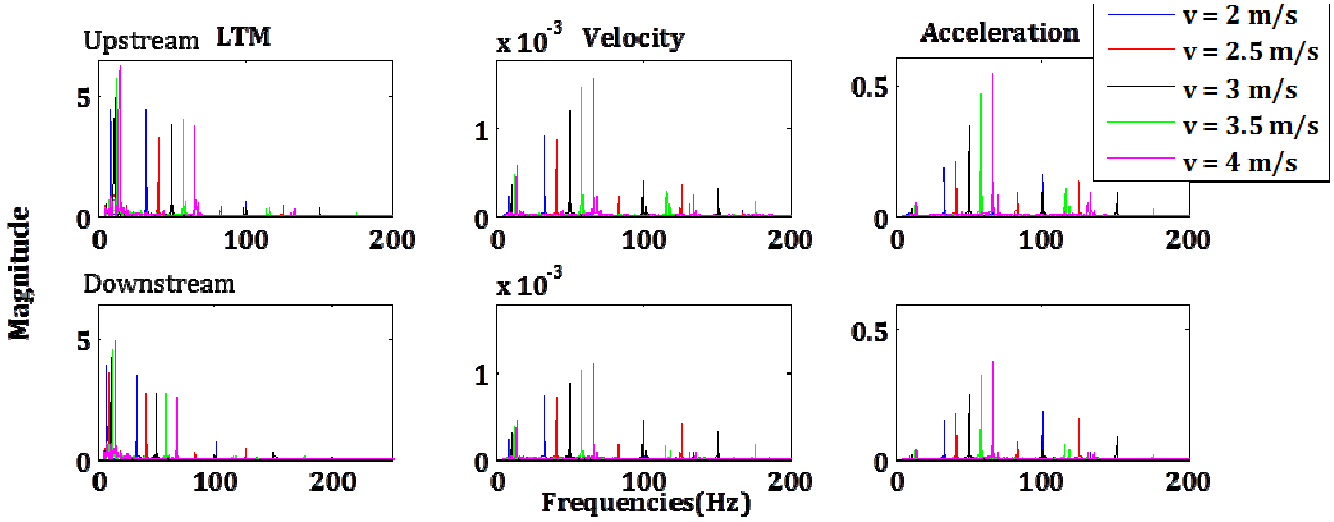

Figure 2.6: (a) Tape's lateral displacement, velocity and acceleration at T = 0.5 N, v = 2 m/s

(b) FFT of Tape's lateral displacement, velocity and acceleration at T = 0.5 N

(a)

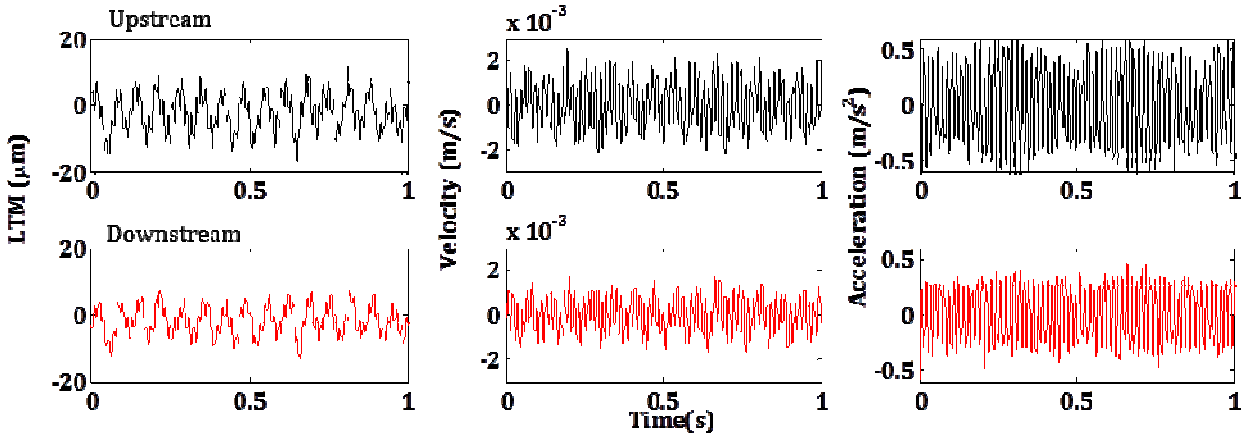

(b)

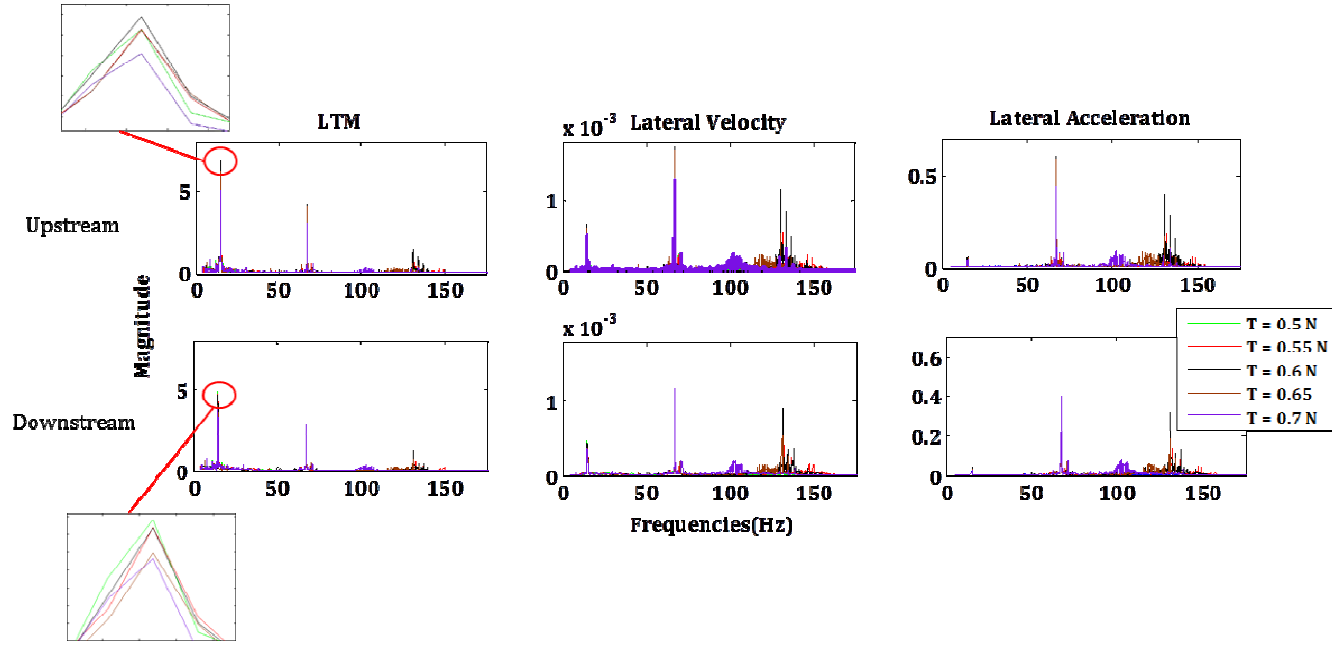

Figure 2.7: (a) Tape's Lateral displacement, velocity and acceleration at T = 0.5 N, v = 4 m/s

(b) FFT of Tape's lateral displacement, velocity and acceleration at v = 4 m/s

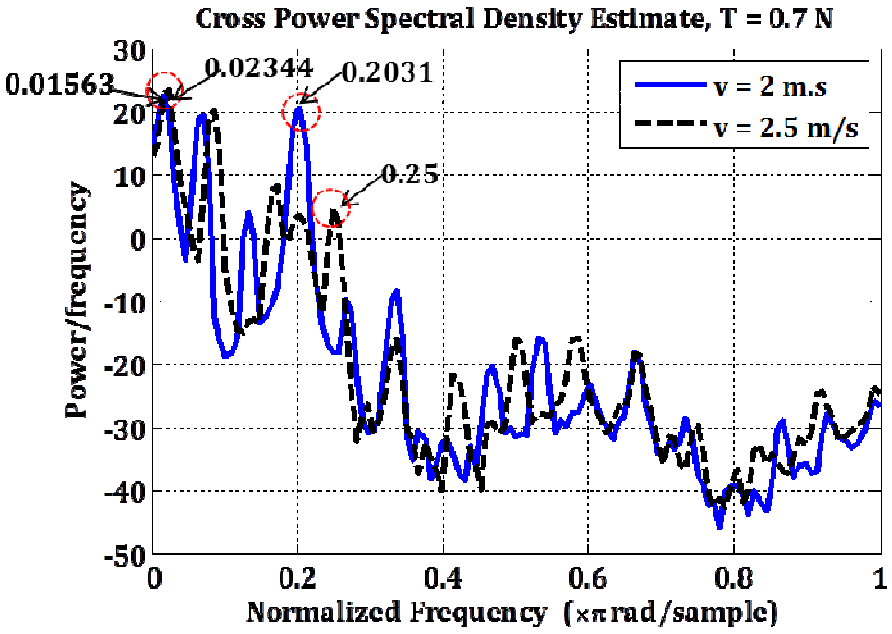

(a)

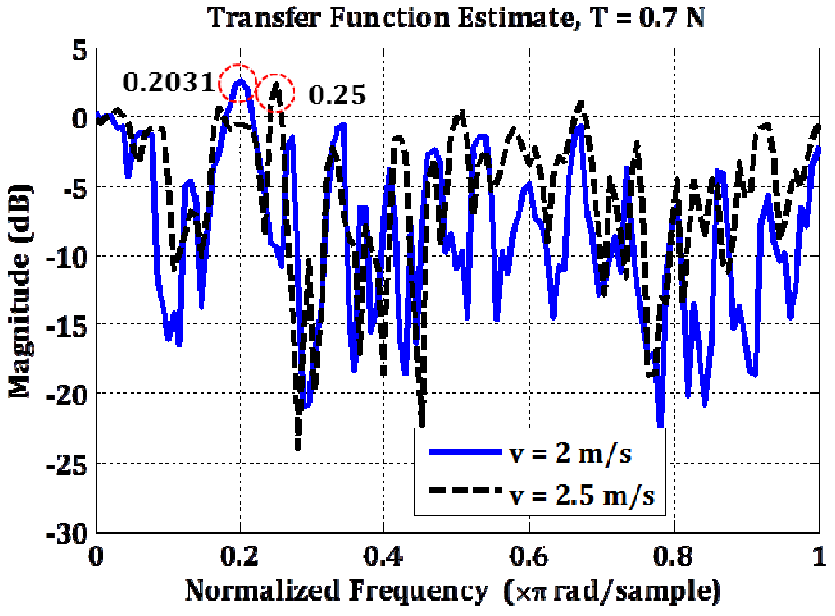

(b)

Figure 2.8: (a) Cross power spectral density at T = 0.7 N & v = 2 m/s, 2.5 m/s (b) Transfer function estimate at T = 0.7 N & v = 2 m/s, 2.5 m/s

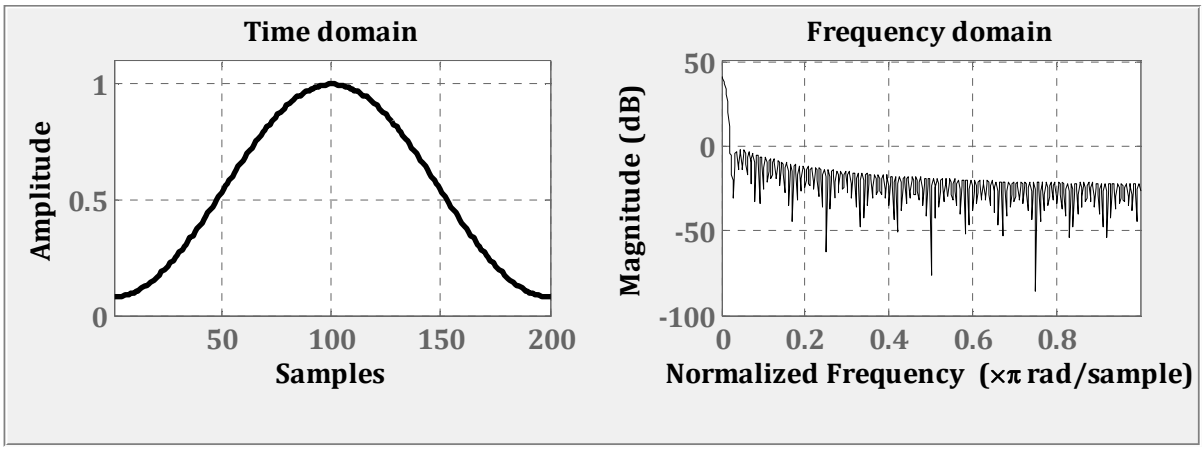

Figure 2.9: Hamming window of length 200 in time and frequency domain

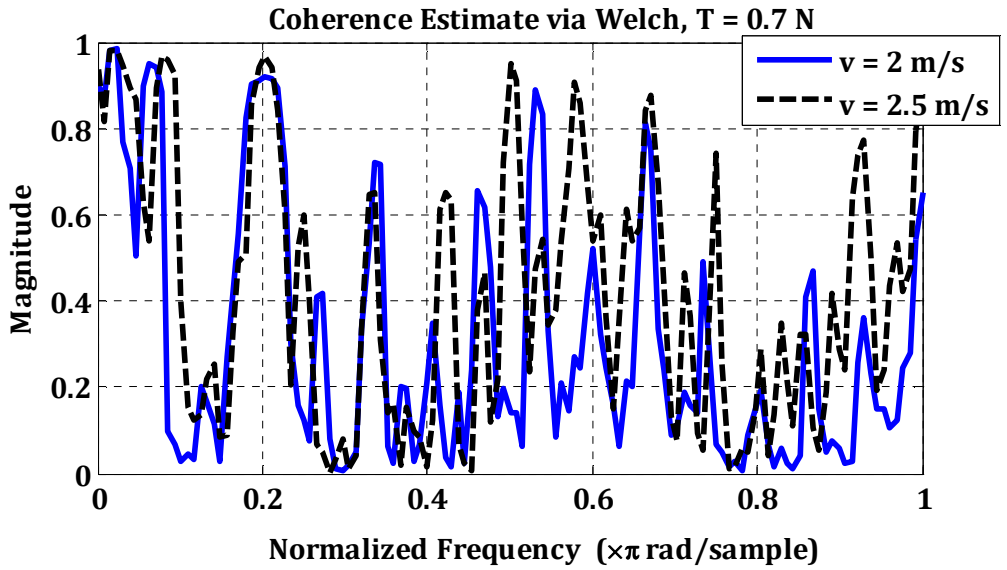

(a)

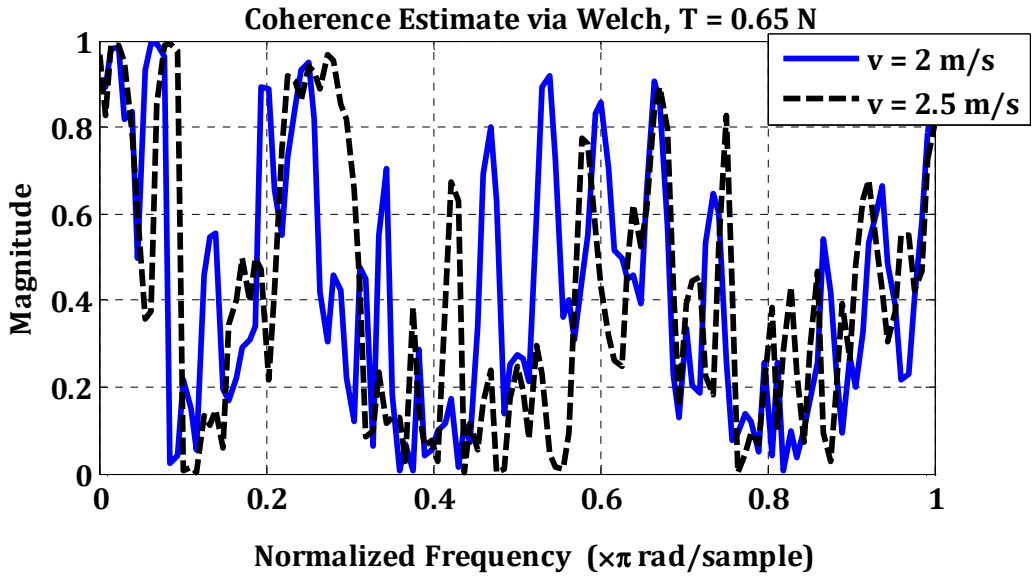

(b)

Figure 2.10: Coherence estimate at (a) T = 0.7 N, v = 2 m/s & 2.5 m/s and at (b) T = 0.65 N, v = 2 m/s & 2.5 m/s

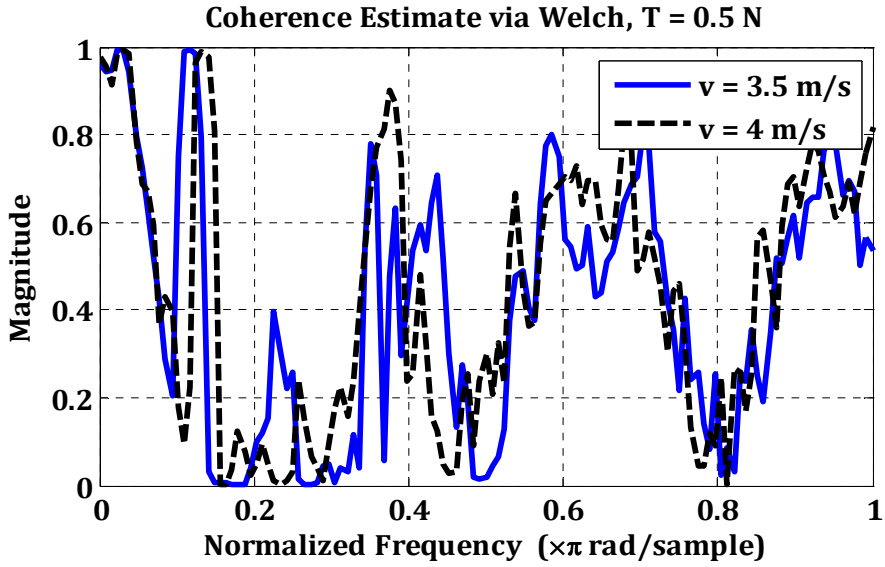

(a)

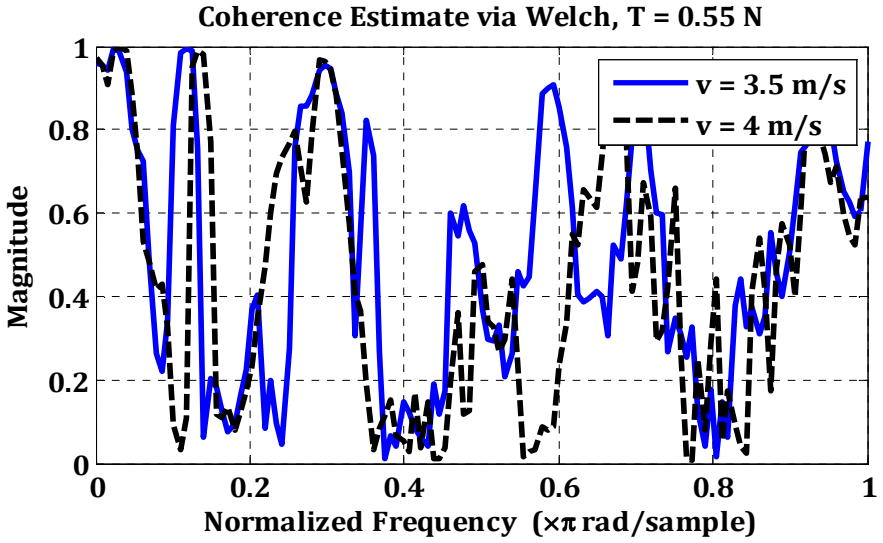

(b)

Figure 2.11: Coherence estimate at (a) T = 0.5 N, v = 3.5 m/s & 4 m/s and at (b) T = 0.55 N, v = 3.5 m/s & 4 m/s

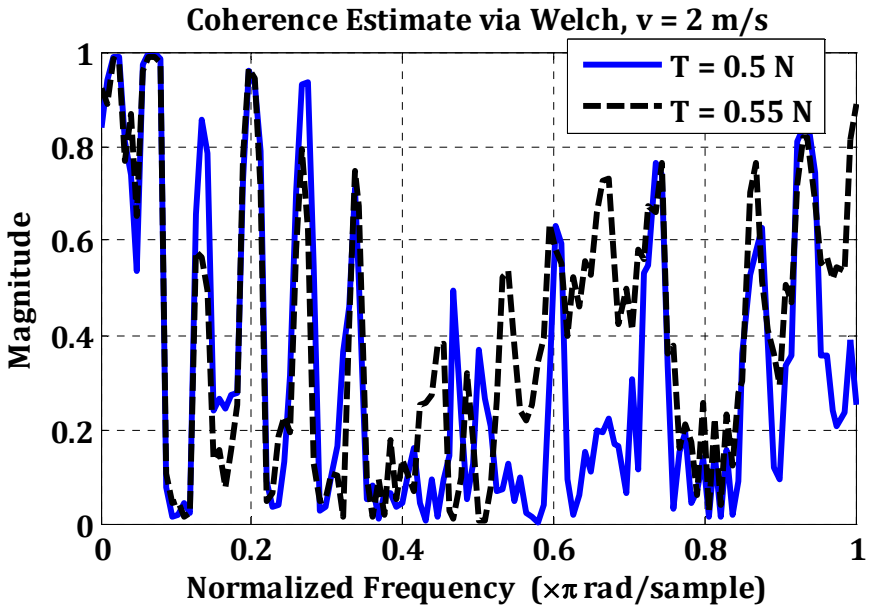

Figure 2.12: Coherence estimate at v = 2 m/s, T = 0.5 N & 0.55 N

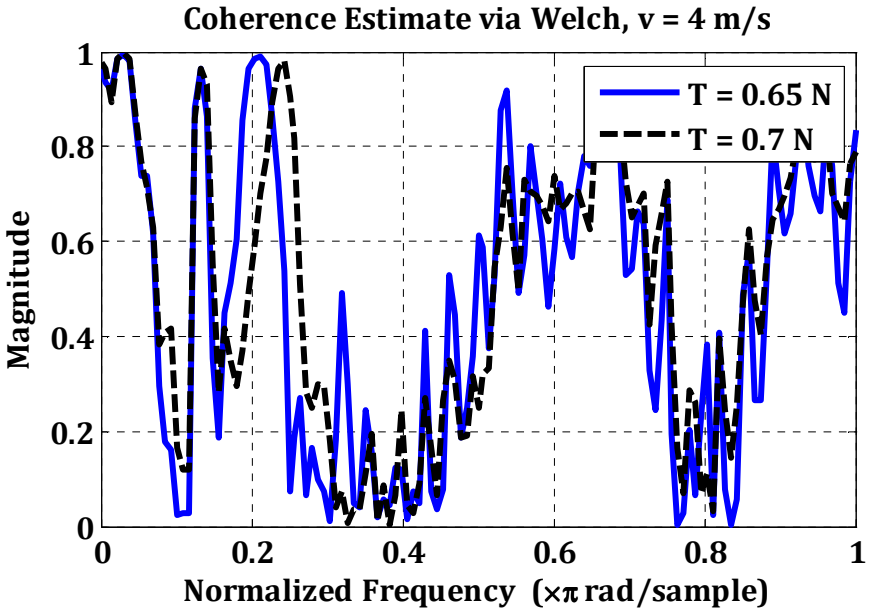

Figure 2.13 Coherence estimate at v = 4 m/s, T = 0.65 N & 0.7 N

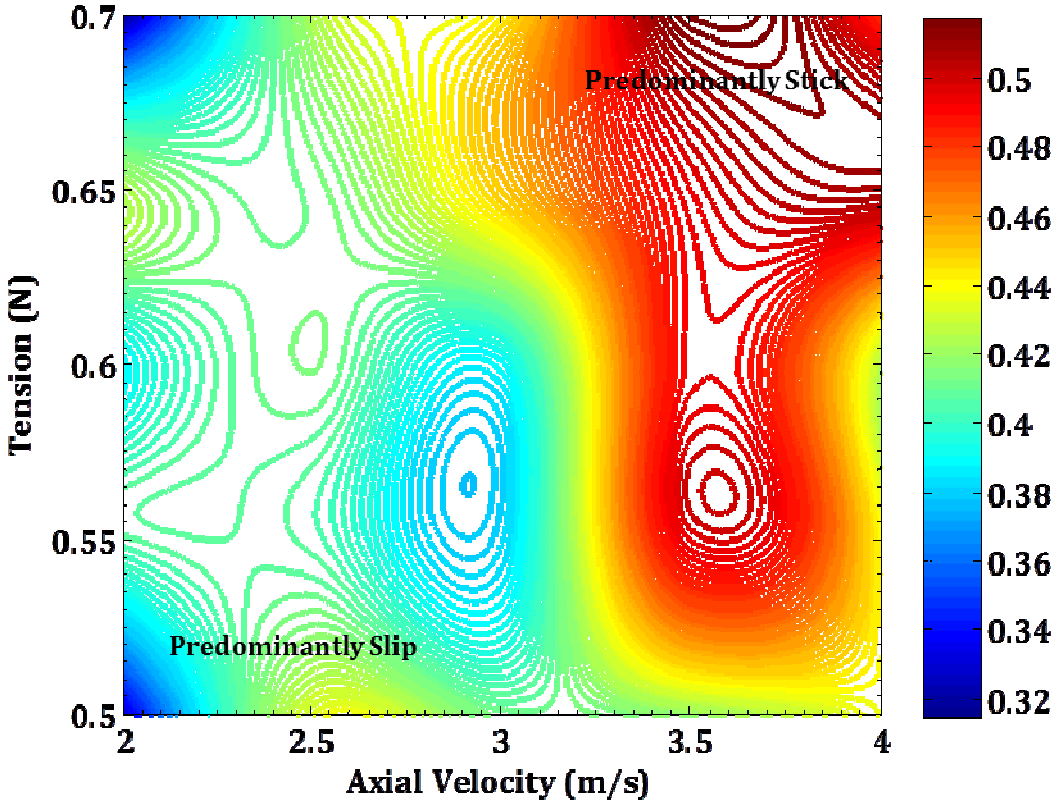

Figure 2.14: Coherence metric to demarcate stick/slip predominance

Appendix

Excitation sources

In each set of measurements, magnetic tape is unwinding from the rotating supply pack at constant speed, thereby causing the pack to lose mass at a constant rate. Pack's axial runout and impacts between pack flanges and tape edge are two major sources of excitation for tape's LTM with others such as impact between tape and stationary guide's flanges, surface friction between tape and guide surfaces and other random sources in the tape-path. The magnitude and frequency of excitation from pack axial runout and flange impacts depend on the rotational speed and instantaneous mass of the pack and, thus, varies with time as the tape unwinds from the pack. The resultant lateral force exerted by the pack on tape is,

$$F_L = \dot{P}_L = \dot{M} * v_L \quad (1)$$

$\dot{P}_L$ is the rate of change of lateral momentum of the pack, $\dot{M}$ is the rate of change of pack mass and v_L is its lateral velocity. If v is the transport speed of tape, ω is the rotational speed and r the radius of the pack then

$$\omega = \frac{v}{r}$$

For lateral motion of the pack, we have, $v_L \propto \omega$ and $v_L \propto v$ (2)

$\dot{M} \propto v$, since rate of mass change is proportional to transport speed. Hence, from (1) & (2),

$$\dot{P}_L \propto v^2$$

In our analysis we have considered finite length samples of 5 seconds from the original non-stationary process of vibration measurement. Keeping the tension constant and varying the axial velocity, we made sure that the samples we compared were from a finite time interval when all external excitation sources producing lateral vibration of the tape (except the surface friction) were approximately equal. We, thus, chose samples which were 5s in length, at times when the rate of change of momentum of the pack with tape traveling at different velocities (2 – 4 m/s) was proportionate, resulting in an approximately constant excitation force.

Cross Power Spectral Density

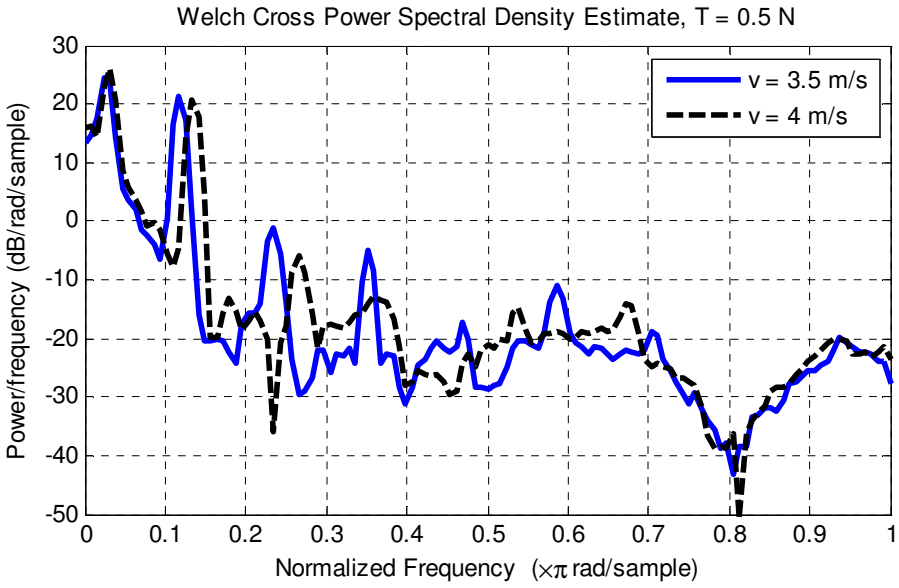

Figure 2.15: Cross power spectral density estimate for T = 0.5 N & v = 3.5 m/s, 4 m/s

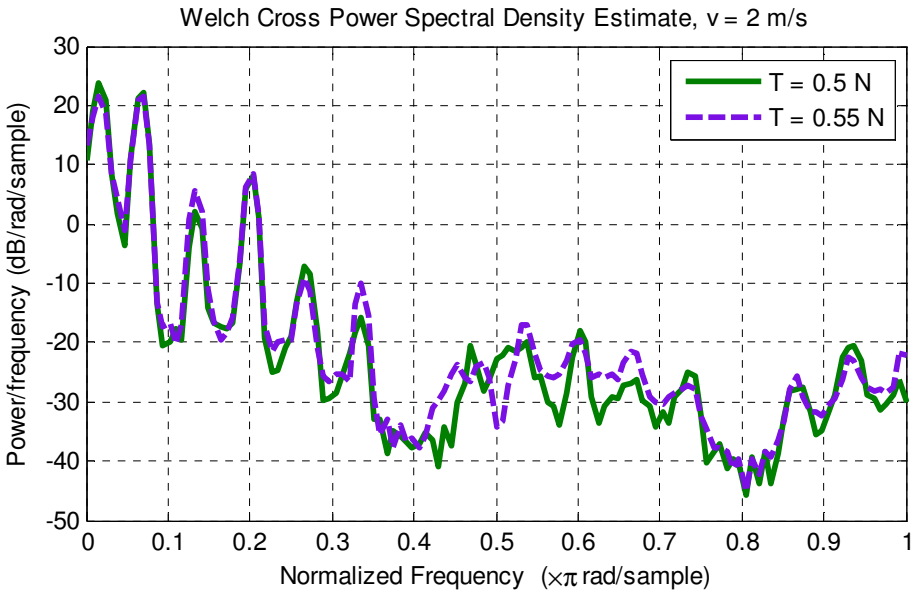

Figure 2.16: Cross power spectral density estimate for T = 0.5 N, 0.55 N & v = 2 m/s

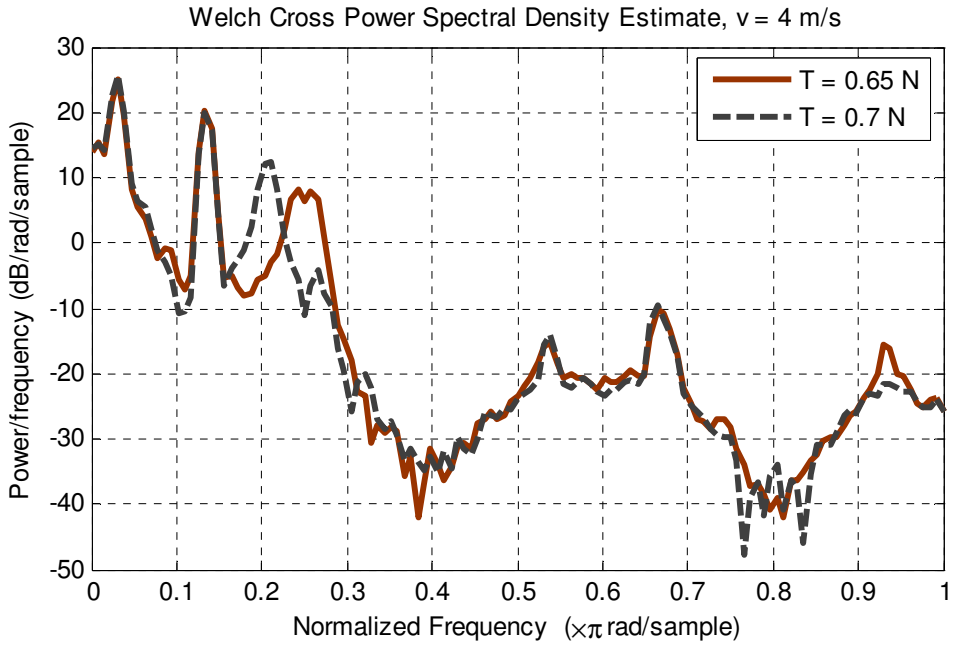

Figure 2.17: Cross power spectral density estimate for T = 0.65 N, 0.7 N & v = 4 m/s

Fig. 2.15, Fig. 2.16 and Fig. 2.17 show the cross power spectral density between upstream and downstream signals across the tape-roller interface for low tension-high velocity, low tension-low velocity and high tension-high velocity cases respectively; estimated using Welch's method. It can be seen that it shows two peaks at the first two harmonics of the tape's lateral vibration where power is transferred across the interface.

Transfer Function

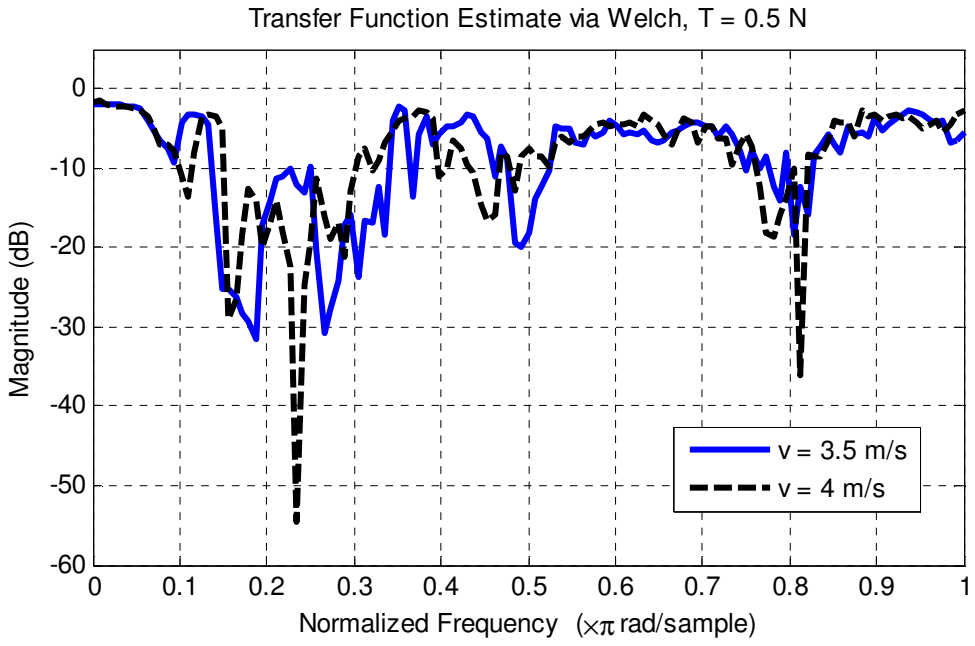

Figure 2.18: Transfer function estimate for T = 0.5 N & v = 3.5 m/s, 4 m/s

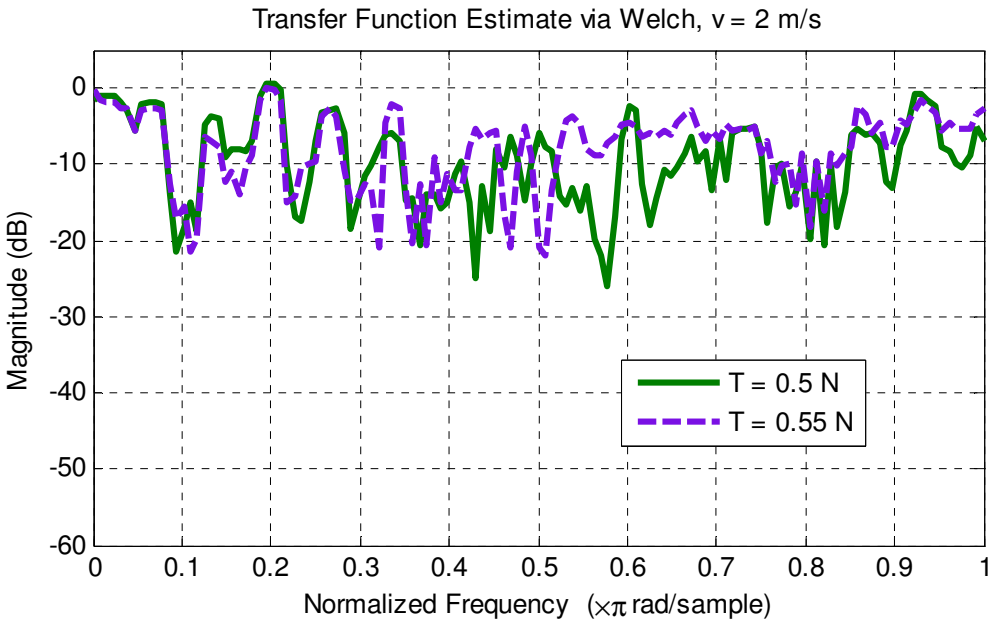

Figure 2.19: Transfer function estimate for T = 0.5 N, 0.55 N & v = 2 m/s

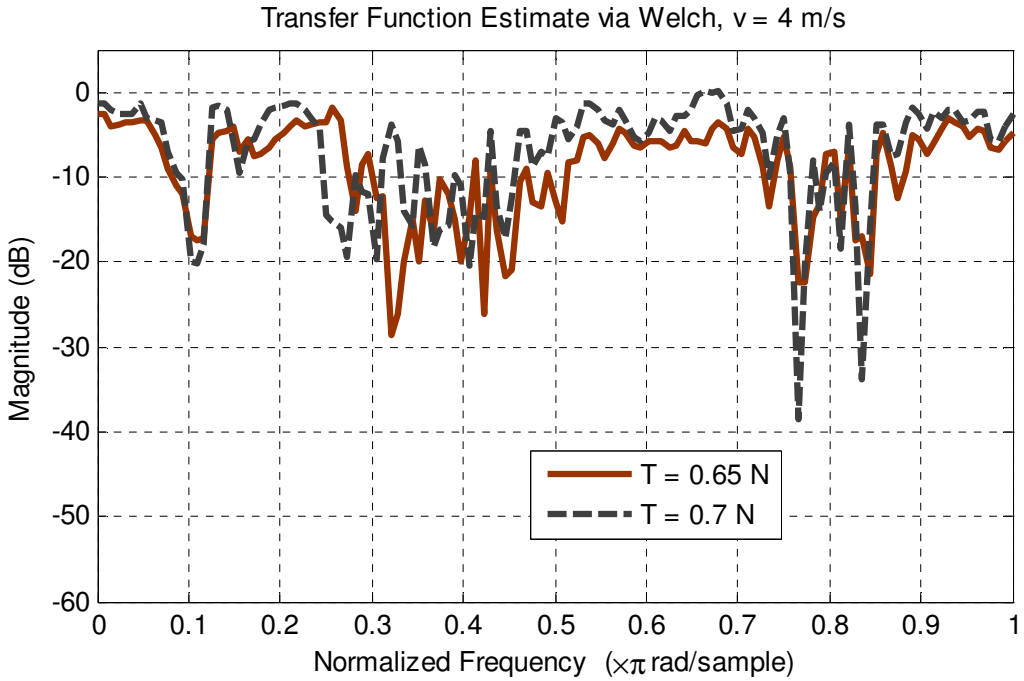

Figure 2.20: Transfer function estimate for T = 0.65 N, 0.7 N & v = 4 m/s

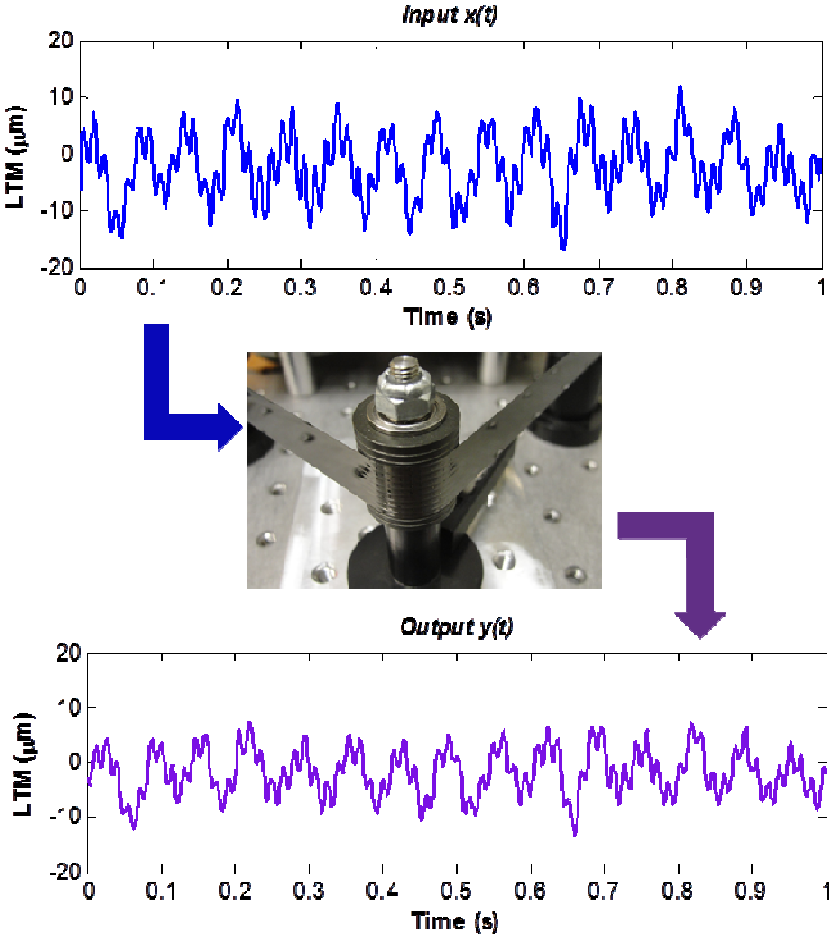

Figure 2.21: Upstream-downstream LTM-relationship across tape-roller interface

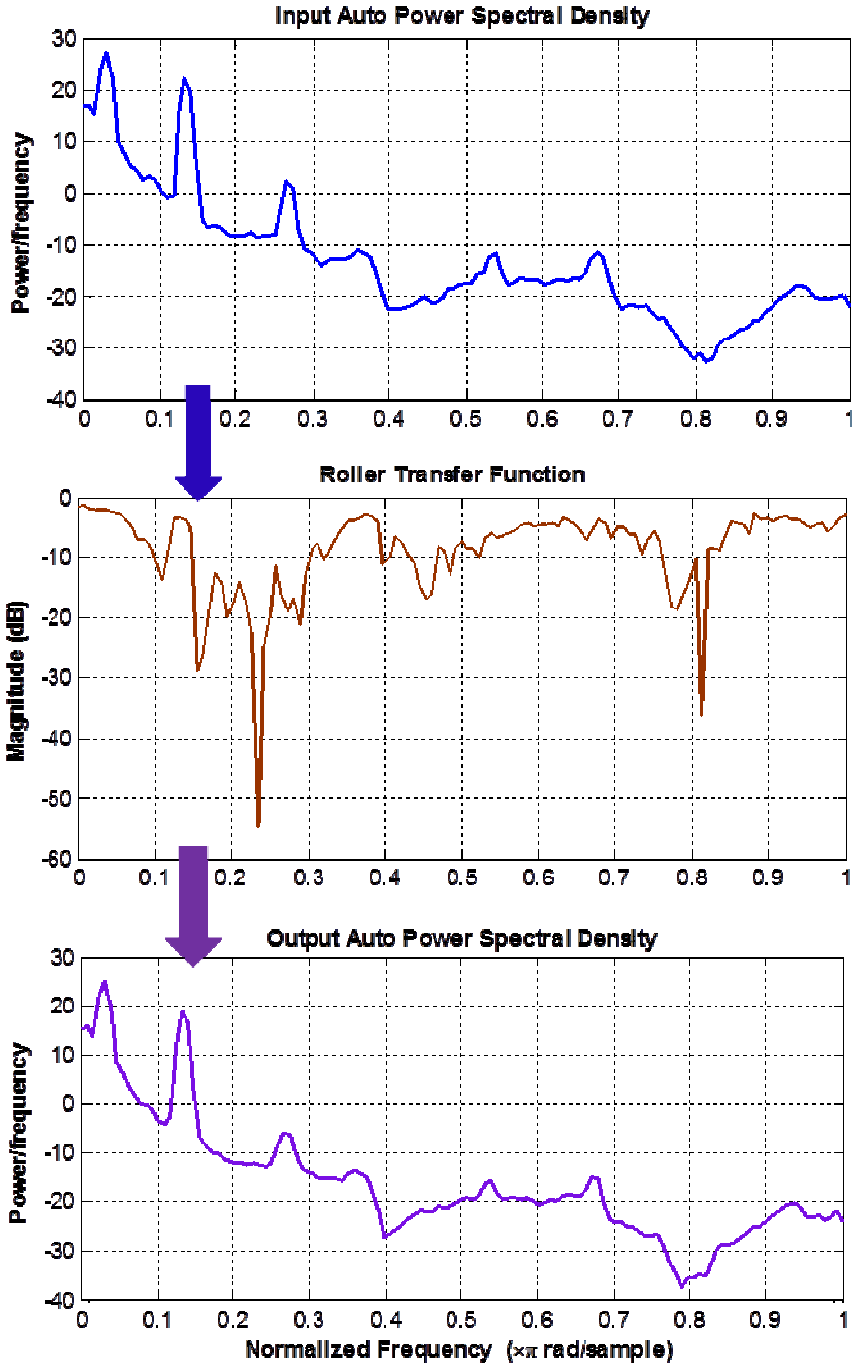

Figure 2.22: Upstream-downstream PSD-relationship across tape-roller interface

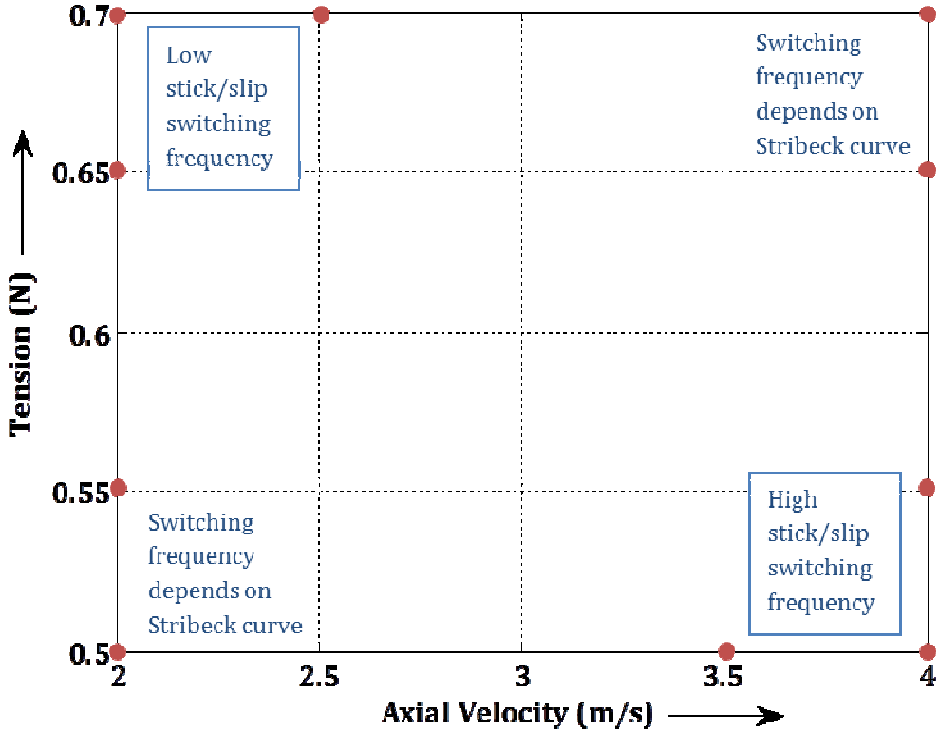

Figure 2.23: Experimental stiffness-velocity phase-space

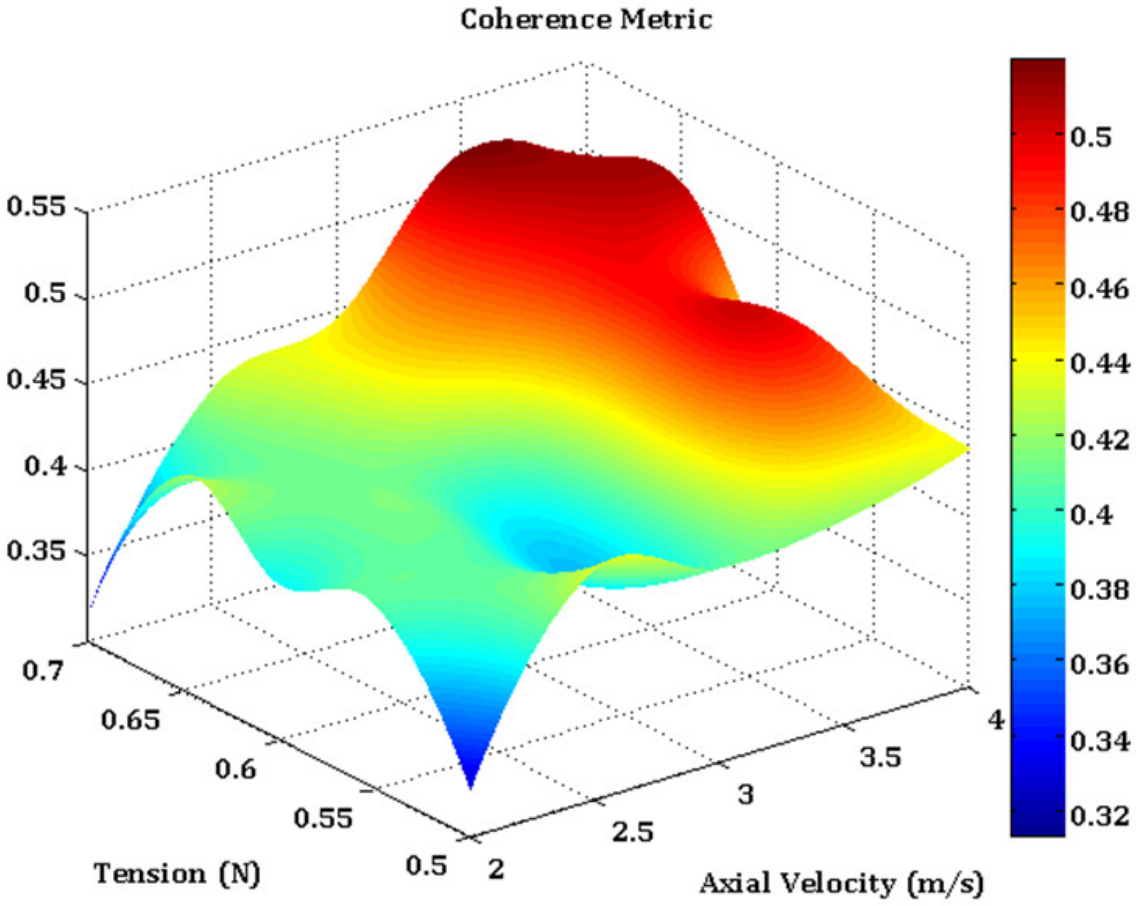

Figure 2.24: 3-D view of normalized area under coherence function plotted over the experimental stiffness-velocity phase-space

Chapter 3

Lateral vibration of axially moving tensioned Euler-Bernoulli beam with stick-slip end condition

S. S. Jape, J.A. Wickert and B. Ganapathysubramanian

Department of Mechanical Engineering, Iowa State University, Ames, IA-50011, U.S.A.

Abstract

Lateral in-plane vibration of tape's narrow edge is a major cause of misalignment between data tracks on tape and position of the read/write head and leads to reduced digital storage capacity in magnetic tape storage devices. One of the methods to attenuate this vibration is using surface friction guides (which include grooved rollers, porous rollers, or roughened rollers) that apply frictional force on the wide tape surface to control its lateral motion throughout the tape-path. It thus becomes necessary to investigate and understand the frictional coupling between tape and roller surface to predict and minimize tape's lateral vibration elsewhere in tape-path. In this article, we have developed a numerical model to study the frictional interaction between a rotating roller surface and the tape that travels over it. Tape is modeled as an axially moving, tensioned, viscoelastic Euler-Bernoulli beam subjected to disturbances arising from supply and take-up pack run-out along with Coulomb friction between the tape and the roller surface. As a result of frictional constraints between

Euler-Bernoulli beam and roller surface, the beam sticks on roller surface if axial force is smaller than frictional force and slips if axial force increases beyond frictional force.

Governing equations of lateral vibration of the beam are discretized through finite element method using Galerkin approximation and cubic Hermite polynomials as elemental basis functions. Considering a periodic stick-slip motion, the axial force is represented by a saw-tooth waveform and the boundary condition at beam-roller interface is modeled to change states from pinned (slip) to fixed (stick) at a constant stick-slip transition frequency. The model is used to numerically quantify the possibility of sticking or slipping between the surfaces in contact, as a function of the beam parameters -- tape axial velocity and tension. Lateral vibration measurements from an experimental setup for a range of axial tension and velocity are used to validate the finite element model.

3.1 Introduction

Axially moving continua, commonly modeled as either second order systems (traveling strings) or fourth order systems (traveling tensioned beams), find application in such areas as high speed magnetic tapes, automotive belt drives, power transmission chains, conveyor belts, band saws, pipes carrying fluids and aerial cable tramways. Processing of paper, plastic film, cloth fabrics and strip steel employs the guiding and transport of webs. Recent applications of axially moving media include flexible robotic manipulators and spacecraft antennas. Previous work on second order systems focuses on natural frequencies and resonance conditions of the system [1] and on effects of axial velocity on wave propagation in the medium [2] , where the forced vibration was formulated as a variational problem. In fourth order systems modeled as traveling Euler Bernoulli beam with axial tension, the effect

of axial velocity and velocity dependent axial tension on the flexural natural frequencies was investigated [3]. Approximate methods to calculate the natural frequencies of these fourth order systems were presented in [4]. The response of second and fourth order system to arbitrary excitations and initial conditions was calculated using modal analysis and Green's function method and the sufficient conditions for stability of a tensioned, axially moving beam were discussed [5]. Stylianou and Tabarrok [6], [7] discretized the equation of motion of axially moving beam and modeled the coupling of axial and transverse motion by finite element method using variable-domain elements. This paper also discussed the use of variable-domain elements for related problems like axially moving beam with a tip mass, link moving through a prismatic joint and pipes conveying liquids.

Lateral vibration of such media, especially in the case of magnetic tape libraries, causes misalignment of the data tracks and the read/write heads, and needs to be investigated and minimized. Lateral vibration of the magnetic tape modeled as an axially moving Euler Bernoulli beam arises from excitation sources such as pack and guide run-out and tilt, tape and guide flange impacts and imperfections or weave in the tape edge. In the application of axially moving continua in tape transport technology, Wickert [8] investigated the self-excited longitudinal vibration of an axially moving tape caused by nonlinear frictional contact with a recording heard or a guide, focusing on the effect of transport speed and location of contact point on the amplitude of response. The contribution of the convective terms in the equation of motion increases with transport speed and vicinity to the frictional point of contact and are crucial from a modeling standpoint. Kartik and Wickert [9] studied the free and forced lateral vibration of axially moving tape modeled as a fourth order system

in the presence of distributed friction guiding with sub-ambient pressure features. Parametric studies with respect to the pressure coefficient, transport speed, and guide placement established their effects on the dissipation of the lateral vibration amplitude. Brake and Wickert [10] developed a frictional model for the vibration transmission from a laterally moving surface to a traveling tensioned beam, and examined the design parameters that affect the extent of vibration transmission.

Despite these advancements, there still is a need for developing analytical and numerical models to predict the effect of stick-slip friction between tape and surface guides on the magnitude and frequency of lateral vibration of tape. The objective of this paper is to investigate the frictional coupling between a tape modeled as axially moving tensioned Euler Bernoulli beam and a rotating roller and the effects of this coupling on the lateral vibration of the beam. Three modes are possible for the nature of the frictional contact: (1) circumferential stick, (2) circumferential slip, (3) non-linear circumferential stick-slip. Spatial derivatives in the equation of motion of Euler-Bernoulli beam are discretized through finite element method using Galerkin approximation whereas the temporal derivatives are approximated using backward Euler finite difference method. Boundary conditions are specified according to the nature of frictional interaction at the boundaries of the tape. Experimental vibration measurements are used to validate the numerical model. Using this numerical model, the occurrence of stick or slip or both and its effect on the lateral vibration is studied for parameters of the system, such as, axial tension and velocity and coefficient of friction of the roller surface and beam span length.

3.2 Stick-slip friction model

Stick-slip motion friction arises in sliding systems because of the difference between static and kinetic friction coefficients. The system shown in Fig. 3.1 contains a sliding block of mass M and elastic properties represented by spring constant k, sliding on a rough surface. It undergoes steady sliding, if spring force equals the kinetic friction force, but exhibits periodic or chaotic stick-slip motion if the spring force is not equal to kinetic friction force. The spring force F has a profile of a saw-tooth waveform in time with respect to the kinetic friction force F_b as shown in Fig. 3.2.

In roller-tape frictional interface, the tape slides over roller surface with a constant velocity v, with axial tension T in tape acting as a restoring spring force as shown in Fig. 3.3. The tape is modeled according to the Kelvin-Voigt model for viscoelastic materials, with a purely elastic spring and a purely viscous damper in parallel. As a result of the viscoelastic nature, for certain values of coefficient of friction between the tape and roller surface and axial tension (spring force) the system exhibits stick-slip frictional behavior, wherein the tape periodically sticks and slip on the roller surface.

In this numerical analysis, the tape is modeled as an axially travelling linear Euler-Bernoulli beam and stick-slip friction is modeled in the form of a periodically changing boundary condition at the beam-roller interface end [17]. We refer to our discussion in section 2.6.2 model the boundary conditions for a pure stick and a pure slip friction phase between the Euler-Bernoulli beam and the roller surface. For a pure stick case, displacement and slope of the tape modeled as beam is frozen at the point of contact between beam and roller surface. Assuming that both displacement and slope of the point on beam in contact with roller are

restricted, stick phase of the frictional coupling is modeled as a fixed support. On the other hand, pure slip friction corresponds to a state where displacement and slope of a particle damped across the tape-roller interface. Thus, we assume that at slip, the displacement and curvature of the point of beam in contact with roller are restricted. Slip phase is thus modeled as a simple support at the beam's end. Fig. 3.5 represents these two phases of the beam-roller coupling. The boundary switches between a fixed support and simple support with a frequency that is equal to the stick to slip transition frequency of the beam-roller interface. Fig. 3.6 show a beam-roller interface switching between stick (fixed support) and slip (simple support) with a frequency of 10 Hz (which indicates 10 transitions of equal duration between fixed and simple support in 1s).

3.3 Numerical model of magnetic tape

In the numerical analysis, we consider a portion of the tape-path that consists of an axially traveling magnetic tape supported between a stationary guide and a roller. The end corresponding to the stationary guide restricts tape's motion via its flanges and is represented by a simple support. At the roller end, surface friction controls the lateral motion of tape and is represented by the time-varying boundary as shown in Fig. 3.5. This simple portion of the tape-path is depicted in Fig. 3.7 where the span-length is 10 cm (following the experimental span-length we used in previous chapter). The magnetic tape is modeled as an axially traveling tensioned linear Euler-Bernoulli beam and its governing equation in the span is discretized using finite element and finite difference methods with a grid-size of 100.

3.3.1 Governing equation

The magnetic tape is modeled as an axially moving Euler Bernoulli beam with axial tension with governing equation [4],

$$EIu_{,xxxx} + \rho A(u_{,tt} + 2vu_{,xt} + v^2 u_{,xx}) - Tw_{,xx} = f(x,t) \qquad \text{---------- (A)}$$

Where u = Lateral displacement of beam, EI= Flexural stiffness of the beam,

ρA = Inertia, T = Axial Tension, f = Lateral forces on beam

We further nondimensionalized this equation as follows [5];

Introducing, $c_1 = \sqrt{\dfrac{EI}{\rho AL^2}}$ ---------- Flexural wave speed

$$c_0 = \sqrt{\frac{T}{\rho A}} \qquad \text{---------- Transverse wave speed}$$

Nondimensionalizing the variables and using new parameters: $x' = \dfrac{x}{L}, u' = \dfrac{u}{L}, t' = \left(\dfrac{c_1}{L}\right)t$

$$v = \frac{c}{c_1} = c\sqrt{\frac{\rho AL^2}{EI}} \qquad \text{---------- Dimensionless transport speed}$$

$$T_o^2 = \frac{T}{\rho c_1^2 A} = \frac{TL^2}{EI} \qquad \text{---------- Dimensionless axial tension}$$

Representing the notation u' with u, the equation of motion in its nondimensionalized form:

$$u_{,tt} + 2vu_{,xt} + v^2 u_{,xx} - T_o^2 u_{,xx} + u_{,xxxx} = 0 \qquad \text{---------- (B)}$$

3.3.2 Finite element analysis

Finite element method is used to discretize and solve spatial derivatives and finite difference method to solve temporal derivatives in the beam's governing equation. Finite element library FEMLib is used for both these methods.

(1) Temporal derivatives

Using Euler backward difference scheme for temporal derivatives,

$$u_{,tt} = \left(\frac{u^{i+1} - 2u^i + u^{i-1}}{(\Delta t)^2} \right) \qquad u_{,t=} \left(\frac{u^{i+1} - u^i}{\Delta t} \right)$$

The equation becomes;

$$u_{,xxxx}^{i+1} + (v^2 - T_o^2) u_{,xx}^{i+1} + \left(\frac{2v}{\Delta t} \right) u_{,x}^{i+1} + \left(\frac{1}{(\Delta t)^2} \right) u^{i+1} = \left(\frac{2v}{\Delta t} \right) u_{,x}^{i} + \left(\frac{1}{(\Delta t)^2} \right) \left(2u^i - u^{i-1} \right)$$

Constructing weak form of the equation with weight function *w;*

$$\int_0^L u_{,xxxx} w dx + (v^2 - T_o^2) \int_0^L u_{,xx} w dx + \left(\frac{2v}{\Delta t} \right) \int_0^L u_{,x} w dx + \left(\frac{1}{(\Delta t)^2} \right) \int_0^L uw dx =$$

$$\left(\frac{2v}{\Delta t} \right) \int_0^L u_{,x}^i w dx + \left(\frac{1}{(\Delta t)^2} \right) \int_0^L \left(2u^i - u^{i-1} \right) w dx$$

Evaluating integrals and considering zero values for the boundary integrals,

$$\int_0^L u_{,xx} w_{,xx} dx + (T_o^2 - v^2)\int_0^L u_{,x} w_{,x} dx + \left(\frac{2v}{\Delta t}\right)\int_0^L u_{,x} w dx + \left(\frac{1}{(\Delta t)^2}\right)\int_0^L uw dx \quad =$$

$$\left(\frac{2v}{\Delta t}\right)\int_0^L u^i_{,x} w dx + \left(\frac{1}{(\Delta t)^2}\right)\int_0^L \left(2u^i - u^{i-1}\right) w dx$$

---------- (C)

(2)Spatial derivatives

We use finite element method with Galerkin formulation for the domain $0 \le x \le L$ .Here $u_h^e(x) = [N]\{u\}$, $[N]$ being the elemental shape functions and $\{u\}$ being the nodal degrees of freedom of the finite element, is used for the spatial derivatives in the equation. This is a 4th order partial differential equation and consists of 2 degrees of freedom viz. displacement (u) and slope ($u_{,x}$) of the beam element. Thus, Hermite cubic polynomials, as shown in Fig. 3.8, must be used to represent $u_h^e(x)$

$$u_h^e(\xi) = a_0^e + a_1^e \xi + a_2^e \xi^2 + a_3^e \xi^3 \qquad u_h^e(\xi) = \begin{bmatrix} N_1^e(\xi) & N_2^e(\xi) & N_3^e(\xi) & N_4^e(\xi) \end{bmatrix} \begin{Bmatrix} u_1 \\ u_1' \\ u_2 \\ u_2' \end{Bmatrix}$$

$$N_1^e(\xi) = \frac{1}{4}(1-\xi)(1-\xi)(2+\xi) \qquad N^e_{1,\xi\xi}(\xi) = \frac{3}{2}\xi$$

$$N_2^e(\xi) = \frac{h}{8}(1-\xi)(1-\xi)(1+\xi) \qquad N^e_{2,\xi\xi}(\xi) = -\frac{h}{4}(1-3\xi)$$

$$N_3^e(\xi) = \frac{1}{4}(1+\xi)(1+\xi)(2-\xi) \qquad N^e_{3,\xi\xi}(\xi) = -\frac{3}{2}\xi$$

$$N_4^e(\xi) = -\frac{h}{8}(1-\xi)(1+\xi)(1+\xi) \qquad N^e_{4,\xi\xi}(\xi) = \frac{h}{4}(1+3\xi)$$

And,

Using the Galerkin formulation, weight function $w(x) = \begin{bmatrix} N_1^e(\xi) \\ N_2^e(\xi) \\ N_3^e(\xi) \\ N_4^e(\xi) \end{bmatrix}$

In problems pertaining to transverse bending or beams, a class of finite elements called as *sub-parametric* finite elements is used [19]; wherein we use linear interpolation functions to represent geometry of the finite elements and cubic Hermite interpolation functions to represent the displacement. These functions are then used to explicitly calculate derivatives of shape functions in the element stiffness and matrices.

Thus, $$x = \frac{x_1 + x_2}{2} + \left(\frac{x_2 - x_1}{2} \right) \xi = x_c + \frac{h}{2} \xi$$

$$N_{a,x} = N_{a,\xi} \xi_{,x} = \frac{2}{h} N_{a,\xi} \qquad N_{a,xx} = N_{a,\xi\xi} (\xi_{,xx})^2 = \frac{4}{h^2} N_{a,\xi\xi}$$

And equation (C) can be written as, $\left([K] + [C_1] + [C_2] + [M] \right) \{u\} = [F]$

Where,

Stiffness matrix due to bending:

$$[K] = \int_0^L \begin{bmatrix} N_{1,xx}^e(x) & N_{2,xx}^e(x) & N_{3,xx}^e(x) & N_{4,xx}^e(x) \end{bmatrix} * \begin{bmatrix} N_{1,xx}^e(x) \\ N_{2,xx}^e(x) \\ N_{3,xx}^e(x) \\ N_{4,xx}^e(x) \end{bmatrix} * \begin{Bmatrix} u_1 \\ u_1' \\ u_2 \\ u_2' \end{Bmatrix} dx$$

Stiffness matrix due to axial tension:

$$[C_1] = \left(T_o^2 - v^2\right)\int_0^L \left[N^e_{1,x}(x) \quad N^e_{2,x}(x) \quad N^e_{3,x}(x) \quad N^e_{4,x}(x)\right] * \begin{bmatrix} N^e_{1,x}(x) \\ N^e_{2,x}(x) \\ N^e_{3,x}(x) \\ N^e_{4,x}(x) \end{bmatrix} * \begin{Bmatrix} u_1 \\ u_1' \\ u_2 \\ u_2' \end{Bmatrix} dx$$

Gyroscopic damping matrix:

$$[C_2] = \left(\frac{2v}{\Delta t}\right)\int_0^L \left[N^e_{1,x}(x) \quad N^e_{2,x}(x) \quad N^e_{3,x}(x) \quad N^e_{4,x}(x)\right] * \begin{bmatrix} N^e_1(x) \\ N^e_2(x) \\ N^e_3(x) \\ N^e_4(x) \end{bmatrix} * \begin{Bmatrix} u_1 \\ u_1' \\ u_2 \\ u_2' \end{Bmatrix} dx$$

Mass matrix:

$$[M] = \frac{1}{(\Delta t)^2}\int_0^L \left[N^e_1(x) \quad N^e_2(x) \quad N^e_3(x) \quad N^e_4(x)\right] * \begin{bmatrix} N^e_1(x) \\ N^e_2(x) \\ N^e_3(x) \\ N^e_4(x) \end{bmatrix} * \begin{Bmatrix} u_1 \\ u_1' \\ u_2 \\ u_2' \end{Bmatrix} dx$$

Forcing matrix:

$$[F] = \int_0^L \begin{bmatrix} \frac{1}{(\Delta t)^2}(2u^i - u^{i-1})^1 * N_1^e(x) \\ \frac{1}{(\Delta t)^2}(2u_{,x}^i - u_{,x}^{i-1})^1 * N_2^e(x) \\ \frac{1}{(\Delta t)^2}(2u^i - u^{i-1})^2 * N_3^e(x) \\ \frac{1}{(\Delta t)^2}(2u_{,x}^i - u_{,x}^{i-1})^2 * N_4^e(x) \end{bmatrix} dx + \int_0^L \begin{bmatrix} \frac{2v}{\Delta t}(u_{,x}^i)^1 * N_1^e(x) \\ \frac{2v}{\Delta t}(u_{,xx}^i)^1 * N_2^e(x) \\ \frac{2v}{\Delta t}(u_{,x}^i)^2] * N_3^e(x) \\ \frac{2v}{\Delta t}(u_{,xx}^i)^2] * N_4^e(x) \end{bmatrix} dx$$

3.3.3 Numerical Integration

For integration of stiffness and mass matrices, the highest order of polynomial we encounter is order six in the mass matrix. And in Gaussian quadrature, an N^{th} order quadrature can integrate a polynomial of order 2N-1 exactly. So we use the fourth order Gaussian quadrature scheme.

3.4 Validation of numerical model using analytical solution

Using the finite element framework FEMLib, we solve the nondimensionalized partial differential equation of Euler-Bernoulli beam's lateral vibration for a simple case where the beam (magnetic tape) is transported at constant axial tension and axial velocity between a stationary guide and a roller. In the beam's equation, sub-isoparametric Hermite cubic polynomials are used for spatial discretization and Euler's backward difference method for temporal discretization. To test the validity of numerical model, we compared it with analytical solution of the beam's original governing equation.

$$EIu_{,xxxx} + \rho A(u_{,tt} + 2vu_{,xt} + v^2 u_{,xx}) - Tw_{,xx} = f(x,t)$$

Boundary conditions: $U(0,t) = U_{,xx}(0,t) = 0$ $U(L,t) = U_{,xx}(L,t) = 0$

Where, analytical solution for lateral displacement of beam:

$$u(x,t) = f_0 \sin\left(\frac{\pi x}{L}\right)\sin\left(\omega t\right)$$

And the appropriate forcing term:

$$f(x,t) = A f_0 \sin\left(\frac{\pi x}{L}\right)\sin(\omega t) \; + \; B f_0 \cos\left(\frac{\pi x}{L}\right)\cos(\omega t)$$

$$f_{,x}(x,t) \; = \; A f_0 \left(\frac{\pi}{L}\right)\cos\left(\frac{\pi x}{L}\right) \; \sin(\omega t) \; - \; B f_0 \left(\frac{\pi}{L}\right)\sin\left(\frac{\pi x}{L}\right)\cos(\omega t)$$

With, $A = EI\left(\frac{\pi}{L}\right)^4 - m\omega^2 - mv^2\left(\frac{\pi}{L}\right)^2 + To\left(\frac{\pi}{L}\right)^2$ $\qquad$ $B = 2mv\omega\left(\frac{\pi}{L}\right)$

$EI = 0.0143 \; Nm^2$ = measured value of bending stiffness of the tape.

$m = 12.945 \; kg/m$ = tape's mass per unit length.

Axial tension $To = 6 \; N$ and axial velocity $v = 30 \; m/s$

$f_0 = 0.082 \; N \; \& \; \omega = 50.37 \; Hz$

(The approximate magnitude of force exerted by the supply pack in experiment is $f_0 = 0.0082N$. Since using this value gives a zero output, force is multiplied by 10 and $f_0 = 0.082N$ is used.) Convergence of numerical solution for forced vibration of beam with grid-size = 100, and time-step $dt = 0.01$ s with the analytical solution in time and frequency domain is shown in Fig. 3.9.

3.5 Results

From the stick-slip friction model in Section 3.2, pinned boundary condition in the finite element model represents the beam-stationary guide interface and a time-varying boundary condition that switches between fixed and pinned support represents the beam-roller interface. Using a grid-size of 100, numerical value of tape's lateral displacement at a point 1 cm upstream of the tape-roller interface (91st finite element; considering a span as shown in Fig. 3.7) is calculated at stick-slip transition frequencies of 80 - 160 Hz and a constant axial tension and velocity. We chose these particular values of transition frequency since they give an approximate match between the numerical and experimental FFT of lateral vibration. The numerical lateral vibration is calculated for axial tension values of 0.5 N – 0.7 N at 0.05 N intervals and axial velocity values 2 m/s – 4m/s at 0.5 m/s intervals. We examine the numerical lateral vibration using following two methodologies.

3.5.1 Constant axial tension

Fig. 3.10 shows the response and frequency content of vibration of the beam for a constant axial tension 0.6N and varying axial speeds from 2m/s to 4m/s, mimicking the parameters in our experiment. We used stick/slip switch frequencies of 80, 100, 120, 140, 160 Hz respectively for the 5 set of parameters, to match the frequency content in the experimental output. In the numerical model, increasing the stick-slip transition frequency at constant axial tension and increasing axial velocity ensures that the frequency content of the lateral vibration increases, as observed in FFT of experimental lateral vibration. *It is thus observed that at constant axial tension, an increase in axial velocity causes increase in the stick/slip switching rate thereby shifting the frequency spectrum towards higher frequency region.*

3.5.2 Constant axial velocity

Fig. 3.11 shows the response and frequency content of vibration of the beam for a constant axial velocity 4m/s and varying axial tension from 0.5 N to 0.7. We used stick/slip switch frequency of 160 Hz to match the frequency content in the experimental output. Following the experiments, frequency content of lateral vibration remains unchanged at constant velocity and varying tension. This phenomenon is replicated by keeping stick-slip transition frequency constant at 160 Hz. *Thus, at constant axial velocity, an increase in axial tension has no observable effect on the stick/slip switching frequency; which in turn has no effect on the frequency spectrum of lateral vibration.*

3.6 Conclusion

The numerical model developed in this chapter is capable of predicting the lateral displacement of an axially moving linearly elastic Euler-Bernoulli beam with axial tension. We have used Galerkin approximation method to discretize the spatial derivatives and Euler's backwards difference method to discretize the temporal derivatives in the equation of lateral vibration of the beam. With a few modifications in the equation, the model can also be used to calculate lateral displacement of a static beam, a beam without axial tension or transport velocity and a tensioned beam without axial velocity. We have also introduced a parameter viz. frequency of transition between stick and slip friction at the tape-roller interface. This frequency, along with tape's axial tension and axial velocity are used to study the lateral displacement of the traveling tensioned beam.

The main conclusions of this work are:

1. The numerical model is capable of predicting tape's lateral displacement for a beam length around ~ 10 cm and time-steps 0.01 s and 0.001 s. Physical properties of tape's material are calculated from experiments and are used in the numerics. However, some of the quantities need to be magnified to get a reasonable output (for example, the tape's bending stiffness).
2. At constant axial tension, with increasing axial velocity, the stick-slip transition frequency needs to be proportionately increased in order to match the frequency content in experimental lateral vibration.
3. At constant velocity, with increasing axial tension, there is no observable change in the lateral vibration's frequency content. Hence, stick-slip transition frequency remains constant at constant velocity.

3.7 Future Work

The numerical model is in the preliminary stage and needs to be developed to be able to calculate lateral vibration for beams of arbitrary length for arbitrarily small time-steps. We plan to apply Newmark-beta numerical integration method to solve the time derivatives in beam's governing equation, since its better accuracy and stability than Euler's method for structural vibration problems. We also plan to improve the stick-slip friction model by introducing varying time-periods of stick and slip friction, with the system switching between stick and slip and staying in both phases for unequal times.

References

[1] F.R. Archibald, A.G. Emslie, The vibration of a string having a uniform motion along its length, ASME Journal of Applied Mechanics 25 (1958) 347-348

[2] R.D. Swope, W.F. Ames, Vibrations of a moving threadline, Journal of Franklin Institute 275 (1963) 36-55

[3] C.D. Mote Jr., A Study of band saw vibrations, Journal of Franklin Institute 279 (1965) 430-444

[4] C.D. Mote Jr., S. Naguleswaran, Theoretical and experimental band saw vibrations, Transactions of the ASME 88 (1966) 151-156.

[5] J. A. Wickert, C. D. Mote, Jr., Classical vibration analysis of axially-moving continua, ASME Journal of Applied Mechanics 57 (1990) 738-744.

[6] M. Stylianou, B. Tabarrok, Finite element analysis of an axially moving beam, Part I: Time integration, Journal of Sound and Vibration 178 (1994) 433-453

[7] M. Stylianou, B. Tabarrok, Finite element analysis of an axially moving beam, Part II: Stability analysis, Journal of Sound and Vibration 178 (1994) 455-481

[8] J.A. Wickert, Analysis of self-excited longitudinal vibration of a moving tape, Journal of Sound and Vibration 160 (1993) 455-463

[9] V. Kartik, J.A. Wickert, “Surface Friction Guiding for Reduced High Frequency Lateral Vibration of Moving Media,” ASME Journal of Vibration and Acoustics, 129 (2007) 371-379

[10] M.R. Brake, J.A. Wickert, Frictional Vibration Transmission from a Laterally Moving Surface to a Traveling Beam, Journal of Sound and Vibration, 310 (2008) 663-675

[11] F. Kozin, R.M. Milstead, The stability of a moving elastic strip subjected to random parametric excitation, Journal of Applied Mechanics, 46 (1979) 404-410

[12] M. Moustafa, F.K. Salman, Dynamic properties of a moving thread line, Journal of Engineering for Industry 98 (1976) 868-875

[13] V. Kartik, J.A. Wickert, Vibration and guiding of moving media with edge weave imperfections, Journal of Sound and Vibration 291 (2006) 419-436

[14] M.R. Brake, J.A. Wickert, Optimizing vibration isolation flex circuits in hard disk drives, Journal of Vibration and Acoustics, 127 (2005) 165-172

[15] G.E. Young, J.J. Shelton, C. Kardamilas, Modeling and control of multiple web spans using state estimation, Journal of Dynamic Systems, Measurement, and Control 111 (1989) 505-510

[16] Richard C. Benson, Lateral dynamics of a moving web with geometrical imperfection, Journal of Dynamic Systems, Measurement, and Control 124 (2002) 25-34

[17] R.N. Miles and S.P. Bigelow, Random vibration of a beam with a stick-slip end condition, Journal of Sound and Vibration 169 (1994) 445-457

[18] J.A. Wickert, C.D. mote Jr., On the energetics of axially moving continua, Journal of Acoustical Society of America 85 (1989) 1365-1368

[19] Ahmed A. Shabana, Computational continuum mechanics, Cambridge University Press, 286-314

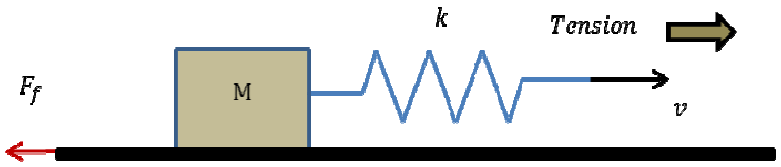

Figure 3.1: Spring-mass system to demonstrate stick-slip

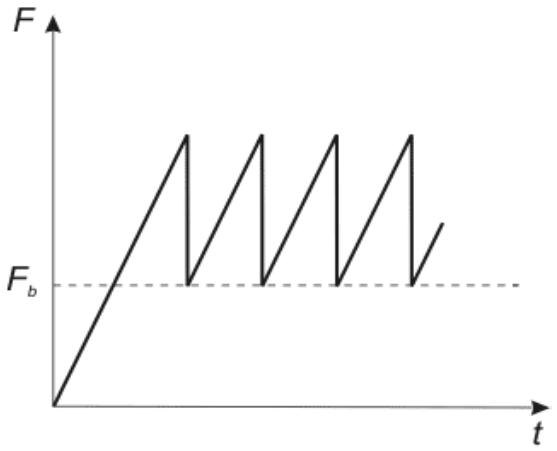

Figure 3.2: Sawtooth profile of spring force

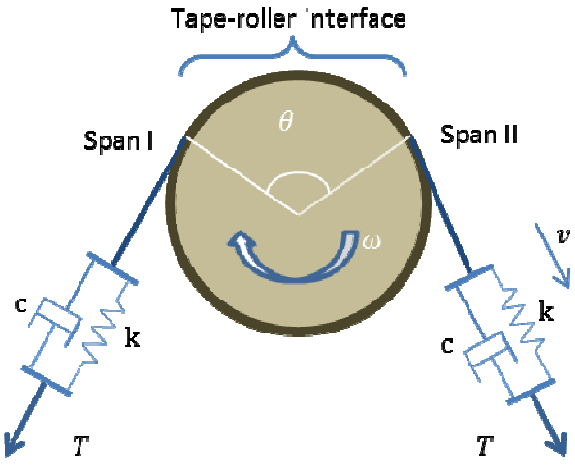

Figure 3.3: Tape-roller interface depicting upstream and downstream spans and Kelvin-Voight model of viscoelasticity for magnetic tape

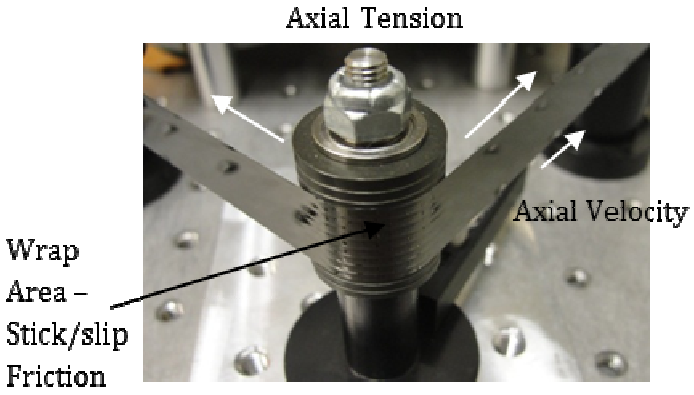

Figure 3.4: Tape-roller interface depicting the wrap area, axial tension and axial velocity of magnetic tape

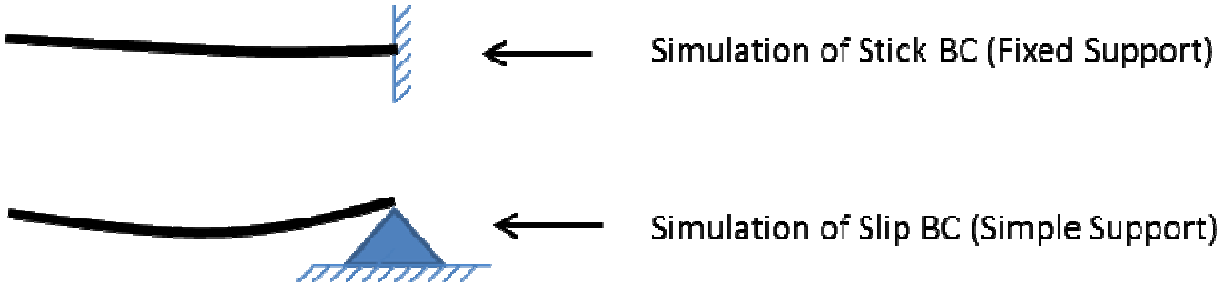

Figure 3.5: Numerical model for stick-slip friction showing the boundary condition switching between fixed and simple support

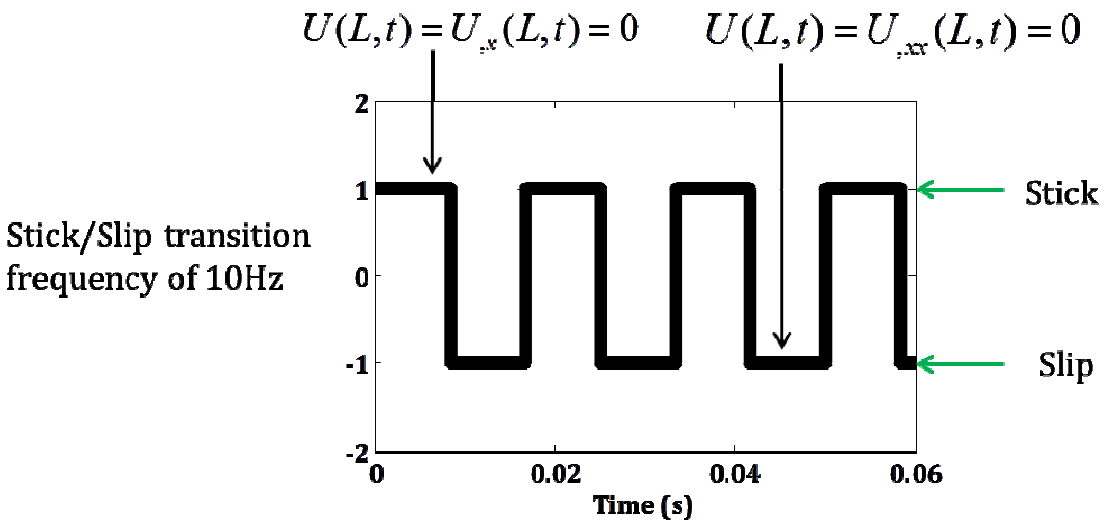

Figure 3.6: Switching between fixed support (stick) and simple support (slip) with a frequency of 10 Hz

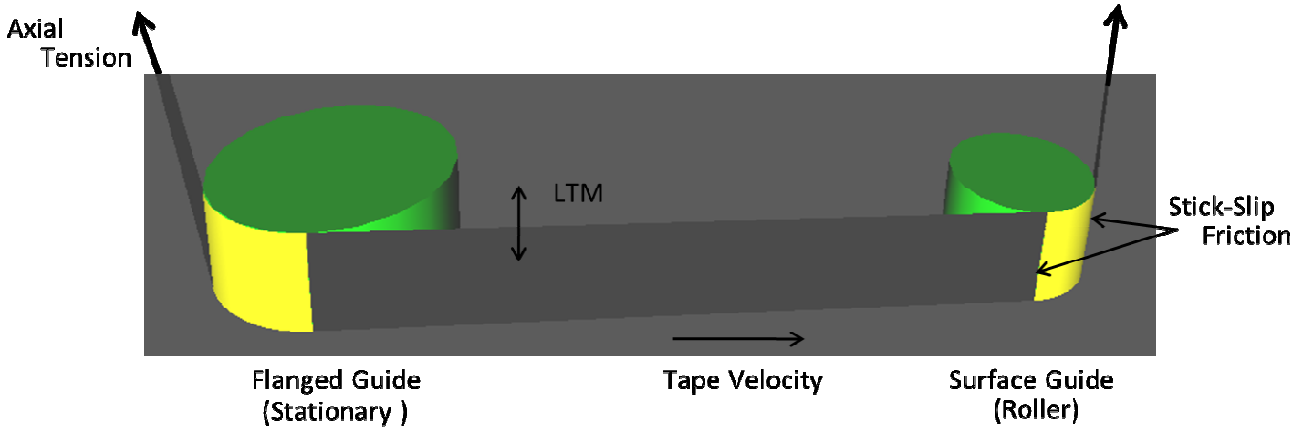

Figure 3.7: Simple tape-path model for finite element analysis showing stationary flanged guide, traveling tensioned tape and surface guide (roller)

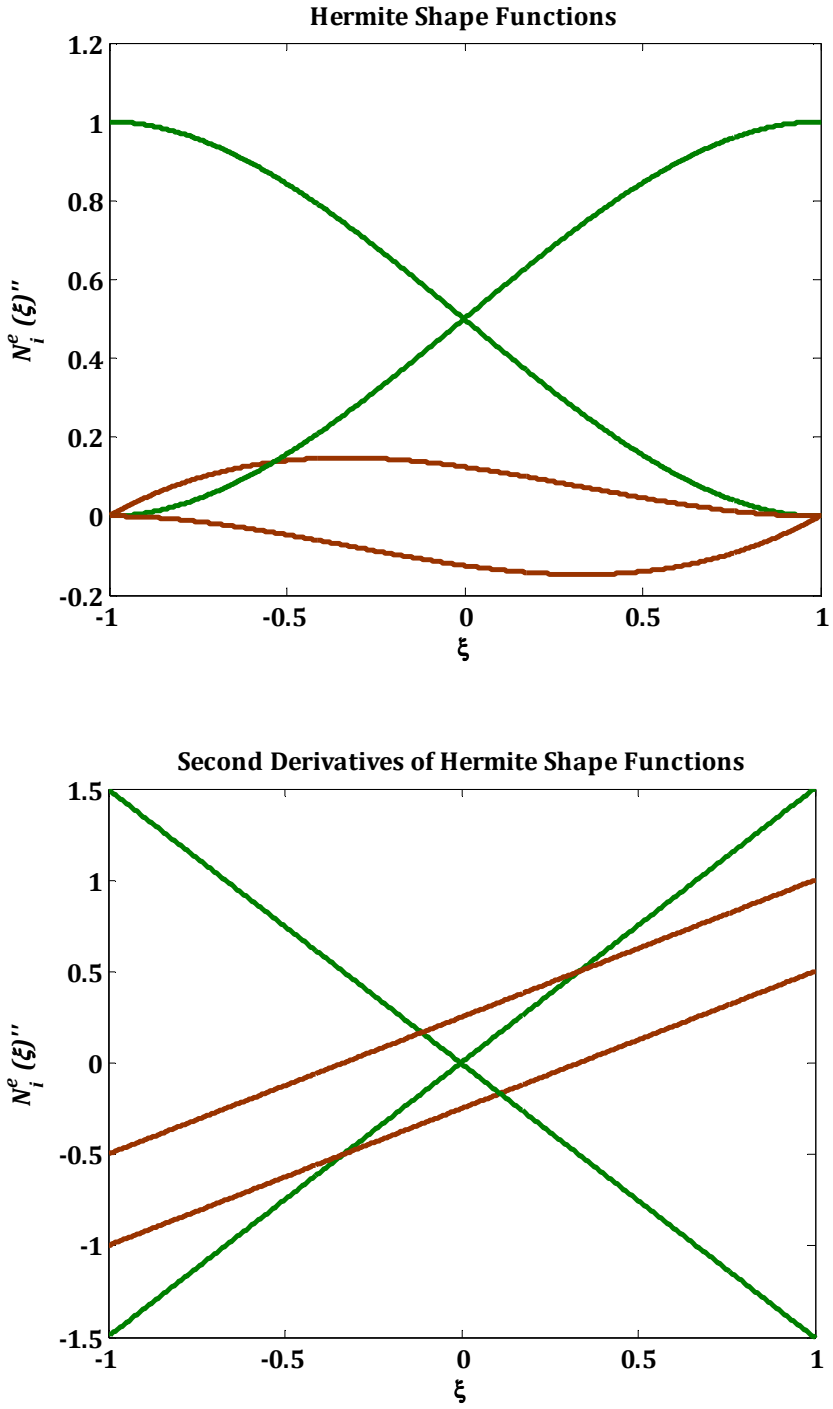

Figure 3.8: (a) Hermite cubic interpolation functions (b) Second derivatives of Hermite cubic interpolation functions

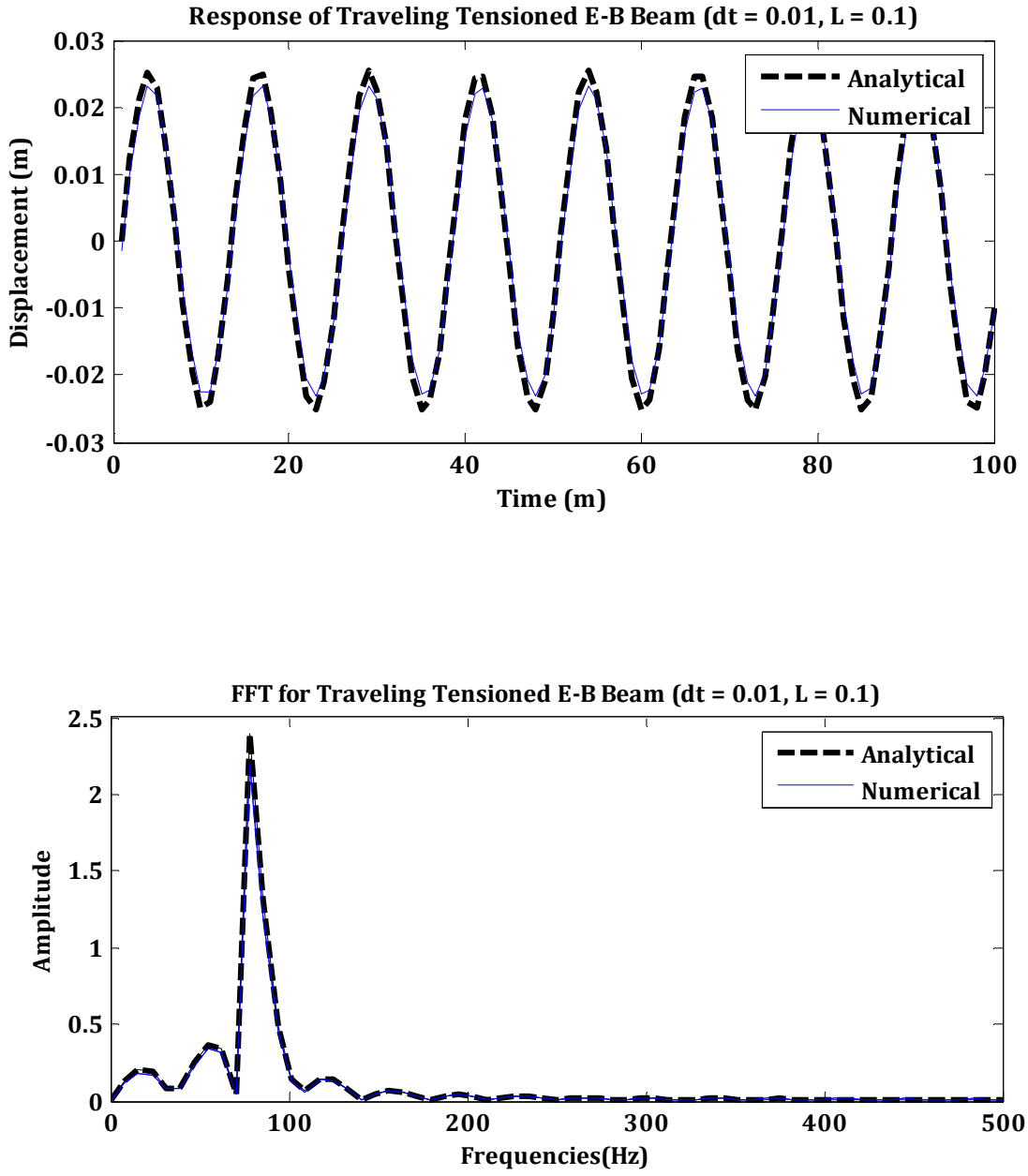

Figure 3.9: Comparison between (a) analytical and numerical lateral displacements (b) analytical and numerical FFTs of lateral displacements - of traveling tensioned Euler-Bernoulli beam with grid-size = 100, dt = 0.01 s and L = 0.1 m

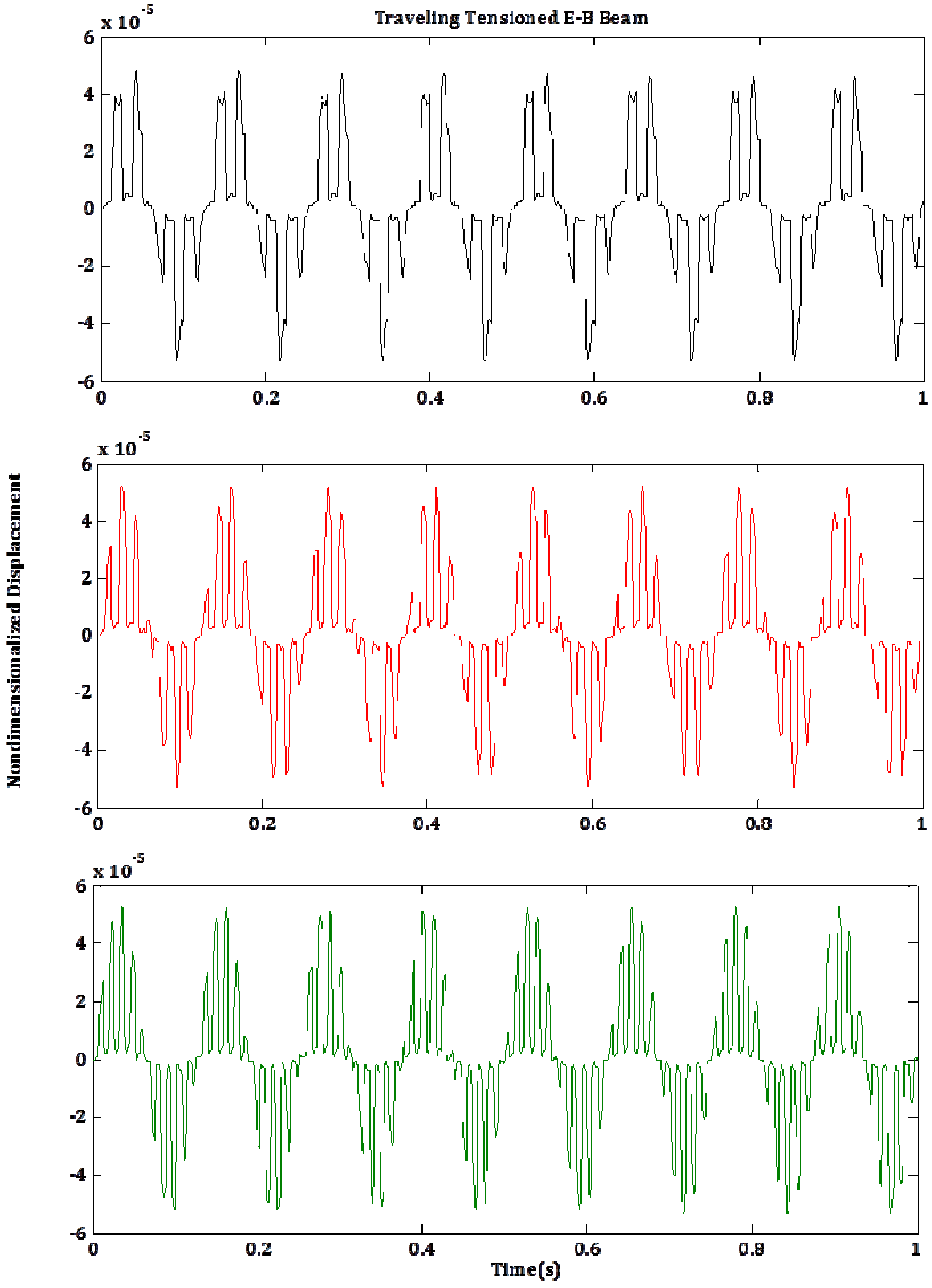

Figure 3.10: (a) Numerical lateral vibration at upstream point at tension 0.6 N and varying axial velocities 2 m/s, 3 m/s and 4 m/s

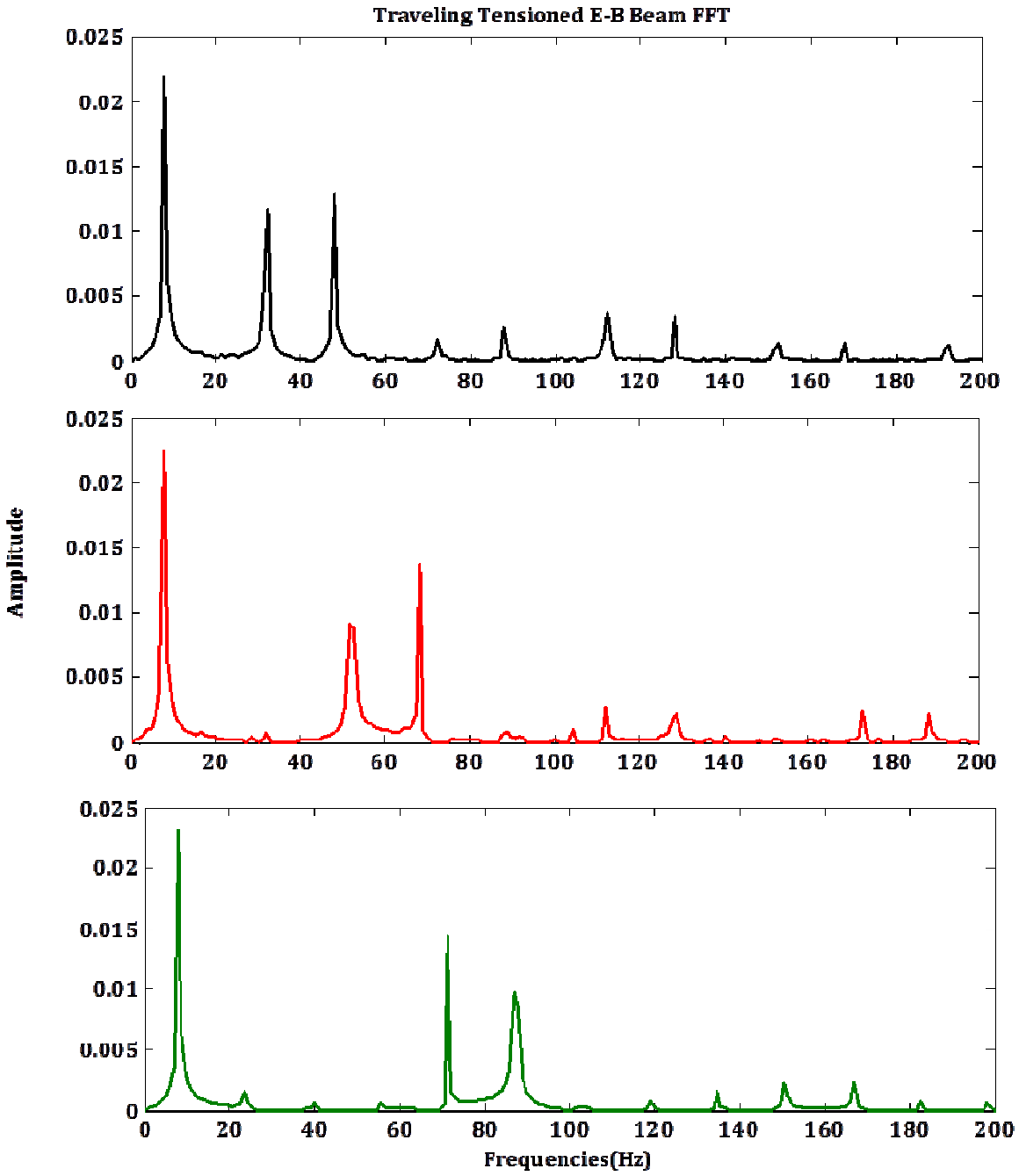

Figure 3.11: (b) FFT of numerical lateral vibration at upstream point at tension 0.6N and varying axial velocities 2 m/s, 3 m/s and 4 m/s

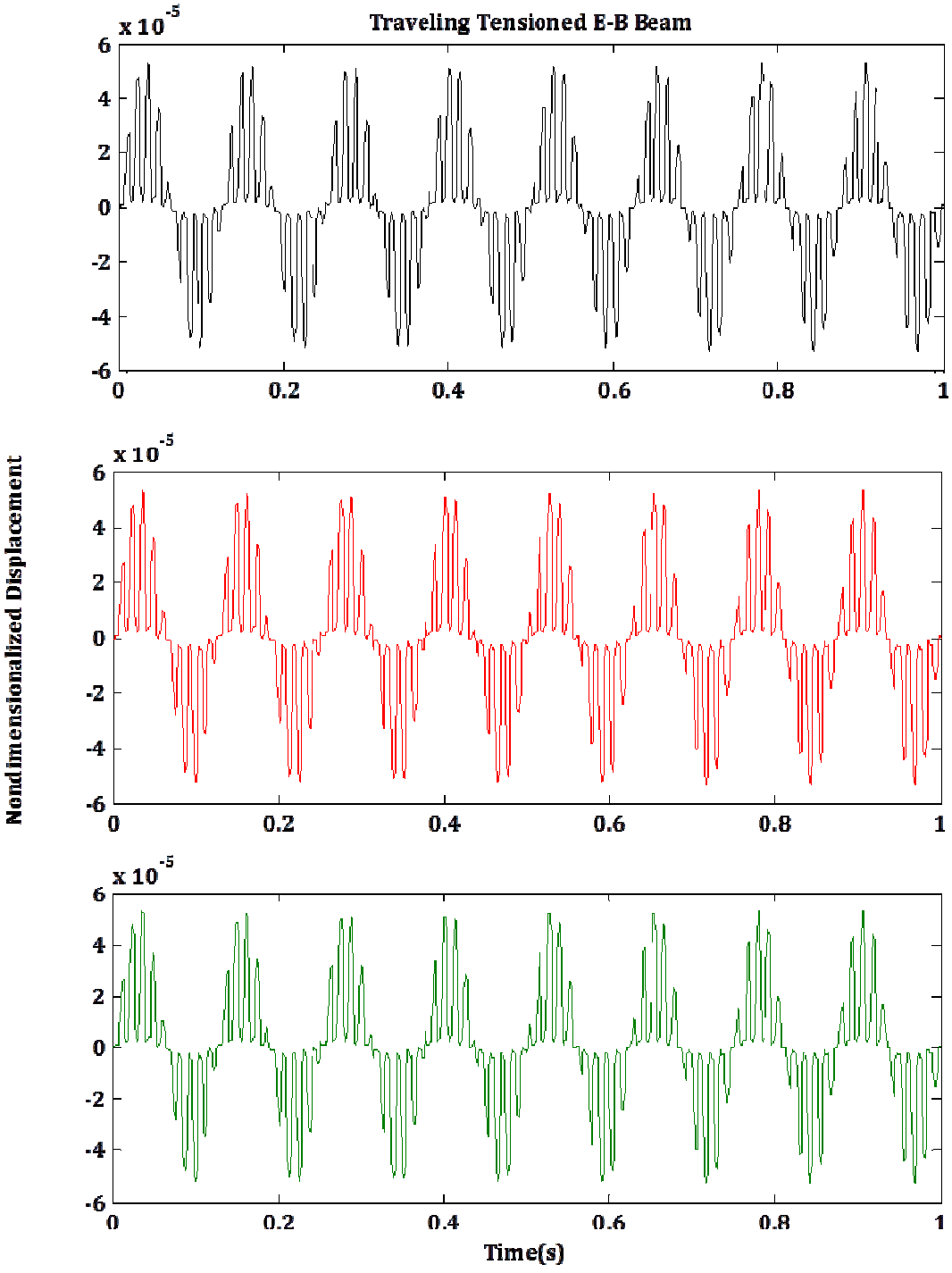

Figure 3.12: (a) Numerical lateral vibration at upstream point at axial velocity 4m/s and varying tensions 0.5 N, 0.6 N and 0.7 N

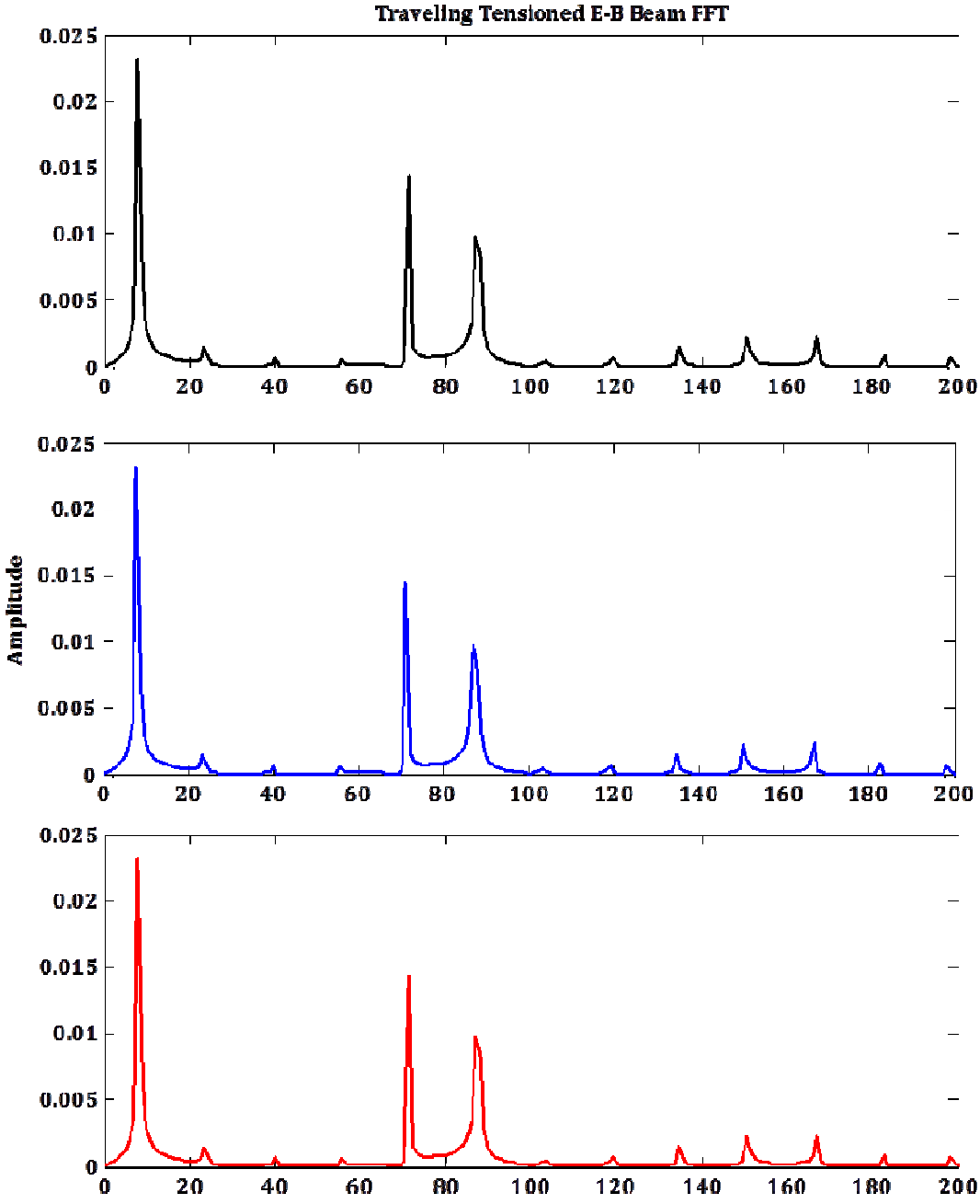

Figure 3.13: (b) FFT of numerical lateral vibration at upstream point at axial velocity 4m/s and varying tensions 0.5 N, 0.6 N and 0.7 N

Node	Quadrature Points		Weights
	$+X_i$	$-X_i$	W_i
1	0.3399810	- 0.3399810	0.65214 515
2	0.8611363	-0.8611363	0.34785 485

Table 3.1: Gaussian quadrature points and weights

Chapter 4

Effect of stick-slip friction transition on the lateral vibration of magnetic tapes – Flanged and smooth rollers

4.1 Introduction

In this chapter, we experimentally investigate the effect of stick-slip friction transition on the lateral vibration of magnetic tape for the case of the flanged grooved roller (Fig. 4.1) and the flangeless roller with fine grooves (Fig. 4.2) (we will refer to this as smooth roller henceforth). This analysis is carried out in the similar manner as that for the flanged grooved roller in chapter 1. Vibration measurements are carried out for five values of axial tension and axial velocity of the tape at points on the upstream and downstream of the tape-roller interface. These measurements are then used to understand the stick-slip behavior of the interface for both flanged roller and smooth roller and demarcate areas on the stiffness-velocity phase-space that exhibit predominantly stick or predominantly slip behavior. The analysis and conclusions are presented in subsequent sections.

The experimental setup in Fig. 4.3 shows the smooth roller placed between two stationary flanges and supply and take-up packs and an LTO-4 generation tape is transported through the tape-path at a constant axial tension and axial transport speed. The setup is connected to a computer via a serial port and the winding/unwinding of tape from the supply and take-up packs is controlled by a Matlab program. The length of tape's span between the roller and each flanged guide is fixed to be 10 cm and two optical edge sensors are placed at a distance

approximately 1 cm to the upstream and downstream side of the interface. These sensors collect real time lateral displacement measurements of the tape's narrow edge.

4.2 Lateral vibration analysis using spectral techniques

4.2.1 Basic definitions

Recalling the analysis in chapter 1, advanced correlation techniques from spectral analysis were used to investigate the relationship between the downstream and upstream LTM signals. Briefly restating the basic definitions pertinent to this analysis; Considering the tape-roller interface as a system represented by upstream and downstream lateral vibration signals, cross power spectral density between them is a measure of the mutual power between these two signals. It is given by,

$$S_{xy}(\omega) \;=\; \frac{1}{2\pi} \int_{-\infty}^{\infty} R_{xy}(\tau)\; e^{-i\omega t}\, d\,\tau$$

Transfer function or frequency response function of a system is the quotient of cross power spectral density $S_{yx}(\omega)$ of $x(t)$ and $y(t)$ and auto-power spectral density $S_{xx}(\omega)$ of $x(t)$. It is given by a time-invariant transfer function,

$$T_{xy}(\omega) \;=\; \frac{S_{yx}(\omega)}{S_{xx}(\omega)}$$

Coherence function between the signals *x(t)* and *y(t)* is a real valued quantity defined by,

$$\gamma_{xy}^2(\omega) \;=\; \frac{\left|S_{yx}(\omega)\right|^2}{S_{xx}(\omega) S_{yy}(\omega)}$$

where $S_{xx}(\omega)$ and $S_{yy}(\omega)$ are the individual auto-power spectral densities. Here $0 \leq \gamma_{xy}^2 \leq 1$ and it represents the degree of correlation between vibration signals in the frequency domain. A raised cosine Hamming window of length 200 is used which minimizes the nearest side lobe and is given in frequency domain by,

$$\omega(n) = 0.54 - 0.46 \cos\left(\frac{2\pi n}{N-1}\right)$$

4.2.2 Classification of axial tension and velocity

Similar to chapter 2, to simplify our analysis, we have divided our experimental stiffness-velocity phase-space (0.5 N-0.7 N and 2 m/s-4 m/s) into four distinct sections, viz.

(1) High tension-low velocity (T = 0.65 N, 0.7 N and *v* = 2 m/s, 2.5 m/s)

(2) Low tension-high velocity (T = 0.5 N, 0.55 N and *v* = 3.5 m/s, 4 m/s)

(3) Low tension-low velocity (T = 0.5 N and *v* = 2 m/s, 2.5 m/s)

(4) High tension- high velocity (T = 0.7 N and *v* = 3.5 m/s, 4 m/s)

4.3 Flanged roller

(1) Low tension – high velocity

Coherence function estimates for tension T = 0.5 N and velocities *v* = 3.5 m/s and 4 m/s in Fig. 4.3 show that the coherence γ_{xy}^2 has values ~ 1 around the low frequency range 0.05 – 0.15 and in a higher frequency range around 0.55 – 0.80 on the normalized frequency scale. This suggests an overall good coherence for the low tension-high velocity case.

(2) High tension – low velocity

Fig. 4.4 for velocity 2 m/s and 2.5 m/s and tension 0.7 N shows good coherence between the upstream and downstream vibration signals at higher frequencies (0.6 – 0.75) in a relatively

narrower range. In the low frequency region, the coherence estimate is close to 1 for a narrow band of frequencies in the range 0.05 to 0.1, and has a low value elsewhere. Thus, the high tension-low velocity case shows relatively poor coherence.

(3) Low tension – low velocity

Fig. 13 for velocity 2 m/s and tensions 0.5 N and 0.55 N shows bad coherence between the upstream and downstream vibration signals at lower frequencies (0.05 – 0.15). In the high frequency region, the coherence estimate is close to 1 for at a narrow band of frequencies in the range 0.6 to 0.75 for T = 0.5 N & 0.55 N.

(4) High tension – high velocity

For velocity 4 m/s and tensions 0.65 N and 0.7 N shows good coherence at higher frequencies (0.5 – 0.8) and in the low frequency region (0.05 – 0.15) on the normalized scale. Thus the overall coherence is good for high tension-high velocity case of a flanged roller.

4.3.1 Coherence metric

We calculated area enclosed under the coherence curve and plotted its normalized form on the experimental stiffness-velocity phase-space, as shown in Fig. 4.7. The normalized area is a measure of total amount of coherence between upstream and downstream signals across the entire frequency domain. Greater value of the area indicates better coherence which in turn suggests that the system stays in stick phase for a comparatively longer time. It is observed that the right half portion of the contour in Fig. 7 shows higher values of normalized area. This indicates that the system exhibits predominantly stick characteristics for velocities above 3.5 m/s, particularly at tensions 0.5 N and 0.6 N. Smaller value of the area denotes a

comparatively bad coherence which suggests the system's tendency to slip more often. Thus, for lower values of velocity, i.e. velocities less than 3 m/s and tension 0.65 N and 0.7 N, the systems exhibits predominantly slip characteristics.

4.4 Smooth Roller

(1) Low tension-high velocity

The system shows good coherence at both low and high frequency regions for low tension-high velocity case. The value of coherence function is close to 1in the region around 0.05 – 0.2 and around 0.4 on the normalized scale. Coherence functions is also ~ 1 in the high frequency range around 0.75 – 0.85 on the normalized scale.

(2) High tension-low velocity

For T = 0.7 N and v = 2 m/s & 2.5 m/s, the system shows very good coherence across the entire frequency domain as seen in Fig. 4.9. Although the coherence function is not close to 1, it is consistently high (around 0.5 – 0.6) for a relatively wider range of frequencies. It means that power is being transferred across the tape-roller interface at a wider range of frequencies of tape's lateral vibration.

(3) Low tension-low velocity

As seen in Fig. 4.10, the coherence is extremely poor for T = 0.5 N and v = 2 m/s across the entire frequency domain. However, for T = 0.55 N, the coherence function shows relatively higher values at both low (0.05 – 0.15), mid-range (0.3 – 0.45) and high (0.7 – 0.85) frequency range. Power is being transferred at greater rates for T = 0.55 N & v = 2 m/s in these frequency regions.

(4) High tension-high velocity

Coherence is consistently good across the entire frequency domain for T = 0.65N, 0.7 N and v = 4 m/s, as observed in Fig. 4.11. This suggests a stable power transfer across the tape-roller interface over the entire frequency domain and indicates a system with stick characteristics.

4.4.1 Coherence metric

The contour in Fig. 4.12 shows the distribution of normalized value of area under the coherence curve, over the experimental stiffness-velocity phase-space. Greater values of the coherence area metric indicates that the total amount of coherence over the entire frequency domain is higher; lower values of coherence area metric indicate a lower amount of coherence over the domain. From Fig. 4.12, it can be observed that the system exhibits predominantly stick characteristics for tension above 0.65 N and for all values of axial velocity. Predominantly slip behavior is seen at low tension – low velocity cases, especially when T = 0.5 N and v = 2 m/s & 2.5 m/s.

Figure 4.1: (a) Flanged Grooved Roller

Figure 4.2: (b) Flangeless Smooth Roller

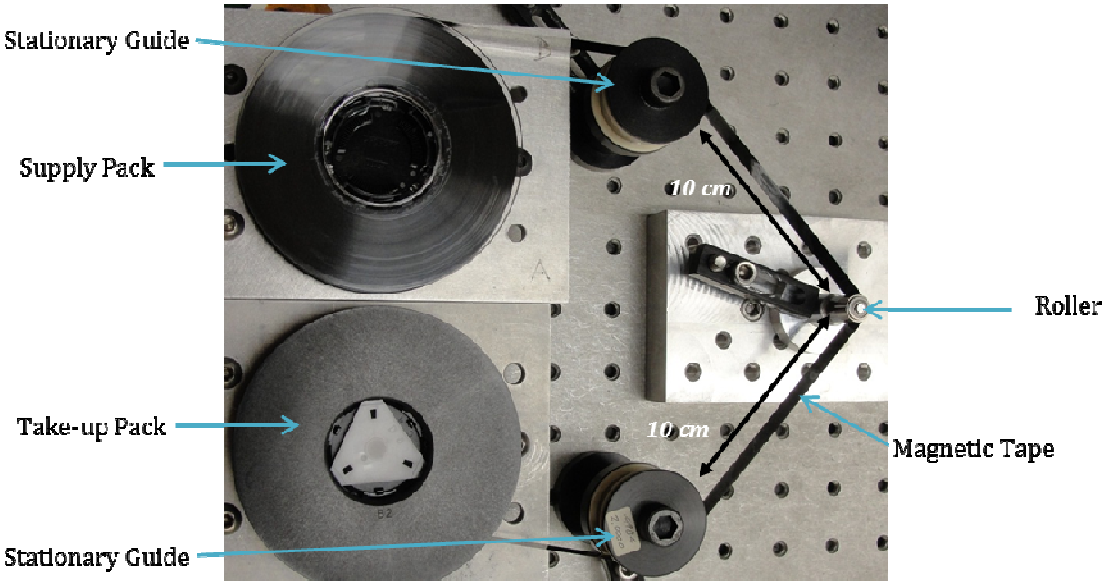

Figure 4.3: Photograph of "JAWS" experimental setup showing tape-path with supply and take-up packs, two stationary flanged guides and a flangeless smooth roller

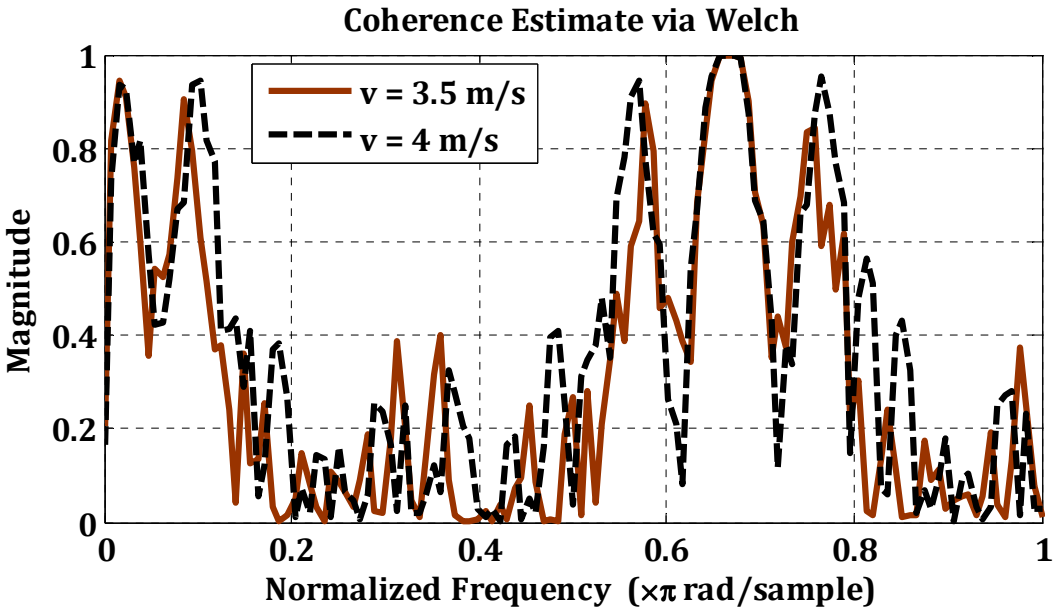

Figure 4.4: Coherence estimate at T = 0.5 N, v = 3.5 m/s & 4 m/s

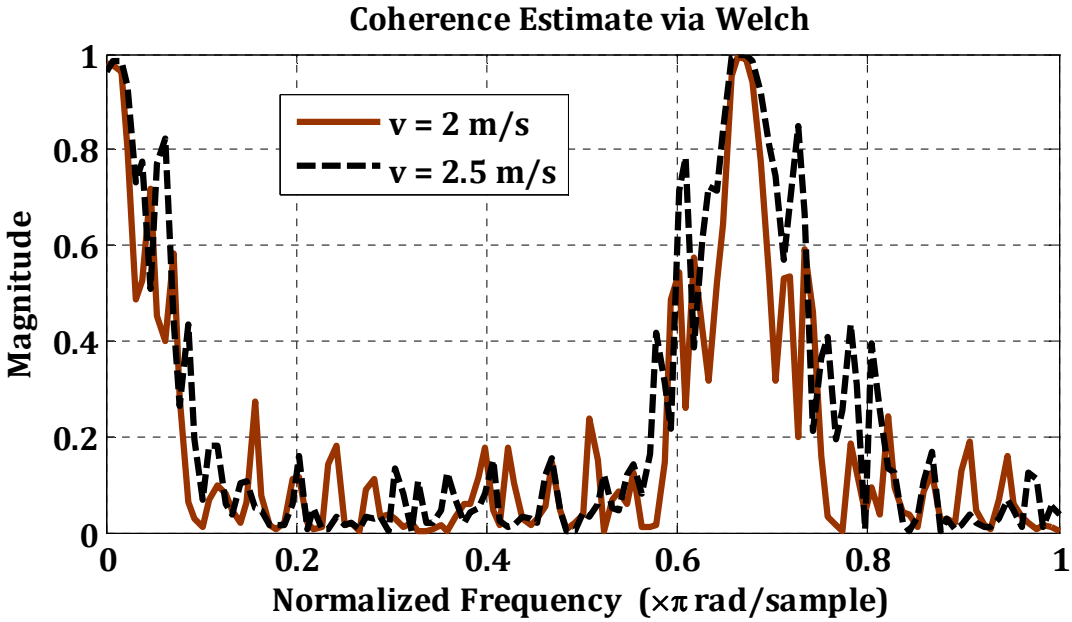

Figure 4.5: Coherence estimate at T = 0.7 N, v = 2 m/s & 2.5 m/s

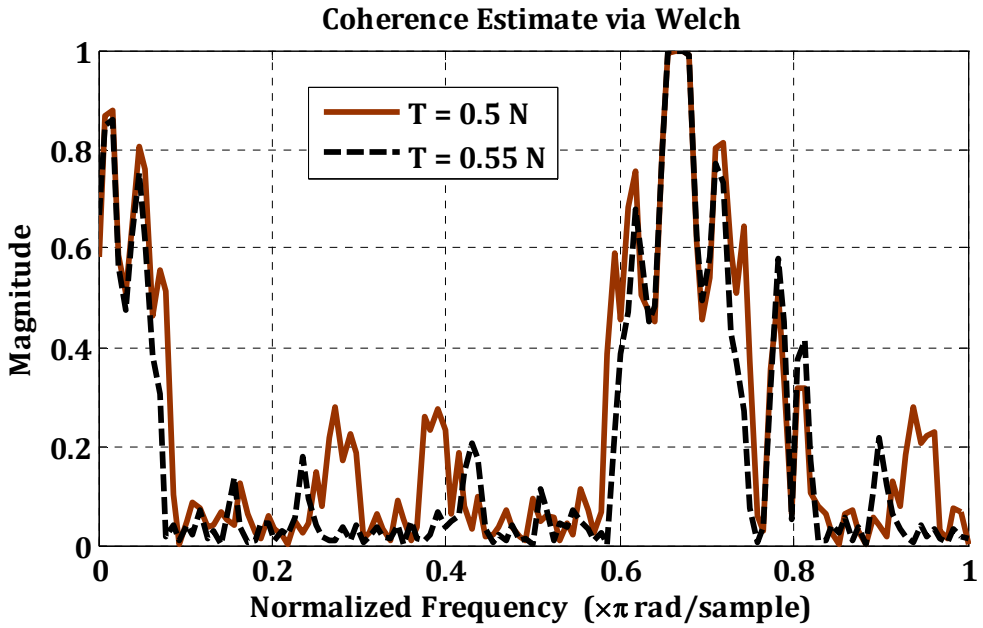

Figure 4.6: Coherence estimate at T = 0.5 N & 0.55 N, v = 2 m/s

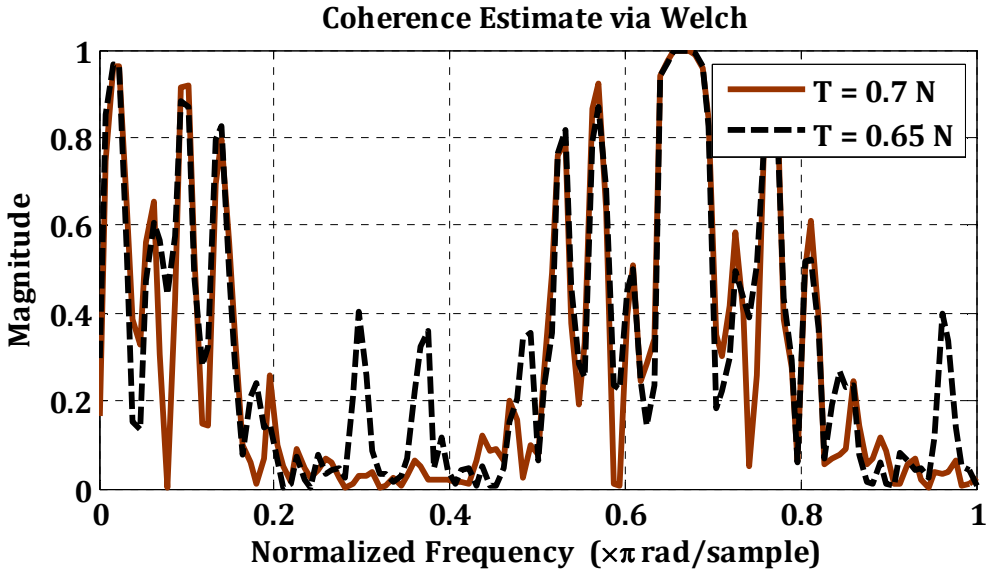

Figure 4.7: Coherence estimate at T = 0.7 N & 0.65 N, v = 4 m/s

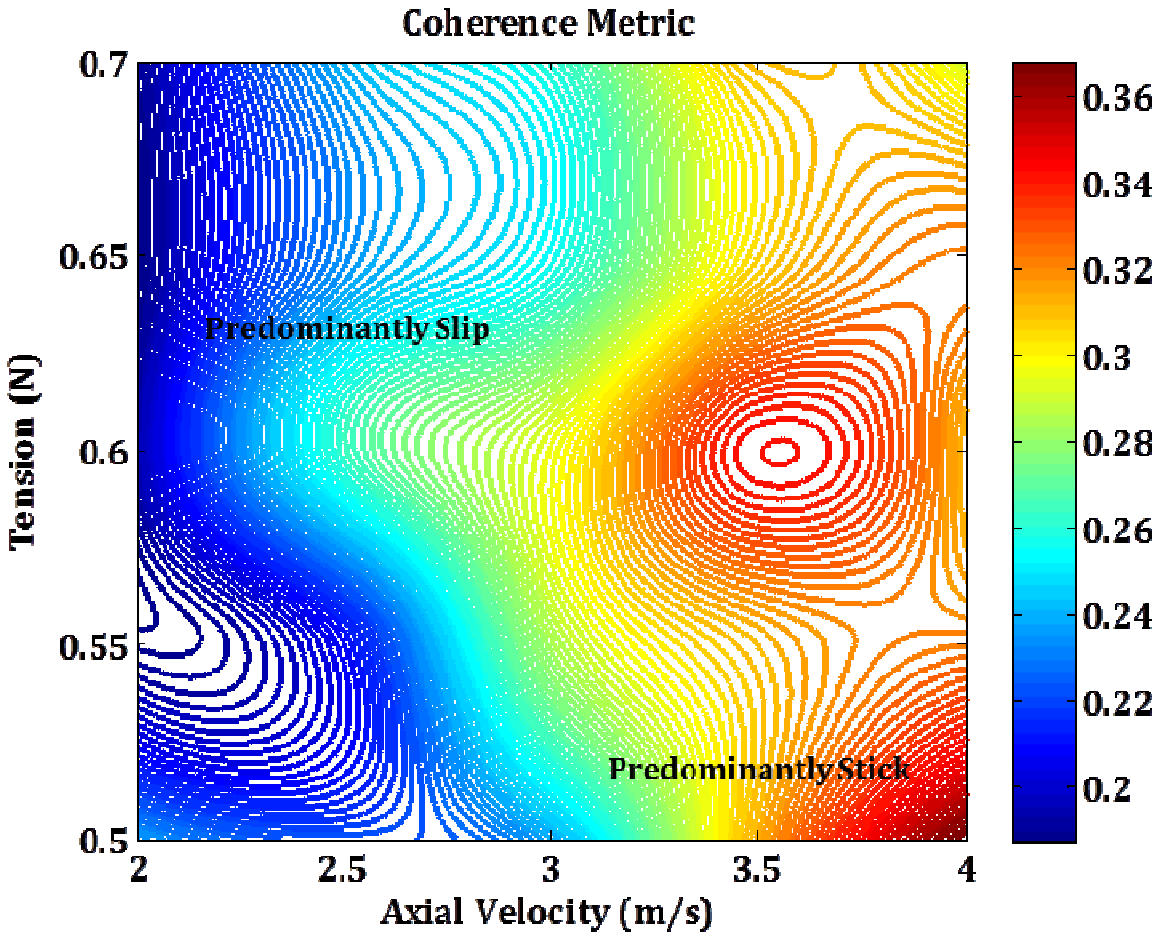

Figure 4.8: Coherence metric to demarcate stick/slip predominance

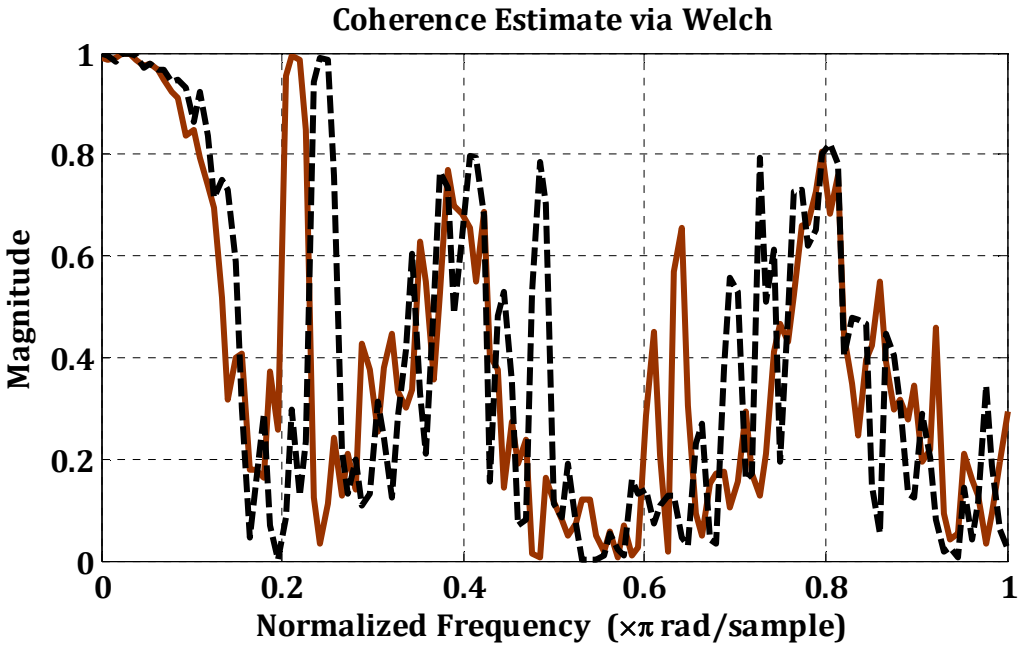

Figure 4.9: Coherence estimate at T = 0.5 N, v = 3.5 m/s & 4 m/s

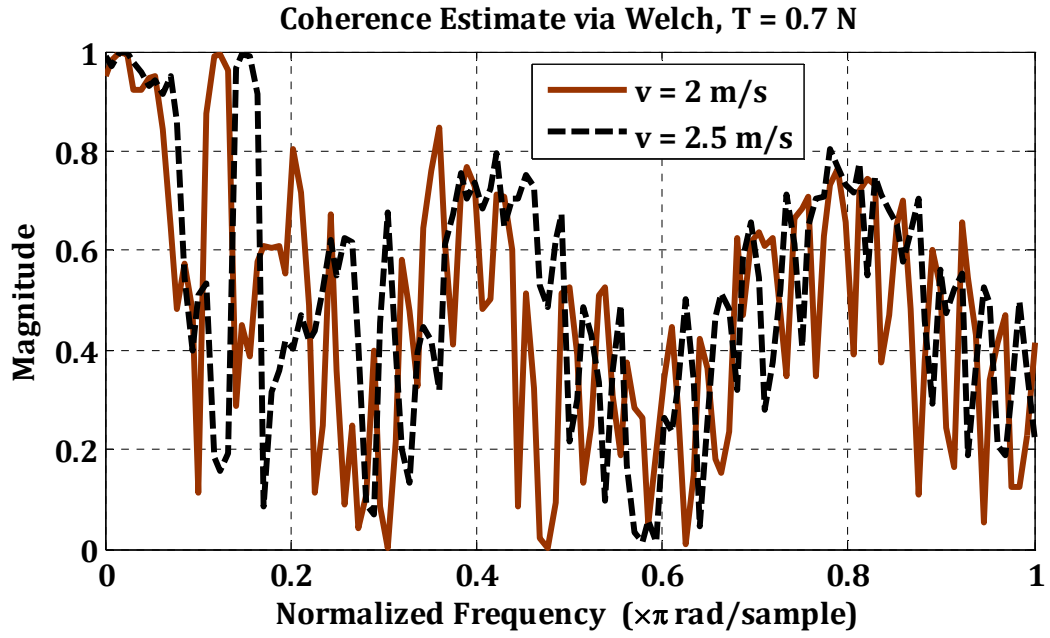

Figure 4.10: Coherence estimate at T = 0.7 N, v = 2 m/s & 2.5 m/s

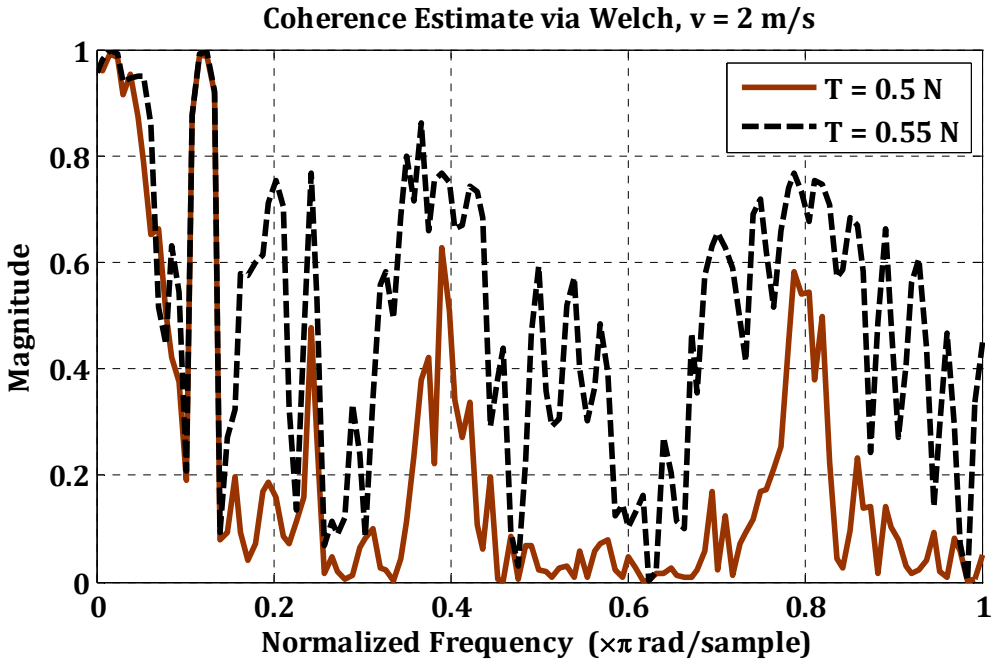

Figure 4.11: Coherence estimate at T = 0.5 N & 0.55 N, v = 2 m/s

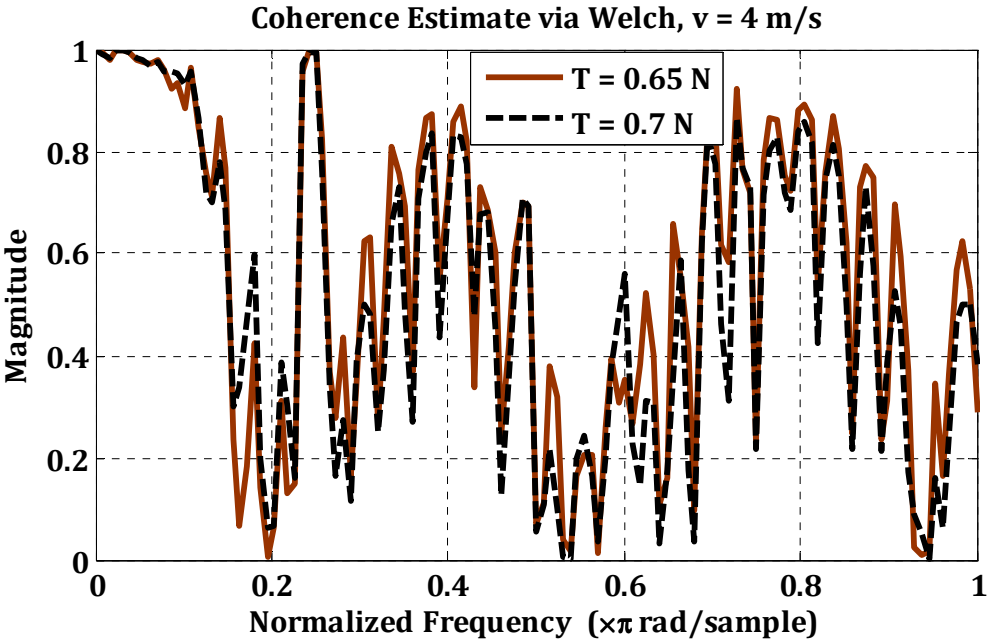

Figure 4.12: Coherence estimate at T = 0.65 N & 0.7 N, v = 4 m/s

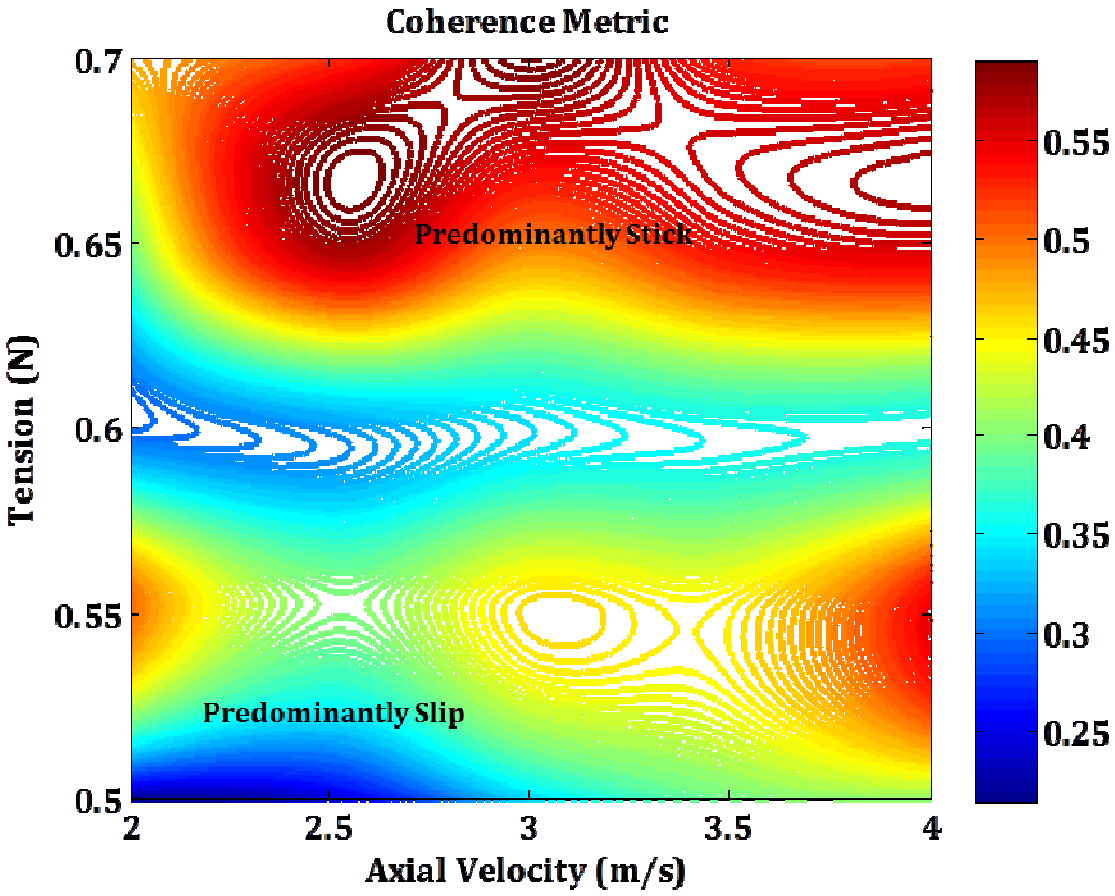

Figure 4.13: Coherence metric to demarcate stick/slip predominance

Chapter 5

Conclusions and future work

5.1 Experimental analysis

The nature of stick/slip friction between tape and roller surface on and its effect on lateral vibration of the tape is analyzed experimentally by controlling tape parameters viz. axial tension and axial transport velocity of the tape. The analysis is carried out for three different roller types.

5.1.1 Flangeless grooved roller

- Nature of friction between tape and roller surface is qualitatively understood from Fig. 2.15, which shows areas of stick predominance, slip predominance and their combination.
- The tape and roller surface stick to a greater degree in the stiffness-velocity region T = 0.65-0.7 N and v = 3.5-4 m/s.
- The region on the left half around T= 0.5 N and v = 2 m/s is where the two surfaces in contact slip to a greater extent.

5.1.2 Flanged grooved roller

- In Fig. 4.7 right half of the contour exhibits predominantly stick characteristics for velocities above 3.5 m/s, at tensions 0.5 N and 0.6 N.

- For lower values of velocity (i.e. less than 3 m/s) and tension 0.65 N and 0.7 N, the systems exhibits predominantly slip characteristics.

5.1.3 Flangeless smooth roller

- In Fig. 4.12 the system exhibits predominantly stick characteristics for tension above 0.65 N and for all values of axial velocity.
- Predominantly slip behavior is seen at low tension – low velocity cases, when T = 0.5 N and v = 2 m/s & 2.5 m/s.

5.2 Numerical Analysis

The numerical model developed in this work can predict lateral displacement of an axially moving linearly elastic Euler-Bernoulli beam with axial tension. We used Galerkin approximation method to discretize the spatial derivatives and Euler's backwards difference method to discretize the temporal derivatives in the equation of lateral vibration of the beam.

The main conclusions of this work are:

- At constant axial tension, with increasing axial velocity, the stick-slip transition frequency needs to be proportionately increased in order to match the frequency content in experimental lateral vibration.
- At constant velocity, with increasing axial tension, there is no observable change in the lateral vibration's frequency content. Hence, stick-slip transition frequency remains constant at constant velocity.

5.3 Future work

We envisage the future of this work in both experimental and numerical aspects. The vibration measurements as described in chapter 2 and chapter 4 can be conducted for a broader spectrum of tape's axial tension and velocity. Other parameters that can be controlled are: tape span-length (spans shorter than 10 cm), angle of wrap at the tape-roller interface, surface roughness of roller and using multiple rollers and investigating their combined effect on tape's lateral motion. It is also suggested to obtain vibrations measurements at multiple points across both upstream and downstream tape spans using multiple edge sensors. An accurate measurement of the pack and guide runout and lateral velocity will be helpful in constructing the forcing function in numerical model. Moreover, taking the measurements at higher sampling frequencies (10 kHz or higher) will ensure the capture of higher frequency lateral vibration of the tape.

In the numerical model, firstly, we want to obtain an accurate estimate of the lateral forces acting on the tape to get more realistic values of the numerical displacement. Secondly, we plan to improve the stick-slip friction model by employing varying time-periods for stick and slip; the time-periods depending on the combination of axial stiffness and velocity of the system. Thirdly, we plan to incorporate terms from tape material damping and tape edge weave into the governing equation of the traveling tensioned Euler-Bernoulli beam. Lastly, to get a more accurate and realistic depiction of tape's lateral behavior, we (a) construct the beam's governing equation by incorporating elastic nonlinearities in the Euler-Bernoulli equation and (b) implement the Timoshenko model to represent beam's lateral displacement.

Bibliography

[1] International magnetic storage roadmap, Information Storage Industry Consortium, September (2008) 117-120

[2] K. Ono, Lateral motion of an axially moving string on a cylindrical guide surface, ASME Journal of Applied Mechanics 46(1979) 905–912

[3] R.J. Yang, Steady motion of a thread over a rotating roller, ASME Journal of Applied Mechanics 61(1994) 16–22

[4] J.E. Rhodes, Parametric self-excitation of a belt into transverse vibration, ASME Journal of Applied Mechanics 37(1970) 1055–1060

[5] J.J. Shelton, K.N. Reid, Lateral dynamics of an idealized moving web, ASME Journal of Dynamic Systems, Measurement, and Control 3(1971) 187–192

[6] J.J. Shelton, K. N. Reid, Lateral dynamics of a real moving web, ASME Journal of Dynamic Systems, Measurement, and Control 3(1971) 180–186

[7] G.E. Young, J. J. Shelton, B. Fang, Interaction of web spans: Part II—Dynamics, ASME Journal of Dynamic Systems, Measurement, and Control 111 (1989) 497–504

[8] G.E. Young, K.N. Reid, Lateral and longitudinal dynamic behavior and control of moving webs, ASME Journal of Dynamic Systems, Measurement, and Control 115 (1993) 309–317

[9] V. Kartik, J.A. Wickert, Vibration and guiding of moving media with edge weave imperfections, Journal of Sound and Vibration 291 (2006) 419–436

[10] V. Kartik, J.A. Wickert, Surface friction guiding for reduced high frequency lateral vibration of moving media, ASME Journal of Vibration and Acoustics 129 (2007) 371-379

[11] M.R. Brake, J.A. Wickert, Frictional vibration transmissions from a laterally moving surface to a traveling beam, Journal of Sound and Vibration 310 (2008) 663-675

[12] Ryan J. Taylor, Frank E. Talke, Investigation of roller interactions with flexible tape medium, Tribology International 38 (2005) 599-605

[13] Bart Raeymaekers, Frank E. Talke, Lateral Motion of an axially moving tape on a cylindrical guide surface, Journal of Applied Mechanics 74 (2007) 1053-1056

[14] R.N. Miles, S.P. Bigelow, Random vibration of a beam with a stick-slip end condition, Journal of Sound and Vibration 169 (1994) 445-457

[15] R.A. Ibrahim, Friction-induced vibration, chatter, squeal, and chaos Part II: Dynamics and modeling, Applied Mechanics Review 47 (1994) No. 7

[16] Mark Denny, Stick-slip motion: an important example of self-excited oscillation, European Journal of Physics 25 (2005) 311-322

[17] K. Popp, P. Stelter, Stick-slip vibration and chaos, Philosophical Transactions of the Royal Society London 332 (1990) 89-105

[18] Chun Bo, D. Pavelescu, The friction-speed relation and its influence on the critical velocity of stick-slip motion, Wear 82 (1982) 277-289

[19] www.mathworks.com

[20] Dean Karnopp, Computer simulation of stick-slip friction in mechanical dynamic systems, ASME Journal of Dynamic Systems, Measurement, and Control 107 (1985) 100-103

[21] Barney E. Klamecki, A catastrophe theory description of stick-slip motion in sliding, Wear 101 (1985) 325-332

[22] D E Newland, An introduction to random vibrations and spectral analysis, Longman Group Limited, 2nd edition, 21-51

[23] A.V. Oppenheim, R.W. Schafer, Discrete-Time Signal Processing, Upper Saddle River, NJ: Prentice-Hall, (1999) 730-754

[24] Michael Norton, Denis Karczub, Fundamentals of noise and vibration analysis for engineers Second Edition, Cambridge University Press, (2003) 352-380

[25] André Preumont, Random vibration and spectral analysis, Kluwer Academic Publishers, (1994) 135-141

[26] Julius S. Bendat, Allan G. Piersol, Engineering applications of correlation and spectral analysis, John Wiley & Sons, (1980) 78-96

[27] F.R. Archibald, A.G. Emslie, The vibration of a string having a uniform motion along its length, ASME Journal of Applied Mechanics 25 (1958) 347-348

[28] R.D. Swope, W.F. Ames, Vibrations of a moving threadline, Journal of Franklin Institute 275 (1963) 36-55

[29] C.D. Mote Jr., A Study of band saw vibrations, Journal of Franklin Institute 279 (1965) 430-444

[30] C.D. Mote Jr., S. Naguleswaran, Theoretical and experimental band saw vibrations, Transactions of the ASME 88 (1966) 151-156.

[31] J. A. Wickert, C. D. Mote, Jr., Classical vibration analysis of axially-moving continua, ASME Journal of Applied Mechanics 57 (1990) 738-744.

[32] M. Moustafa, F.K. Salman, Dynamic properties of a moving thread line, Journal of Engineering for Industry 98 (1976) 868-875

[33] J.A. Wickert, Analysis of self-excited longitudinal vibration of a moving tape, Journal of Sound and Vibration 160 (1993) 455-463

[34] V. Kartik, J.A. Wickert, Vibration and guiding of moving media with edge weave imperfections, Journal of Sound and Vibration 291 (2006) 419-436

[34] M. Stylianou, B. Tabarrok, Finite element analysis of an axially moving beam, Part I: Time integration, Journal of Sound and Vibration 178 (1994) 433-453

[35] R.N. Miles and S.P. Bigelow, Random vibration of a beam with a stick-slip end condition, Journal of Sound and Vibration 169 (1994) 445-457

[36] V. Kartik, J.A. Wickert, Vibration and guiding of moving media with edge weave imperfections, Journal of Sound and Vibration 291 (2006) 419-436

[37] G.E. Young, J.J. Shelton, C. Kardamilas, Modeling and control of multiple web spans using state estimation, Journal of Dynamic Systems, Measurement, and Control 111 (1989) 505-510

[38] F. Kozin, R.M. Milstead, The stability of a moving elastic strip subjected to random parametric excitation, Journal of Applied Mechanics, 46 (1979) 404-410

[39] M.R. Brake, J.A. Wickert, Optimizing vibration isolation flex circuits in hard disk drives, Journal of Vibration and Acoustics, 127 (2005) 165-172

[40] Richard C. Benson, Lateral dynamics of a moving web with geometrical imperfection, Journal of Dynamic Systems, Measurement, and Control 124 (2002) 25-34

[41] M. Stylianou, B. Tabarrok, Finite element analysis of an axially moving beam, Part I: Stability analysis, Journal of Sound and Vibration 178 (1994) 455-481

[42] J.A. Wickert, C.D. mote Jr., On the energetics of axially moving continua, Journal of Acoustical Society of America 85 (1989) 1365-1368

[43] G.E. Young, J. J. Shelton, B. Fang, Interaction of web spans: Part I—Statics, ASME Journal of Dynamic Systems, Measurement, and Control 111 (1989) 490–496

[44] Chao Gao, Doris Kuhlmann-Wilsdorf, David D. Make1, Fundamentals of stick-slip, Wear 162-164 (1993) 1139-1149

[45] Chao Gao, Doris Kuhlmann-Wilsdorf, David D. Make1, The dynamic analysis of stick-slip motion, Wear 173 (1994) 1-12

[46] A. Galip Ulsoy, Coupling between spans in the vibration of axially moving materials, Journal of Vibration, Acoustics, Stress, and Reliability in Design 108 (1986) 207-212

[47] W.L. Miranker, The wave equation in a medium in motion, IBM Journal (1960) 36-42

[48] Eric M. Mockenstrum, Jianping Guo, Nonlinear vibration of parametrically excited, viscoelastic, axially moving strings, Journal of Applied Mechanics, 72 (2005) 374-380

[49] R.A. Ibrahim, Friction-induced vibration, chatter, squeal, and chaos Part I: Mechanics of contact and friction, Applied Mechanics Review 47 (1994) 209-226

[50] J.A. Wickert, Analysis of self-excited longitudinal vibration of a moving tape, Journal of Sound and Vibration, 160 (1993) 455-463

[51] J. Petera, J.F.T. Pittman, International Journal for Numerical Methods in Engineering, 37 (1994) 3489-3519

[52] Kee-Hyun Shin, Soon-Oh Kwon, Member, Sang-Hoon Kim, Seung-Ho Song, Feedforward control of the lateral position of a moving web using system identification, IEEE Transactions on Industry Applications, 40 (2004) 1637-1643

[53] Lisa Sievers, Mark J. Balas, Andreas von Flotow, Modeling of web conveyance systems for multivariable control, IEEE Transactions on Automatic Control, 33 (1988) 524-531

[54] John B. Yerashunas, J. Alexis De Abreu-Garcia, Tom T. Hartley, IEEE Transactions on Control Systems Technology, 11 (2003) 684-693

[55] Günter Reiter, A. Levent Demirel, John Peanasky, Lenore L. Cai, Steve Granick, Stick to slip transition and adhesion of lubricated surfaces in moving contact 101 (1994) 2606-2615

[56] A.A. Shabana, Vibration of discrete and continuous systems, Springer-Verlag New York, Inc., 2nd Edition, 206-262

[57] Leonard Meirovitch, Principles and techniques of vibrations, Prentice-Hall Inc., 587-629

[58] Haym Benaroya, Mechanical vibration – Analysis, uncertainties, and control, Prentice-Hall Inc., 413-439

[59] Maurice Peyt, Introduction to finite element vibration analysis, Cambridge University Press, 414-449

[60] Peter Hagedorn, Anirvan DasGupta, Vibration and waves in continuous mechanical systems, John Wiley & Sons Ltd., 113-178

[61] Leonard Meirovitch, Fundamentals of vibrations, McGraw-Hill Higher Education, 374-612

[62] Singiresu S. Rao, Vibration of continuous systems, John Wiley & Sons Ltd., 317-390

[63] Zdeněk Bittnar, Jiří Šejnoha, Numerical methods in structural mechanics, American Society of Civil Engineers, 174-209

[64] Ahmed A. Shabana, Computational continuum mechanics, Cambridge University Press, 286-314

[65] Thomas J.R. Hughes, The finite element method-Linear static and dynamic finite element analysis, 1-175, 363-376

[66] Klaus-Jürgen Bathe, Edward L. Wilson, Numerical methods in finite element analysis, Prentice-Hall Inc., 308-361

[67] A.I. Beltzer, Variational and finite element methods-A symbolic computation approach, Springer-Verlag New York, Inc., 150-208

[68] Alain Berlioz, Philippe Trompette, Solid mechanics using the finite element method, John Wiley & Sons Ltd., 233-271

[69] Irving H. Shames, Clive L. Dym, Energy and finite element methods in structural mechanics, Hemisphere Publishing Corporation, 326-342, 487-520

[70] J.N. Reddy, An introduction to the finite element method, McGraw-Hill Higher Education, 3rd Edition, 233-261, 525-569

[71] Gang Sheng, Friction-induced vibrations and sound-Principles and applications, CRC Press, 194-198

[72] Roger E. Bohn, James E. Short, How Much Information? - Report on American Consumers, (2009), http://hmi.ucsd.edu/howmuchinfo_research.php

[73] Sun Microsystems, http://www.oracle.com/us/sun